Predicting crashes of foiling ocean racing yachts by means of a DVPP

Msc Thesis Ship Hydromechanics
Jelle Lourens

TUDelft

(This page is intentionally left blank)

Thesis for the degree of MSc in Marine Technology in the specialization of Ship Hydromechanics

Predicting crashes of foiling ocean racing yachts by means of a DVPP

by

Jelle Lourens

to be defended publicly on Friday, December 13, 2024, at 14:00.

Company Supervisors
Responsible supervisor: Dr. Ir. P. Wellens

Thesis exam committee
Chair: Dr. Ir. P. Wellens
Staff member: Dr. Ir. I. Akkerman
Staff member: Ir. M. Bockstael

Author Details
Study number: 4961897
Author contact e-mail: jelle@jellelourens.nl

Cover: Biotherm sailing - Biotherm Ronan Gladu under CC BY-NC 2.0 (Modified)

TUDelft

Preface

This thesis marks the completion of the past seven years of my academic journey. Throughout this period, I have always been sailing at a high level, and this experience, combined with my curiosity about hydrodynamics and sailboat design, has led me to pursue this research. Over the last couple of ocean races, more reports showed that big waves significantly impact sailboat racing. This sparked the idea of doing research into this phenomenon. Therefore, this thesis is of interest to people with similar interests in ocean racing and the hydrodynamic modeling of such boats.

This thesis would not have been feasible without the support of numerous people, so I would like to thank a few of them. Firstly, I want to thank Peter Wellens for guiding and supporting me in this master's thesis. I came up with this idea without knowing if it would be a viable research subject and if it could be solved. But he was enthusiastic, supported me, and guided me to the right parts of the literature to complete this research.

Secondly, I want to thank my sailing friends for their curiosity in this subject and for listening to me when we were going to races. Lastly, I want to thank my academic friends who helped and listened to me during this thesis.

Jelle Lourens
Delft, December 2024

Summary

This report aims to investigate the dynamic simulation of an IMOCA 60 sailing yacht in big wave conditions. These yachts are equipped with hydrofoils, which significantly increases their speed. However, this increase in speed introduces a challenge: when encountering large waves, the yacht can experience a "crashing" behavior, where rapid acceleration leads to a collision with the wave ahead. These crashes can be severe enough to cause injuries to the crew onboard, making it essential to understand and mitigate these occurrences.

A Dynamic Velocity Prediction Program, DVPP, was developed to explore the yacht's behavior in waves. This DVPP systematically models all the forces acting on the yacht, allowing them to be solved in the time domain. Particular attention was given to hydrodynamic forces, with a nonlinear Froude-Krylov force calculation to accurately represent the effect of waves on the yacht's hull. Next to this, a correction has been applied to the diffraction and radiation forces to take the effect of foiling into account. Furthermore, a correction has been applied to the aerodynamic forces to account for the flapping of sails due to changes in apparent wind angle.

To validate the DVPP's accuracy regarding hydrodynamic and static forces, a heave decay test and RAOs of a Wigley hull were calculated. Based on these results, the DVPP agrees with the reference data, which gives confidence in the DVPP. A qualitative validation was conducted to evaluate the DVPP's ability to simulate an IMOCA 60 in wave conditions. These simulations demonstrated that the DVPP with the implemented corrections could accurately simulate an IMOCA 60 yacht in waves, as the results corresponded with those from a DVPP developed for an ocean-racing trimaran.

Further investigation was performed on the effect of the foils on the yacht. A parametric study revealed a clear correlation between the yacht's behavior and sea state: higher sea states lead to more severe crashes. Further investigations into foil chord length and rake angle were also conducted. The analysis showed that a longer chord length tends to result in less influence of waves on the yachts speed, likely due to the increased drag associated with a longer chord, which limits the yacht's speed.

Additionally, it was found that a lower rake angle leads to more severe slowdowns. This is attributed to the influence of wave orbital motion on the foils; at a lower rake angle, the increased angle of attack generated by the orbital movement increases lift as the wave approaches the stern of the yacht, leading to higher speeds and more significant impacts with the wave ahead. Furthermore, recovery from these crashes is slower with a lower rake angle, as the hydrofoil produces less lift overall. Based on this parametric study, it can be concluded that a larger chord length and a higher rake angle are preferred to minimize accelerations during slowdowns. However, further investigation is needed to understand how the yacht's overall design influences its behavior in waves.

Lastly, a longer simulation, with challenging environmental conditions, was performed to investigate whether the DVPP could be used to simulate crashes in waves of an IMOCA 60. The results showed several slowdowns where the G force was above the threshold for a crash. This indicates that the DVPP can simulate these extreme events. Upon further analysis, it was concluded that the first part of the slowdown occurs due to the foil submergences, and a second slowdown occurs when the hull enters the water. Based on the results of the parametric study, the recommendations of a larger foil chord length and higher rake angle were applied to the simulation case; with these changes, the slowdowns were much lower, and the occurrence of crashes was reduced.

Furthermore, it is recommended that future research focus on enhancing the accuracy of the DVPP, particularly in the modeling of nonlinear hydrodynamic forces, radiation, and diffraction effects. Since an engineering solution was implemented, incorporating unsteady sail forces into the simulation to account for the effects of sail trimming on the yacht's performance is also crucial for stable results in big waves. Further research is needed to present a method that is backed by further physics.

Contents

List of Figures

List of Tables

Nomenclature

Abbreviations

Abbreviation	Definition
AWA	Apparent wind angle
AWS	Apparent wind speed
BEM	Boundary Element Method
BSP	Boatspeed
Cd	Drag coefficient
CFD	Computational Fluid Dynamics
Cl	Lift coefficient
DoF	Degrees of Freedom
DVPP	Dynamic Velocity Prediction Program
DSYHS	Dell Systematic Yacht Hull Series
NACA	National Advisory Committee for Aeronautics
ORC	Offshore Racing Congress
PISO	Pressure-Implicit with Splitting of Operators
RANS	Reynolds-averaged Navier-Stokes
RAO	Response Amplifier Operator
TWA	True wind angle
TWS	True wind speed
URANS	Unsteady reynolds-averaged navier-stokes
VOF	Volume-Of-Fluid
VPP	Velocity Prediction Program

Symbols

Symbol	Definition	Unit
A_f	Facet area	[m^2]
A_∞	A-matrix at infinite frequency	[kg]
A_{w0}	Wetted surface	[m^2]
ar	Aspect ratio	[-]
b	Wetted beam	[m]
B_∞	B-matrix at infinite frequency	[N/(m/s)]
B_{wl}	Beam at water line	[m]
C	Cord length	[m]
C_d	Drag coefficient	[-]
C_f	Frictional resistance coefficient	[-]
C_l	Lift coefficient	[-]
C_p	Prismatic coefficient	[-]
C_t	Resistance coefficient	[-]
c_τ	scaling factor impulse response	[-]
$C_{r,DSYHS}$	Residuary resistance coefficient	[-]
F	Force vector	[N]
F_{Aero}	Aerodynamic force	[N]
F_{App}	Appendage forces	[N]
F_{grav}	Gravity force	[N]

Symbol	Definition	Unit
F_{HD}	Hydrodynamic force	[N]
F_{HS}	Hydrostatic force	[N]
F_{rad}	Radiation force	[N]
F_{res}	Resistance	[N]
f	Frequency	[rad/s]
f_c	Facet center	[m]
f_m	Modal frequency	[rad/s]
g	Gravitational constant	[m/s^2]
H	Distance to the free surface	[m]
H_s	Significant wave height	[m]
I	Inertia tensor	[kg m^2]
k	Wave number	[-]
K	Impulse Response function	[N/m]
LCB	Latitudinal center of buoyancy	[m]
LCF	Latitudinal center of flotation	[m]
L_s	Selection matrix	[-]
L_{wl}	Length water line	[m]
M_{HS}	Hydrostatic moment	[Nm]
M_{rb}	Mass rigid body matrix	[kg]
m	Mass	[kg]
N_f	Facet normal	[m]
OG	Position center of gravity	[m]
P_{HS}	Hydrostatic pressure	[N/m^3]
R	Resistance	[N]
$R_{b,n}$	Rotation matrix body to ned	[-]
R_{fh}	Frictional resistance	[N]
R_{rh}	Residuary resistance	[N]
R_{vk}	Viscous resistance	[N]
Re	Reynolds number	[-]
S_f	Wave spectrum	[-]
S_w	Underwater volume	[m^3]
S_{w0}	Underwater volume at water line	[m^3]
t	Time	[s]
t^*	Cut off time	[s]
T_o	angular velocity rotation matrix	[-]
U	Velocity	[m/s]
V	Velocity vector	[m/s]
$\mathbf{S}$	State vector	[m]
z_{mid}	z-position middle point	[m]
z_p	z-position point	[m]
α_k	Prony coefficient	[-]
β_k	Prony coefficient	[-]
β	Deadrise angle	[deg]
Δ	Displacement	[kg]
λ	Wet keel length	[m]
μ	Wave angle	[deg]
ϕ	Rotation over x-axis	[rad]
ϕ_d	Phase diffraction force	[rad]
Φ	Wave velocity potential	[m]
ψ	Rotation over z-axis	[rad]
ρ_w	Water density	[kg/m^3]
θ	Rotation over y-axis	[rad]
τ	Trim angle	[deg]
τ	Time step	[s]

Symbol	Definition	Unit
ω	Angular velocity	[rad/s]
ω	Wave frequency	[rad/s]
ζ_a	Wave amplitude	[m]

<div align="right">

1

</div>

<div align="right">

Introduction

</div>

The quest for higher speeds in offshore sailing yachts has led to the adoption of hydrofoils across various classes. These hydrofoils generate hydrodynamic lift, allowing the hull to be partially or fully lifted out of the water, thereby significantly reducing hydrodynamic resistance. This innovation is particularly evident in the IMOCA 60 class, where nearly all newly constructed yachts now feature hydrofoils to improve performance (Gorman, 2023).

The development of hydrofoils can be traced back to the 34th America's Cup in 2013 when they were first employed on catamaran hulls. This marked a significant turning point in sailing technology, prompting extensive research and understanding. Initially, hydrofoils were predominantly used on smaller sailing boats operating in calm waters with minimal wave interference. However, the application of hydrofoils in ocean racing expanded when the IMOCA 60 class, a 60-foot monohull designed for single-handed, round-the-world racing IMOCA Class (n.d.), permitted their use in the 2016 race edition. Only a hydrofoil placed along the side of the hull is allowed on these yachts, leading to a semi-foiling mode where the aft portion of the hull remains in the water. Advances in research and design, coupled with the experience gained from the 2016 race, have led to the development of larger and more powerful foils. These modern foils allow the yacht to rise nearly above the water surface, as illustrated in Figure 1.1.

Figure 1.1: Fully foiling IMOCA 60 (Defi-Azimut, 2024)

While this evolution has brought significant speed advantages, the 2023 Ocean Race revealed two critical challenges these foiling yachts face. First, the yachts experience severe slamming when encountering waves. Second, there is a tendency for abrupt pitching or even crashing into the wave ahead, as shown in Figure 1.2. These incidents lead to rapid deceleration, with boats reducing from speeds over 35 knots to nearly a complete stop. Such events have resulted in crew injuries (The Ocean

Race, 2023), highlighting the urgent need for further investigation into the causes and effects of these crashes.

Figure 1.2: Crashing IMOCA in waves (11th-Hour-Racing-Team, 2023)

The severity of this issue is compounded by the remote locations of these races, where rescue operations are often not feasible. Therefore, this research aims to investigate the dynamics of these crashes, focusing on how these yachts can numerically be simulated when sailing in these big waves. Besides, the influence of the foil design on the yacht's behavior in waves is investigated. Specifically, it will examine the dimensions and angle of attack of hydrofoils.

Current literature offers limited insights into this phenomenon. While some studies have explored the dynamic simulation of foiling yachts, only a few have focused on ocean-going vessels. Most notably, a time-domain simulation for an ocean-going trimaran has been conducted. This research seeks to build upon this knowledge by enhancing the understanding of how foiling monohulls behave in wave conditions. The central research question guiding this thesis is:

Can the occurrence of wave-induced crashes be investigated by numerically simulating an IMOCA 60 in high waves?

The research will leverage existing dynamic simulation literature and apply these methodologies to build a numerical simulation for an IMOCA 60. Special attention will be drawn to the implications of sailing in high waves. The dynamic simulation will be validated with reference data, and improvements to the current state-of-the-art simulation method are proposed. Based on this improved dynamic simulation, a parametric study will be conducted to determine which parameters most significantly influence the sailing behavior in waves. These studies will draw conclusions about the dynamics of an IMOCA 60 in waves. Lastly, it is investigated whether dynamic simulation can be used to model the occurrence of extreme decelerations.

The thesis is organized as follows: first, a review of relevant literature is presented in section 2, covering key topics such as velocity prediction, impact dynamics, CFD analysis of floating bodies, green water effects, mathematical wave descriptions, and the IMOCA 60. This review provides a comprehensive overview of the subject matter and identifies potential avenues for further research. The research questions and methodology are then formulated in section 3, firstly addressing the overlap between the literature and the problem statement. Based on this overlap, the research questions are formed. Based on these research questions, an appropriate methodology is proposed.

The first step involves developing a Dynamic Velocity Prediction Program, DVPP, to simulate a yacht's behavior in waves, discussed in section 4. In this section, the framework of the DVPP is presented. Each component is explained, and the relevant implemented formulas are explained. This DVPP is validated in two ways: firstly, a quantitative validation in section 5. This section presents a decay test of a sphere and compares it with reference data. Secondly, RAOs of a wigley hull are calculated and compared with both experimental and numerical results. Based on this validation, a conclusion will be drawn about the accuracy of the DVPP.

Secondly, a qualitative validation is performed in section 6. This qualitative validation is a comparative analysis against a similar DVPP developed by Kerdraon (2021), using identical sea states and wind conditions. This comparison, detailed in section 6, allows for an evaluation of the DVPP's accuracy in big waves. Based on this validation, several improvements to the DVPP are proposed, which enhance the accuracy of a foiling monohull in big waves.

The study then focuses on the behavior of IMOCA 60 in waves by conducting a parametric study that focuses on the environmental and foil parameters. These testing conditions compromise wind speed, foil chord length, and rake angle. The simulation setup and the results are presented in section 7. Lastly, the DVPP is used to investigate whether or not the crashes in waves can be simulated, section 8. By setting a threshold on the G-forces on the yacht, a clear distinction can be made as to whether or not a slowdown is a crash. A longer simulation, combined with extreme environmental conditions, will be the input setting for the DVPP. The results are analyzed, and conclusions on the usefulness of the DVPP for these cases are presented.

The report finishes with a discussion of the applied methodology, validation, and the results, section 9. The thesis concludes with answers to the research questions and suggestions for mitigating crash events in future designs.

2

Background literature

The literature around sailing hydrofoil yachts can be divided into several objects. The first is velocity prediction, which entrails all research surrounding the prediction of velocity and attitude of the vessel in a steady state or in the time domain. This can further be expanded into two different methods, one based on algebraic equations and one based on computational fluid dynamics. Next to the velocity prediction, the background of the issue also focuses on the dynamics of impact; this can be further divided into water entry impact, the hull slamming or crashing in waves, and into green water, water flowing over the deck. Lastly, the mathematical behavior of waves is a source of literature on how waves can be fully captured into mathematical formulas.

2.1. Velocity prediction

Currently, there is little literature on velocity prediction of foiling sailing vessels in waves however, there are some papers on how to model the dynamics of a sailing yacht in 6 degrees of freedom, DoF. Day et al. (2002) started this work by explaining how, from the current type of Velocity Prediction Program, VPP, a non-linear time domain solution for the motions can be obtained. And called this a Dynamic Velocity Prediction Program, DVPP. Based on this work, Boris Horel (2019), Kerdraon et al. (2020), and Knudsen et al. (2022) build several 6-DoF DVPP for various types of hydrofoiling yachts. This work uses the same overall system-based approach to solving the motion equation. In this way the computational time is reduced greatly with respect to CFD methods. Each paper uses a different method to obtain the hydrodynamical forces. For normal sailing yachts most used way to obtain these coefficients is by the Delft Systematic Yacht Hull Series however, Huetz and Alessandrini (2011) explains that these coefficients are not accurate for high speeds or newer types of designs, and therefore a different method is preferred for foiling yachts.

In Boris Horel (2019), the hydrostatic force is calculated by using the hull geometry and obtaining the hydrostatic pressure at each mesh point of the hull. The damping forces are modeled using linear and nonlinear coefficients obtained by experimental and CFD decay tests. The hydrodynamic interaction forces are only modeled in 3-DoF, where the coefficients are identified from captive model tests. The choice for a 3-DoF model comes from the fact that the transition between foiling and displacement only takes place when sailing in a straight line. The transition between these two modes is accounted for by a ratio of the static wetted surface and the instantaneous wetted surface. The appendages are modeled by approximating the shapes of the rudder and foil with elements and assuming a 2d flow over each element. Based on the NACA profile of the appendage, the lift and drag can be calculated. Later Boris Horel and Durand (2019) use the same approach to model an IMOCA 60 while focusing on the deflection of the hydrofoil due to the forces acting on it. In this approach, instead of using experimental and CFD decay tests, he uses BEM to calculate the added mass and damping forces and convert this to a situation where there is a forward speed. This method is numerically efficient because it eliminates the need for CFD or tank tests, instead it uses the faster BEM calculations.

Kerdraon et al. (2020) models the hydrodynamical maneuvering loads not as hydrodynamic derivatives but by computing polynomial response surfaces based on numerical computations for different hull at-

titudes, sinkage, and speeds. Meanwhile, the wave forces are computed using potential flow methods. The appendage loads are modeled using a vortex lattice method because it provides a numerically efficient way to calculate different kinds of lifting surfaces. The aerodynamic loads are calculated using steady-state polars obtained by RANSE calculations. He concludes that the DVPP can be used to perform stability assessments and motion stability criteria and quantities to assess the quality of appendage design. However, further work needs to happen regarding appendage and aerodynamic loads.

Knudsen et al. (2022) obtains the hydrostatical stiffness matrix by various simulations in static conditions while the hydrodynamical constants are obtained from URANS simulations with forces oscillations, the advantage of this is that the viscous damping is included in the coefficients. However the time to compute these coefficients is rather large. They compare the solution to quasi-steady VPP and CFD and conclude that the model is very close to the dynamic CFD simulations.

Next to the hydrostatic and hydrodynamical forces the aerodynamical forces are modeled in different ways, the most used way is the method presented in the ORC-VPP (Offshore Racing Congress, 2022), which obtains the force of the sails by using different lift and drag coefficient for several wind angles. While others use a more dynamic approach based on the Vortex Lattice Method. In addition, Gerhardt et al. (2009) showed how to calculate the added mass of the mainsail and concluded that it has a significant effect on the movement of the vessel.

The main goal of these studies was to model the maneuvers, only Kerdraon et al. (2020) modeled a situation where a foiling ship was sailing downwind in waves typical for the southern ocean. Earlier Angelou and Spyrou (2017) provided a new kind of mathematical model for investigating stability. This work is expanded by Angelou and Spyrou (2019) and Angelou and Spyrou (2021) by using different hydrodynamic and aerodynamic models. In the last paper the attention was to downwind sailing conditions where surf-riding occurs.

Besides the work of system-based DVPP, there is also a class of DVPP that solves the motion equations in a CFD solver. This work started with a 5-DoF coupled VPP and CFD RANSE simulation presented by J. L. Roux (2008a), where RANSE code Fine/Marine is coupled with aerodynamic software of ARAVANTI. In recent work Robin et al. (2023) provided a way where the 6-DoF hydrodynamic and aerodynamics are solved with CFD code, and in this way obtaining steady-state velocity predictions. By doing this combination he obtained more accurate results than conventional VPP. However, the computational time for a racing yacht with foils is still very large and the effect of waves is not included in this work. This work was based on Levin and Larsson (2017) where an empirical sail model is used, this reduces the computational time that is needed. Both mention that waves could be implemented in the calculations which will result in more accurate results.

2.2. Green water, Impact dynamics, CFD calculation of floating bodies

A background literature study was conducted on green water, impact dynamics, and CFD calculations for floating bodies. However, during further stages of the research, it was concluded that these subjects are outside the scope. Therefore, it is not included in the report. The literature study can be found in appendix A.

2.3. Numerical modeling of waves

The first type of linear wave theory was developed by Airy (1845), the equations obtained are valid for fully developed waves, waves that have reached maximum height and length, in deep water. This theory is based on potential flow to describe the motion of the waves. J. L. Roux (2008b) build upon this theory and presents higher-order expressions to calculate the wave profile of different waves. These

equations are modified and simplified to conform the airy wave theory for deep water waves. This is validated using published data based on the JONSWAP field. Based on these equations, he presents a theory for linear waves that propagate into shallow water Y. Roux et al. (2008).

Further enhancement in the modeling of waves is the nonlinear wave theory presented by Stokes (1847), where the potential of the flow is expressed as perturbation series, and using Taylor expansions, a higher-order solution can be obtained. Rahman (1970) provides the fundamentals of the Stokes theory and notes that the second-order Stokes expansion is only valid for wave amplitudes with a max of around 26% of the water depth, otherwise the expansion will not converge. He noted that a breaking wave in shallow water the wave amplitude is almost 40% and therefore the stokes expansion is not a good approximation.

Further more Fenton (1985) provides formulas for fifth-order Stokes waves where the wave steepness is used as an expansion parameter. He provides these formulas for deep and shallow water. Next to this he showed that the provided formulas to describe the fifth-order stokes waves are rather accurate for waves shorter than 10 times the water depth.

2.4. IMOCA 60

The IMOCA 60 featured in this study originated in 1991 with the development of a monohull-type sailing yacht class. This class has an open design, allowing the designers of such boats to have creativity within certain rules. These rules define the main dimensions, the type of sails and appendages that can be used, and the required strength of certain parts (IMOCA Class, n.d.). A general plan of an IMOCA 60 is shown in figure 2.1.
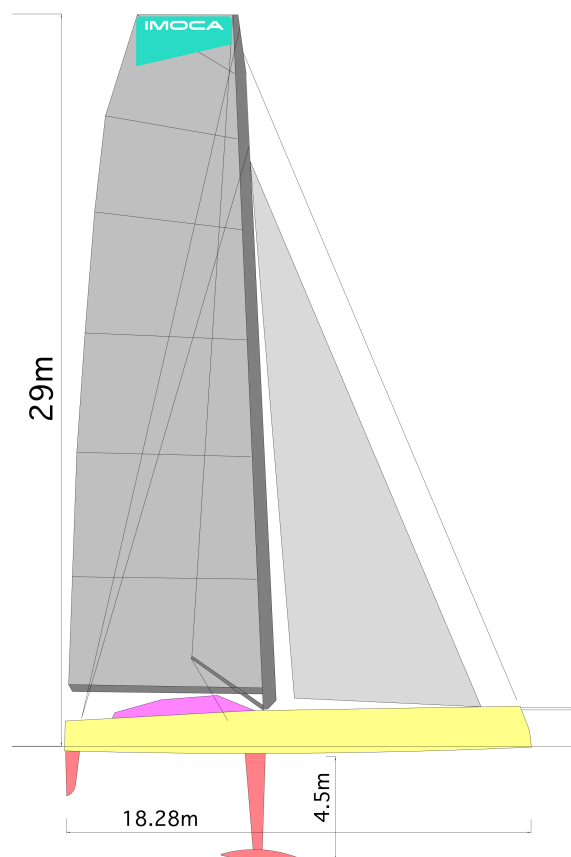
Figure 2.1: General dimensions IMOCA 60 (Wikipedia contributors, 2024)

A schematic of the front profile of an IMOCA 60 is shown in figure 2.2. The appendage rules differ from those of conventional sailing vessels, where there is only a keel and rudder. In this class, a canting keel (item 3 in the figure) is allowed. This keel is able to swivel a maximum of 38 degrees over the x-axis. Additionally, two hydrofoils are permitted on the hull (items 5 and 6 in the figure), which can be rotated around the y-axis (referred to as rake), altering the static angle of attack, and translated in and out of the hull.
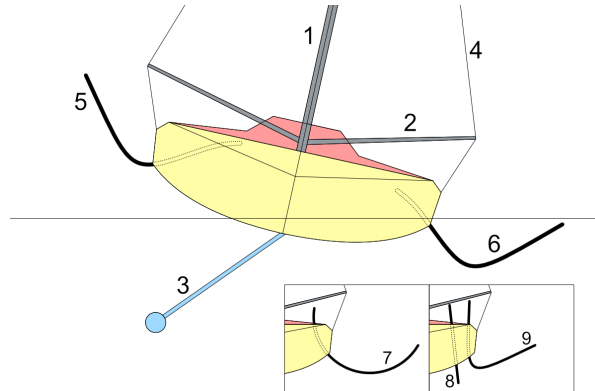
Figure 2.2: Front view IMOCA 60 with canting keel and different hydrofoils shown (Wikipedia contributors, 2024)

The IMOCA 60 sails in various conditions, encountering different wind speeds and angles. The sails carried onboard each have their specific range in wind speed and angle for which they are designed and perform best. This means that there are several different sail combinations, each working in specific conditions. A schematic of the different sails can be seen in figure 2.3.
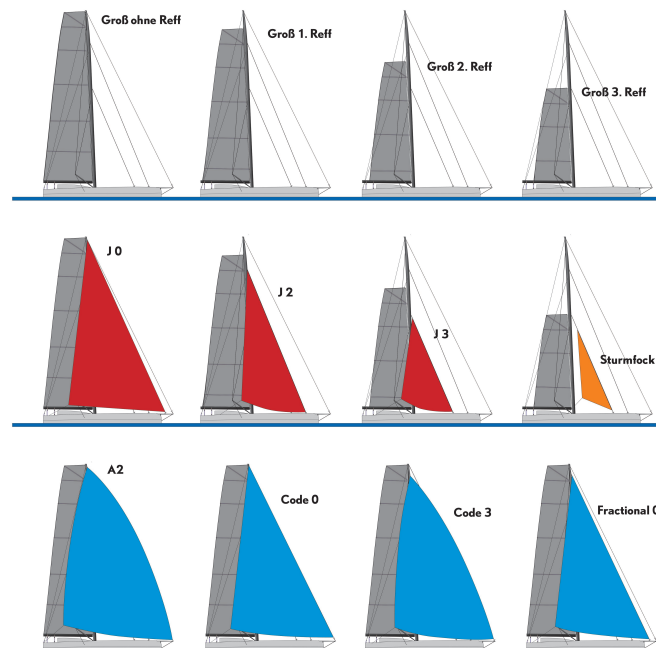
Figure 2.3: Sail configurations IMOCA 60. The top shows different mainsail, the middle shows different jib configurations, and the bottom shows different code-type sails. (Rieker, 2024)

This figure shows that the mainsail can be made smaller by means of a reef, which lowers the entire sail. For the foresail, different options are present. A J-type sail is used when the boat is sailing into the wind, with different numbers representing smaller sails. For off wind conditions, Code type sails are used, designed with more depth and a larger sail area (North Sails, 2022).

<div style="text-align: right; font-size: 3em;">3</div>

Research questions and methodology

Based on the current literature, shown in chapter 2, several research questions surrounding this problem can be formed. The connection between the background, literature, and the problem is shown in paragraph 3.1. From these relationships, the research questions are shown in paragraph 3.2. Lastly, a methodology to solve these research questions is presented in paragraph 3.3.

3.1. Problem statement

The main problem, as stated in the introduction, is that the extra speed due to the hydrofoils fitted to IMOCA 60s leads to significant crashes in waves. During these crashes, the decelerations become so big that humans onboard are thrown from their places, and in the most extreme cases, injury results from this. This phenomenon has not been studied in the current literature, which is the main reason for this study.

Research exists on velocity prediction programs, more specifically dynamic velocity prediction programs, where the yacht's behavior is solved in the time domain instead of the steady state (Day et al., 2002). These programs were originally built to study the maneuvering of traditional yachts. However, several research papers focus on implementing this method on foiling yachts, but there has been no research on foiling monohull yachts sailing in big waves. This leads to the main research question: Can the occurrence of wave-induced crashes in IMOCA 60s be investigated by means of a DVPP.

As for the internals of the DVPP, there is consensus on the main methodology, namely, the system-based approach, in which the forces are individually modeled. As for these individual forces, there has been no consensus on how to model the hydrodynamical and wave forces. For both of these forces there should be a special method to handle the dynamic behavior between foiling and sailing in displacement mode. A huge change in the hull's wetted surface is present between these modes. Some use a non-linear Froude-Krylov method in combination with linear boundary element method damping and added mass, while others use response surfaces built by experimental or RANS tests. Based on this, the question arises: what methodology is most effective for capturing hydrodynamical forces in semi-planing/foiling modes?

Similarly, there are different methods for appendage forces: either using the lift and drag coefficient or the Vortex lattice method. There is a clear method for aerodynamic forces, but various papers recommend that further research focus on unsteady aerodynamics and imperfect sail trim. This limitation could pose issues since this research focuses on yacht behavior in big waves. Therefore, a question arises if perfect sail trim affects the accuracy of the DVPP.

As previously stated, there has been little to no research on a foiling monohull behavior in waves. What parameters are especially important when sailing in big waves? Is it the boat's design or foil, or is it an error in the steering or how the sails are set up? Several papers stated that a DVPP can be used to assess the dynamic stability of the yacht, and Angelou and Spyrou (2017) used a DVPP to investigate stability for a normal sailing vessel. Based on this, the research question arises: how does the foil affect the behavior in waves of an IMOCA 60?

Furthermore, the main problem is the big crashes that happen in waves; based on the previous research

questions, a simulation method is found, and the dependency of the foils is investigated. Based on this information, the question arises whether a DVPP can be used to investigate big crashes in IMOCA 60. And if such crash does occur, what are the contributions to the crash. Since these results lie at the edge of the validity of the DVPP, careful examination of the DVPP and its limitations should be clear.

3.2. Research Questions

Based on the background and literature, a main research question is formed:

Can the occurrence of wave-induced crashes be investigated by numerically simulating an IMOCA 60 in high waves?

Several sub-research questions are formed based on the main research question and the background literature in the previous paragraph. These are listed below:

- What methodology is most effective for capturing hydrodynamical forces in semi-planning/foiling modes?
- What is the most effective way to model the appendage forces, taking into account the change in submerged volume?
- How can the resistance of an IMOCA 60 accurately be represented in a DVPP?
- What are the limitations of a DVPP when simulating an IMOCA 60 sailing in high waves?
- What is the effect of perfect sail trim in simulating an IMOCA 60 in big waves?
- What are the key factors, regarding wind and waves, contributing to behaviour in waves of semi-foiling vessels?
- How do the foil parameters affect the behavior in waves of an IMOCA 60?
- How effectively does the DVPP assess the dynamic stability of an IMOCA 60, particularly in the critical moments leading up to crashing events?
- Can the DVPP be used to investigate the occurrence of crashing events in IMOCA 60?

3.3. Methodology

A methodology is formulated to answer all of the research questions obtained in the previous section. From Robin et al. (2023), it can be concluded that a full 3d time domain simulation of a foiling yacht in CFD can take a long time to obtain results. Therefore, a more time-efficient method is proposed. Namely, a numerical dynamic velocity prediction program. This DVPP will be built to simulate an IMOCA 60 sailing in big waves. This dynamic simulation needs to be validated to ensure the simulation results are closely related to what happens in the real world. Lastly, simulations of an IMOCA 60 in waves can be applied to assess the behavior of such yachts.

However, as stated in previous section using a DVPP to model a yacht sailing in big seas has some limitations regarding the individual force components. Various papers proposed different methods for capturing the hydrostatic and dynamic forces, but no consensus has been reached on the best method. For this research, the same method presented by Kerdraon (2021) in using the boundary element method in combination with the Cummings equation will be used to calculate the hydrodynamical forces. In an ideal scenario, a non-linear method should be used to account for the change in wetted surface. However, as the Cummins equation uses the hydrodynamical coefficients, calculated at a certain wetted surface, to transform from frequency to time domain, a suitable method for addressing this non-linearity has not been found in the literature. This method might not fully capture the hydrodynamical forces but requires less time than the response surfaces method, where URANS or tank test must occur to obtain a response surface for each motion. This method is also more time-efficient when changing hull shapes, as only fast BEM computations need to happen.

As for the aerodynamic forces, the standard approach of using the lift and drag coefficients and the center of effort will be used as proposed by the ORC VPP (Offshore Racing Congress, 2022). This method is used in various papers and gives satisfactory results. As stated, a method to take into account the unsteadiness that happens when sailing in big seas might be required. As for the forces generated by the foils and keel, since the position of the water will change rapidly in the simulation, the

computationally efficient method proposed by Boris Horel and Durand (2019) will be used. This method will be extended with extra corrections to take into account 3d effects and the large shifts in the water level.

The next step is to validate this DVPP. This validation gives confidence in the simulation's results and a further understanding of the DVPP's limitations. This validation should focus mainly on the hydrostatic and dynamic force calculation methods. These two components are important in the case of extreme waves due to the large changes in the wetted surface. Next to this quantitative validation, a qualitative validation will take place. The goal of this validation is to see whether the results of the DVPP are similar to the behavior of a foiling yacht described by Kerdraon (2021).

A more in-depth study of the behavior of an IMOCA 60 will be performed to answer the main research question. Firstly, a parametric study regarding the effect of foil parameters on the behavior of the yacht to crash in waves is performed. This study aims to provide insight into what contributed to a crash and how the occurrence of such crashes can be reduced. This parametric study is done in a systematic way where only one parameter is changed per simulation, in this way only one effect is isolated and conclusions of this parameter can be obtained. Secondly, the ability of the DVPP to simulate a crash will be investigated by pushing the DVPP to its extremes. Using the most extreme environmental conditions in combination with rather high waves. Based on these results, conclusions can be drawn into the occurrence of crashes and what dynamics play a role.

The presented method can be seen as having different stages. Firstly, model the yacht in a dynamic velocity prediction program. Secondly, the DVPP can be validated by using known results. Thirdly, a parametric study of the effect of foil parameters on the behavior of the yacht in waves. And lastly, a the simulation of a crash. The methodology of the different stages is provided below:

- **Stage 1: Dynamic velocity prediction program using:**
  - Hydrostatical forces from the instantaneous wetted surface as proposed by B. Horel et al. (2013)
  - Hydrodynamical forces via BEM calculations and Cummins representation (Kerdraon, 2021)
  - Aerodynamics based on ORC VPP lift and drag coefficients (Offshore Racing Congress, 2022)
  - Appendage loads using finite element representation of the foil (Boris Horel and Durand, 2019)
  - Wave forces according to the decomposition using a velocity potential (Kerdraon, 2021)

- **Stage 3: Validation of DVPP**
  - Validation of hydrostatic and dampening forces
  - Validation of the Froude-Krylov, radiation and diffraction forces
  - Qualitative validation of the yacht foiling behavior in waves

- **Stage 3: Parametric study with regards to behavior in big waves**
  - Systematic approach using different environmental conditions, foil chord length and rake angle
  - Identify which parameters influence the yacht behavior in waves

- **Stage 4: Crash simulation**
  - Investigate if the DVPP can be used to simulate crashes
  - Identifying what forces contribute to the crashing of an IMOCA 60

<div style="text-align: right; font-size: 4em;">4</div>

Dynamic Velocity Prediction Program

The Dynamic Velocity Prediction Program, DVPP, will be used to predict the dynamics of an IMOCA 60. The method proposed by Boris Horel (2019) forms the foundation of this DVPP. Subsequent studies by Boris Horel and Durand (2019), Kerdraon et al. (2020) and Knudsen et al. (2022) have built upon this method. In this study, few alterations to those DVPPs have been made to better model the behavior of a foiling ship in big waves. These alterations are explained in further detail, while the other elements of the DVPP are only briefly explained. Firstly, the used coordinate frame is explained, and after that, each individual force component is highlighted. Lastly, a novelty statement regarding the similarities and differences between the proposed DVPP and the existing literature is shown. The whole DVPP is built in the Simulink software of Matworks (Matworks, n.d.).

4.1. Coordinate frame and wind triangle

The coordinate frame used in this DVPP is consistent with the explanation in Journée (2000) where the x-axis points to the bow of the ship and the z-axis is positive upward. A figure of this coordinate frame can be seen in figure 4.1.
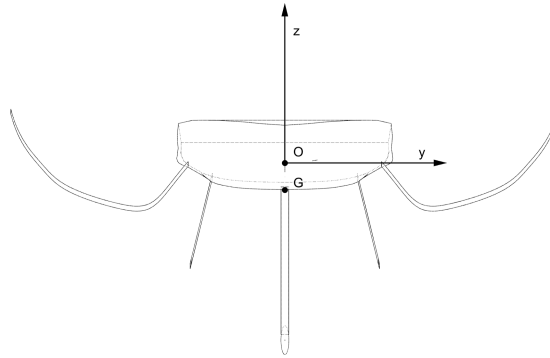
Figure 4.1: Coordinate frame used with O begin origin of the coordinate frame and G the center of gravity of the yacht

This coordinate frame is fixed to the yacht, to transform between this coordinate frame and the earth fixed coordinate frame, a transformation matrix as seen in equation 4.1 is needed, where $R_{b,n}$ is the rotation matrix (Fossen, 2011).

$$R_{b,n} = \begin{bmatrix} 1 & 0 & 0 \\ 0 & \cos\phi & -\sin\phi \\ 0 & \sin\phi & \cos\phi \end{bmatrix} \begin{bmatrix} \cos\theta & 0 & \sin\theta \\ 0 & 1 & 0 \\ -\sin\theta & 0 & \cos\theta \end{bmatrix} \begin{bmatrix} \cos\psi & -\sin\psi & 0 \\ \sin\psi & \cos\psi & 0 \\ 0 & 0 & 1 \end{bmatrix} \tag{4.1}$$

This rotation matrix is used for both the linear velocities and positions; for the angular velocities, a different matrix is used (Fossen, 2011).

$$T_o = \begin{bmatrix} 1 & \sin\phi\sin\theta & \cos\phi\tan\theta \\ 0 & \cos\phi & -\sin\phi \\ 0 & \sin\phi/\cos\theta & \cos\phi/\cos\theta \end{bmatrix} \tag{4.2}$$

Besides the coordinate frame, there is an extra coordinate frame called the wind triangle (Batt, Morison, and Speer, 2000), which relates the wind and boat speed to each other. Starting with the wind that is blowing over the earth, the true wind. This can be split into two parts: the true wind speed, TWS, which represents the wind strength, and the true wind angle, TWA, which indicates the wind angle on the yacht. The movement of the yacht induces wind on itself as it moves through the earth frame. The combination of the true wind and the yacht's movement results in the actual wind experienced by the yacht on its sails, known as the apparent wind. This can be further broken down into the apparent wind angle and speed, AWA and AWS. The apparent wind is the wind the yacht experiences and is the vector sum of both the true wind vector and the boat speed vector. A diagram of this wind triangle can be seen in figure 4.2.
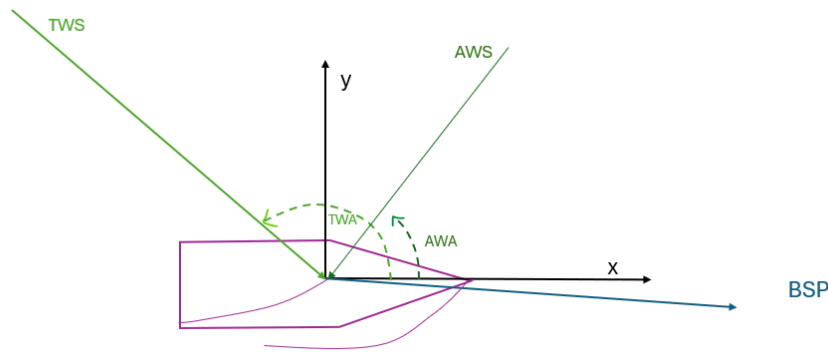
Figure 4.2: Wind triangle of apparent and true wind, TWS and TWA representing the wind in reference with the earth coordinate frame, AWS and AWA representing the wind on the reference frame of the yacht. BSP, the yacht speed.

4.2. Force Modelling

The main physics behind the DVPP is the 6 degrees of freedom rigid body motion equation for a non-inertial coordinate frame. In this equation, m the mass, V the velocity vector, ω the angular velocities, OG the position of the center of gravity, I the inertia tensor, F is the force vector, and M the moment vector.

$$m[\dot{V} + \dot{\omega} \times OG + \omega \times (V + \omega \times OG] = F \tag{4.3}$$
$$I\dot{\omega} + mOG \times \dot{V} + \omega \times I\omega + mOG \times (\omega \times V) = M \tag{4.4}$$

This motion equation is dynamically modeled as obtained by Fjellstad et al. (1994). M_{RB} is the rigid-body inertia matrix, C_{RB} is the Coriolis and centripetal matrix, and F is the external forces. When placing the coordinate frame at the center of gravity, the motion equations will be further simplified as x_g, y_g, and z_g = 0.

$$M_{RB} \cdot \ddot{S} + C_{RB} \cdot \dot{S} = F_{ext} \tag{4.5}$$

$$M_{RB} = \begin{bmatrix} m & 0 & 0 & 0 & mz_g & -my_g \\ 0 & m & 0 & -mz_g & 0 & mx_g \\ 0 & 0 & m & my_g & -mx_g & 0 \\ 0 & -mz_g & my_g & Ixx & -Ixy & -Ixz \\ mz_g & 0 & -mx_g & -Ixy & -Iyy & -Iyz \\ -my_g & mx_g & 0 & -Ixz & -Iyz & Izz \end{bmatrix} \tag{4.6}$$

The DVPP uses a system-based approach, first presented in Boris Horel (2019). This approach splits the forces acting on the ship into individual components. These components are gravity, hydrostatic, resistance, hydrodynamic, aerodynamic, and appendage forces.

$$F_{ext} = F_{grav} + F_{HS} + F_{res} + F_{HD} + F_{Aero} + F_{App} \tag{4.7}$$

4.3. Gravity forces

The gravity forces of an IMOCA 60 consist of several parts: bare hull, canting keel, hydrofoils, rudders, mast, sails, and ballast water. Each of these parts has its own weight and, therefore, gravity force and moment. In the system-based approach, these individual parts independently contribute to the external forces, and therefore, the individual gravity force is calculated in their respective places in the model.

When looking at the bare hull, according to the Rating Certificate, appendix B, an IMOCA 60 consists of 3 water ballast volumes, with their own center of effort. The total weight of the yacht is known from the rating certificate. As is the weight of the keel. Therefore, the weight of the hull can be estimated, and the center of effort can be determined from the rating certificate. However, to simplify the motion equation and the overall DVPP, it is assumed that the center of gravity will not change during the simulation and that the position of the body axis system lies at the center of gravity.

4.4. Hydrostatic forces

Due to the large amplitude of motions that the yacht experiences in calm water and in waves, a nonlinear method to capture the hydrostatic forces is preferred (Kerdraon, 2021). For this nonlinear calculation, two methods were developed, one based on a surface mesh of the yacht or based on sections of the yacht. The surface mesh approach is based on the work of B. Horel et al. (2013), the disadvantage of this method is the rather rough use of the free surface. To overcome this issue, a section method has been developed. Firstly the surface mesh approach is explained and later the section approach.

4.4.1. Surface mesh approach

When a 3-dimensional representation of the yacht is known, the hydrostatic pressure can be obtained by integrating the surface mesh on the total instantaneous immersed surface, equation 4.8. In this equation, ρ_w is the water density, g is the gravitational constant, z_i is the distance from the surface mesh to the water level, and S_W is the immersed surface.

$$F_{hs} = \int \rho_w g z_i dS_W \tag{4.8}$$

In this case, the hull geometry is known, and with the use of RhinoCeros, a surface mesh in an STL file format can be made. In this STL file the surface is discretized in triangular facets. For each triangular facet, f, the normal vector, area, and center are calculated. Based on this information, the immersed surface can be obtained by selecting only the facets whose facet center lies below the water level. With this selection of facets the hydrostatic pressure for each facet is calculated using the following equation, where W_l is the water level and $f_{center,z}$ is the z coordinate of the facet center.

$$P_{HS} = \rho_w \cdot g \cdot (W_l - f_{center,z}) \tag{4.9}$$

Based on this hydrostatic pressure, the hydrostatic force and moment can be calculated using the facet's normal direction and the lever arms of each facet. $A_{f,m}$ is the area of facet m, $N_{f,m}$ the normal of facet m, and $L_{f,m}$ the lever arm of facet m

$$F_{HS} = \sum_{m=1}^{m=n} P_{HS,m} \cdot A_{f,m} \cdot N_{f,m} \tag{4.10}$$

$$M_{HS} = \sum_{m=1}^{m=n} P_{HS,m} \cdot A_{f,m} \cdot N_{f,m} \cdot L_{f,m} \tag{4.11}$$

The sum of all the forces and moments over all the facets that lie under the water line then gives the total hydrostatic force. The selection of facets that lie under the water creates an issue; the force trace becomes non-smooth when the water level changes. This can be limited by making the facets smaller and smaller; however, this increases computational time greatly and does not fully eliminate the problem.

4.4.2. Section approach
To combat the limitation of the surface mesh method, a sectional approach has been developed. In this method, the underwater intersection between the section and the waterline is computed for each section. This point, and the other points of the section lying under the waterline, are used to calculate the hydrostatical forces on each section. The total hydrostatical force is then computed by integrating all the sections. This method is not implemented in the DVPP as it assumes there is only a hull between sections, and there is not a bow of stern. A detailed explanation can be found in appendix C.

4.5. Resistance
Special care should be taken for the resistance calculation, the yacht is sailing between displacement and planing/foiling. For these different situations, different methods for calculating the resistance are preferred. Therefore, an engineering solution has been developed for these different sailing methods. In the case of displacement sailing, and at low speeds, the Delft Systematic Yacht Hull Series, DSYHS, is used. When the speed of the yacht is such that it does not fall into the specified range of the DSYHS, the planing hull resistance calculation presented by Savistky is used. This method differs from the current literature, in which only DSYHS or CFD results are used. But is deemed more accurate because of the limitation of the DSYHS. For both cases the instantaneous yacht characteristics are used, in this way the reducement of resistance due to the hull lifted out of the water is accounted for. In the case that the hull is fully lifted out of the water, the resistance of the hull from either DSYHS or savistky is zero, only air resistance of the hull is calculated.

The resistance of a yacht facing forward velocity can be calculated using the procedure used in the DSYHS (J. A. Keuning, Vermeulen, and De Ridder, 2005). In this formulation, the resistance is split up into frictional, residuary resistance, and viscous resistance. The resistance components of the appendages are not taken into account since, in the system-based approach, these are modeled on their own. Therefore only R_{fh} and R_{rh} remain.

$$F_{DSYHS} = -R_{fh} - R_{rh} - R_{vk} - R_{vr} - R_{rk} \tag{4.12}$$

The frictional resistance component of the hull can be written as equation 4.13 (J. A. Keuning, Vermeulen, and De Ridder, 2005), where U is the yachts speed and C_f the frictional resistance coefficient.

$$R_{fh} = \frac{1}{2}\rho_w U^2 S_w C_f \tag{4.13}$$

The frictional resistance coefficient can be found by using the empirical formula provided in ITTC-57, equation 4.14. In this formula, a form factor k is present. However, for high-speed marine vehicles, such as the IMOCA 60, this factor is assumed to be 0 (Boris Horel and Durand, 2019).

$$C_f = \frac{0.075}{(log_{10}Re - 2)^2} \tag{4.14}$$

The residuary resistance of the bare hull can be approximated using the DSYHS coefficients. Where the coefficients can be found using the work of J A Keuning and Katgert (2008). In this expression, several coefficients are determined from tables for Froude numbers between 0.1 and 0.75.

$$C_{r,DSYHS} = a_0 + (a_1\frac{LCB}{L_{wl}} + a_2C_p + a_3\frac{\nabla_c^{\frac{2}{3}}}{A_w} + a_4\frac{B_{wl}}{Lwl} + a_5\frac{LCB}{LCF} + a_6\frac{B_{wl}}{T_c} + a_7C_m)\frac{\nabla_c^{\frac{1}{3}}}{L_{wl}} \tag{4.15}$$

The total resistance can then be found by adding the individual components of the resistance. In this equation an extra term in the frictional resistance is present, this $\frac{S_w}{S_{w0}}$ is to account for the change in wetted surface when the yacht is in a foiling condition (Boris Horel and Durand, 2019).

$$F_{DSYHS} = \rho\nabla gC_{r,DSYHS} + \frac{S_w}{S_{w0}}C_f\frac{1}{2}\rho V^2 S_w \tag{4.16}$$

As explained, in the case of higher speeds, where the yacht is in planing mode, the planing method of Savitsky (1964) is used. The hydrodynamic drag of a planing surface is given as equation 4.17, where Δ is the displacement of the yacht, λ the wetted keel length, b the wetted beam, β the deadrise angle and τ the trim angle.

$$D = \Delta tan\tau + \frac{\rho U^2 C_f \lambda b^2}{2cos\beta cos\tau} \tag{4.17}$$
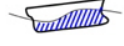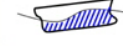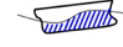
To account for the change from the DSYHS resistance to the resistance calculated by Savistky at higher Froude numbers, a gradual transition region is chosen between Froude numbers 0.6 and 0.75. Above the Froude number of 0.75, the drag, as calculated by Savistky, is used. The formula for the total drag is than:

$$F_{res} = F_{DSYHS} * -\frac{Fn - 0.75}{0.75 - 0.6} + D * \frac{Fn - 0.6}{0.75 - 0.6} \tag{4.18}$$

4.6. Hydrodynamic and wave forces

Hydrodynamical forces are forces due to the presence of waves and are modeled according to the methods of B. Horel et al. (2013), Kerdraon (2021), and Matusiak (2010). Furthermore, the hydrodynamical force is modeled using linear wave theory, where the wave is modeled as a deep water wave potential as proposed in Kerdraon (2021). Since this research focuses on the behavior of an IMOCA 60 in offshore sailing conditions, only the deep water case is considered. This total wave potential can be seen as a superposition of an incident, diffraction, and radiation potential (Journée, 2000). The diffraction and radiation wave potential can be computed from the frequency domain, while the latter is modeled using the Froude-Krylov assumption. The details of these computations is shown in the following subsections.

For numerical simulations, several methods are present to handle hydrodynamic forces. Ranging from linear computations, meaning all the forces are represented as if the boat is still in the water. To fully nonlinear computations, the forces are represented as if the boat is moving in the instantaneous wave profile. The differences of the methods are shown in figure 4.3. It is evident that the linear representation is numerically the easiest and, therefore, computationally preferred. However, in this problem, a more nonlinear approach is necessary since the yacht is sailing in big waves, and the wetted surface changes in significant ways. Therefore a weakly-nonlinear approach is used. In this approach, the Froude-krylov and restoring forces are calculated nonlinearly, that is, on the instantaneous wetted surface. Meanwhile, the other hydrodynamic forces, radiation and diffraction, are calculated in a linear sense by using frequency domain boundary element calculations.

	Linear computation	Weakly−nonli near computation	Weak−scatter computation
Froude−Krylov & restoring force			
Hydrodynamic force			
Numerical implementation	Easy	Easy	Hard
Computational cost	Medium	Medium	Very High

Figure 4.3: Numerical methods for calculating hydrodynamic forces. (Park et al., 2014)

4.6.1. Froude-Krylov forces

As explained, a nonlinear approach is necessary for the hydrostatic and dynamic forces. However, this poses a challenge in using the existing linear airy wave theory, where the pressure is linearized around the mean water level, MWL. In general, the pressure is composed of (Karimirad, 2014).

$$P = \underbrace{\rho g z}_{static-pressure} - \underbrace{\rho \frac{d\phi}{dt}}_{dynamic-pressure} + H.O. \tag{4.19}$$

Where the first part, $\rho g z$, is the hydrostatic pressure, and the second part is the dynamic pressure, also called Froude-Krylov pressure. The dynamic pressure is composed of the time derivative of the velocity potential of the wave (Kerdraon, 2021).

$$\Phi = \zeta_a \frac{g}{\omega} e^{kz} sin(kxcos(\mu) + kysin(\mu) - \omega t) \tag{4.20}$$

$$\frac{d\Phi}{dt} = -\zeta_a g e^{kz} cos(kxcos(\mu) + kysin(\mu) - \omega t) \tag{4.21}$$

In the linear sense, these equations are solved for the mean wetted area. This means that they are modeled as if the boat is still in the water, where z is the distance from the mean water level, MWL.

However, in the nonlinear case, these equations are solved for the instantaneous wetted surface. That is, the yacht moves with the waves, and the submergence is chosen based on the instantaneous wave height. This gives nonlinearity because the wetted surface changes during the simulation.

Moreover, special care should be taken when handling the z-parameter in these equations. To explain, there is a case when the waves are much higher than the freeboard, and the yacht is in its whole above the MWL. In the 'linear' equations, the z-parameter is positive, which gives negative hydrostatic pressure, and the exponential term in the dynamic pressure becomes extremely large due to z being positive in the exponential.

The literature offers two solutions to combat this issue: vertical stretching and Wheeler stretching. For the vertical stretching case, the property that the hydrodynamic pressure at z=0 is the same as the wave elevation is used. Above the MWL the z-term is kept at 0, this means that the hydrodynamic pressure above the MWL will be constant, and mirrors the hydrostatic pressure at the wave surface. This shifts the hydrostatic pressure in the region above the MWL. In the equations, the exponential e^{kz}, z is replaced by $min(z, 0)$ (Karimirad, 2014).

$$\rho\frac{d\phi}{dt}\bigg|_{z>0} = -g\zeta e^{kmin(z,0)}cos(kxcos(\mu) + yxsin(\mu) - \omega t) \tag{4.22}$$

$$= -\rho g\zeta cos(kxcos(\mu) + yxsin(\mu) - \omega t) \tag{4.23}$$

Figure 4.4 shows a schematic of this pressure (Karimirad, 2014). Above the mean wetter level, the dynamic pressure does not vary, hence there will only be a vertical pressure due to hydrostatic loads.
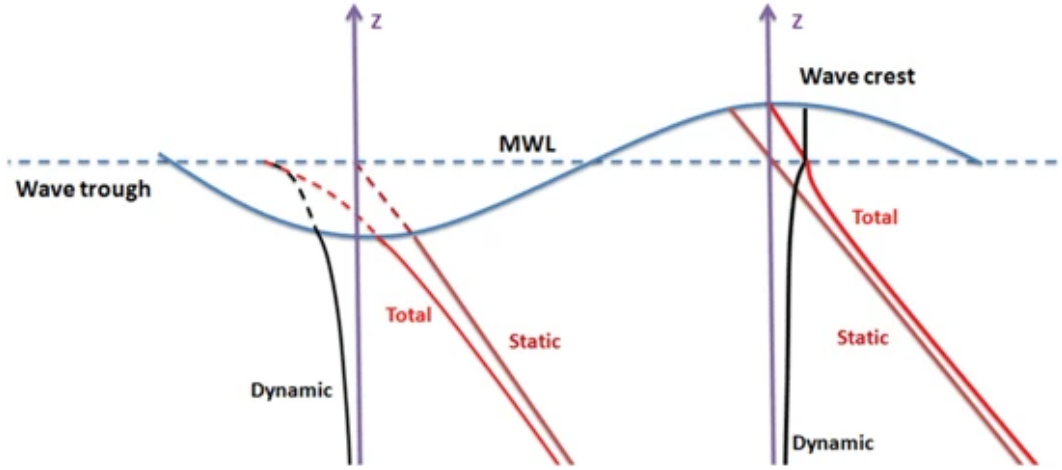
Figure 4.4: Visualisation of the static, dynamic and total pressure. Vertical stretching is applied to the hydrodynamic pressure (Karimirad, 2014)

To combat this issue, Wheeler introduced a different solution. Instead of limiting the dynamic pressure, the whole dynamic pressure is stretched from the mean water level to the actual wave height. A schematic of this can be seen in figure 4.5 (Karimirad, 2014).
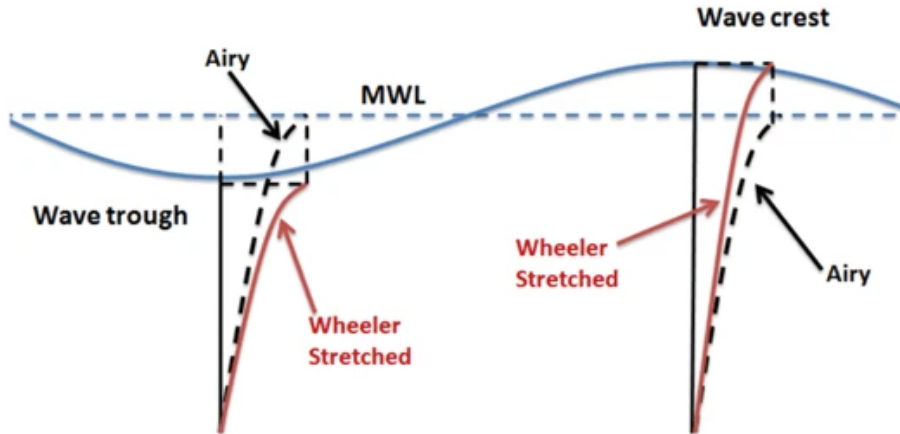
Figure 4.5: Visualisation of Wheeler stretching vs Airy vertical stretching at wave trough and wave crest (Karimirad, 2014)

In the dynamic pressure equation, the z term is replaced by a stretching formula (Matusiak, 2010) where h is the water depth.

$$z = (z - \zeta)\frac{h}{h + \zeta} \tag{4.24}$$

The quotient $\frac{h}{h+\zeta}$ goes to one for deep water, $h >> \zeta$. The total pressure then becomes Matusiak (2010)

$$P = \rho g \zeta e^{k(z-\zeta)} cos(kxcos(\mu) + yxsin(\mu) - \omega t) \tag{4.25}$$

This Wheeler stretching is used in the DVPP, and the force can then be obtained by summing the pressure over all the submerged panels lying under the instantaneous wave height, where n is the number of panels.

$$F_{dym} = \sum_{m=1}^{m=n} P_m A_{f,m} N_{f,m} \tag{4.26}$$

Since the hydrostatic forces are already computed in the hydrostatic force part of the model, this part is excluded from the hydrodynamical forces.

4.6.2. Diffraction Forces

The diffraction loads are computed using frequency domain boundary element method, this means that the forces are calculated around the mean wetted surface and for different wave frequencies. the solution needs to be converted to be linearly modeled in time domain by the DVPP. Kerdraon (2021) poses an equation where the calculated diffraction force for different wave frequencies is converted to a single solution. This formula is given in equation 4.27, in this equation $\mathbf{F_d}$ and ϕ is the modules and phase of the diffraction force and ω_e the encounter frequency.

$$\mathbf{F_{df}} = \zeta_a \mathbf{F_d}(\omega_e) cos(kX - \omega t + \phi_d(\omega_e)) \tag{4.27}$$

The total diffraction force for a system of multiple waves can be found by taking the sum of each wave component. The total wave force is a superposition of the diffraction and Froude-Krylov force components.

4.6.3. Radiation Forces

The radiation forces are similarly computed using the frequency domain. However, instead of using a rather simple transformation to go from frequency to time domain, the Cummins formulation is used (Cummins, 1962). This formulation takes into account movements of the past, which may have an effect on the current position of the yacht. The total radiation force is given as:

$$F_{rad} = -A_\infty(U)\ddot{S} - B_\infty(U)\dot{S} - \int_0^t K(\tau,U)S(t-\tau)d\tau \tag{4.28}$$

Where A_∞ is the added mass matrix at infinite frequency, B_∞ the damping matrix at infinite frequency. These two matrices are the results of the frequency domain calculation which is performed by using the Boundary Element Method program NEMOH (Kurnia and Ducrozet, 2023).

The integral term in the Cummins formulation is the memory effect, which represents the effect of past waves and motions generated by the body on the current state. In this term, K is the impulse response function. Which is calculated with the relationship between time and frequency as explained by Ogilvie (1964).

$$K(\tau,U) = \frac{2}{\pi} \int_0^\infty (B(\omega,U) - B_\infty(U))cos(\omega\tau)d\omega \tag{4.29}$$

However, the calculated A and B matrices are for zero forward speed. Delhommeau and Kobus (1987) establishes a linear formulation based on the slip condition on the hull, which is present when the yacht is sailing at forward speed, to transform these coefficients to cases with forward speed where a boundary layer is present, where U is forward speed, and L_s the selection matrix.

$$A(\omega, U) = A_0(\omega) + U A_u(\omega) \tag{4.30}$$

$$A_u(\omega) = \frac{1}{\omega} B_0(\omega) L_s \tag{4.31}$$

$$B(\omega, U) = B_0(\omega) + U B_u(\omega) \tag{4.32}$$

$$B_u(\omega) = -A_0(\omega) L_s \tag{4.33}$$

$$L_s = \begin{bmatrix} 0 & 0 & 0 & 0 & 0 & 0 \\ 0 & 0 & 0 & 0 & 0 & 1 \\ 0 & 0 & 0 & 0 & -1 & 0 \\ 0 & 0 & 0 & 0 & 0 & 0 \\ 0 & 0 & 0 & 0 & 0 & 0 \\ 0 & 0 & 0 & 0 & 0 & 0 \end{bmatrix} \tag{4.34}$$

Combining these equations with the impulse response function of Ogilvie (1964), a new impulse response function is formulated, which only uses A and B matrices corresponding to zero forward speed.

$$K(\tau, U) = \frac{2}{\pi} \int_0^\infty (B(\omega) - U A_0(\omega) L_s + U A_0(\infty) L_s) cos(\omega \tau) d\omega \tag{4.35}$$

The memory term, the integral from zero to t, presents a numerical difficulty as calculating the integral from t=0 to t at each timestep is a memory-intensive task. Several methods are used to combat this issue. These methods approximate the impulse response, K, in either a state-space approximation or Prony's approximation. This Prony approximation was first implemented in appendix F; however, since the impulse response function is dependent on the forward speed U, the advantage of the approximations, which assumes a constant impulse response, is no longer valid. Therefore, in the DVPP, the whole cummings equation is calculated numerically, as explained by Armesto et al. (2015) where the convolution integral is rewritten by applying the trapezoidal integration method, which can be seen in equation 4.36, where t^* is the cut-off time.

$$\int_0^t K(\tau) \dot{S}(t - \tau) d\tau = \Delta t \left[\frac{K(0)\dot{S}(t) + K(t^*)\dot{S}(t - t^*)}{2} + \sum_{n=0}^{N-1} K(n \Delta t \dot{S}(t - n) \Delta t \right] \tag{4.36}$$

This way of numerically solving the convolution integral has a negative effect on the simulation. Armesto et al. (2015) states that this method can cause a high response near the resonance frequency. This effect needs to be investigated in the validation of the method. To soften the memory burden of the numerical integration, the integral is only solved for the last 10 seconds, that is, the cut-off time, $t^* = 10s$. This approximation can be done since the impulse response converges to zero at this time. In simple terms, this means that events that happened further than 10 seconds ago do not influence the behavior of the ship at the current timestep.

This trancuation of the integral improves the computational time significantly, but the sharp cut-off of the integral can result in a negative dampening at low frequencies, that is a energy feed-in. To combat this issue, a scaling factor has been introduced (Orcaflex, n.d.).

$$c(\tau) = e^{(-\frac{3\tau}{t^*})^2} \tag{4.37}$$

The factor exponentially goes from 1 at τ = 0 to close to zero around $\tau = t^*$. This scales the previous states of the impulse response function to limit the energy feed-in (Orcaflex, n.d.). Furthermore, for both the diffraction and radiation force, a correction for the instantaneous displacement is performed; this is explained later.

4.7. Aerodynamic forces

The aerodynamic forces are calculated using the method presented in Offshore Racing Congress (2022), and for further explanation of the formulas, the documentation should be consulted. As explained in section 2.4, the yachts have several options for which sails to use. Therefore, the DVPP needs to be able to change between these kinds of sails, and thus, several force functions are present that calculate the force for each kind of sail. The reefing of sails, for the mainsail and jib, is taken into account by the Reef parameter, this makes the total area of the sails smaller and reduces the center of effort of each sail. Where the change from an upwind sail, jib, to a downwind sail, flying headsail, is taken into account by a manual switch which will either turn the jib calculation or flying headsail calculation on.

Next to the Reef parameter, a Flat parameter is used, which simulates the reduction of drag and, therefore, also driving force Offshore Racing Congress (2022). In conventional VPP, this parameter, in combination with the Reef parameter, is set such that optimal speed is obtained (Day et al., 2002). However, in the DVPP, these parameters need to be set manually to obtain a stable speed in the simulation.

The dynamical effect of the sails on the dynamics of the yacht is taken into account by using the added mass formulation presented by Gerhardt et al. (2009). This added mass term is especially important for roll motions. Next to the added mass, the wind direction and speed change due to the motions of the yacht; therefore, effective angles are used for the calculation of the lift and drag coefficients; this results in a dampening effect of the sails on the motion of the yacht. A correction factor has been applied to include the effect of flapping sails; this is further explained in a later section.

4.8. Appendage loads

With the appendages, the keel, foils, and rudders are meant. These parts are modeled using the lift and drag coefficient method, and the force is obtained using the following equations for lift and drag. Where the C_l and C_d are dependent on the effective inflow angles and the angle of attack (rake angle) of the foil, α. ρ_w the density of the water, A the area, and U the inflow speed.

$$L = \frac{1}{2}C_l(\alpha)\rho_w AU^2 \tag{4.38}$$

$$D = \frac{1}{2}C_d(\alpha)\rho_w AU^2 \tag{4.39}$$

The method to obtain the total lift and drag force of the appendage is similar as presented by Boris Horel (2019), where the appendage is discretized in several points and a local coordinate frame is used, which lies on the points, in this frame the lift and drag are calculated and transformed back to the coordinate frame of the yacht. However, several corrections are used to include the effects of free surface and 3-dimensional flow. Only for points that lie under the water's surface the lift and drag are calculated. A schematic of this method can be seen in figure 4.6.
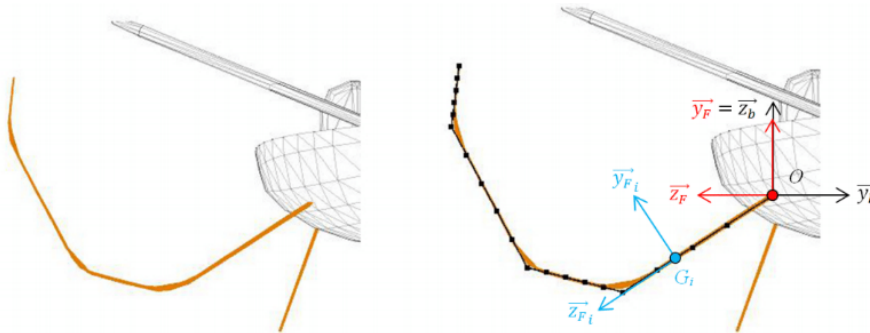
Figure 4.6: Foil geometry and simplified foil geometry with finite elements (Boris Horel, 2019)

However, the method presented is not smooth because only points under the water surface are consid-

ered. Therefore a jump in force is present when the attitude of the yacht changes and a point enters or exits the water. To mitigate this effect, the intersection point between the foil points and the water level is calculated and added to the selected points. This intersection is found by solving the equation of wave height with the equation of the interpolation between the point that lies just above and just below the water level. This equation is solved for Y, which represents the y-coordinate of the intersection.

$$\zeta = \zeta_a \cdot cos(-\omega t + kx + kY) \tag{4.40}$$

$$interpolation = z_p + (z_{p-1} - z_p) \cdot \frac{Y - z_p}{z_{p-1} - z_p} \tag{4.41}$$

Using this method, the force will stay smooth because the intersection point changes when the yacht's attitude changes. Next to this issue, a correction is done due to the foils being close to the free surface Faltinsen (2005) proposes a correction formula, formula 4.42, for the lift coefficient. Where H stands for the distance to the free surface and C is the chord length of the section. In the DVPP this lift reduction is implemented to simulate the effect of the free surface on the yacht.

$$C_l = C_l(\frac{H}{C} = \infty) \cdot [\frac{1 + 16(H/C)^2}{2 + 16(H/C)^2}] \tag{4.42}$$

Besides the correction based on the free surface, an extra correction must occur because the method presented is inherently 2-dimensional, 3D effects are neglected. Fortunately, Stengel (2022) provides empirical formulas to correct 2D lift coefficient to 3D. The formulas presented in his work are incorporated into the DVPP to account for the 3D effects. The formulas used are shown in equations 4.43 to 4.47, where ar is the aspect ratio of the foil and α the angle of attack.

$$ar <= 4 \tag{4.43}$$

$$a = \frac{\frac{dC_l}{d\alpha}}{\sqrt{1 + \frac{\frac{dC_l}{d\alpha}}{(\pi 0.9ar)^2}}} + \frac{\frac{dC_l}{d\alpha}}{\pi 0.9ar} \tag{4.44}$$

$$ar > 4 \tag{4.45}$$

$$a = \frac{\frac{dC_l}{d\alpha}}{1 + \frac{\frac{dC_l}{d\alpha}}{\pi 0.9ar}} \tag{4.46}$$

$$cor_{3d} = \frac{a}{\frac{dC_l}{d\alpha}} \tag{4.47}$$

The added mass of the appendages is taken into account by taking the flat plate assumption as used for the added mass of the sails. Due to the effective angles used for calculating the lift and drag coefficients, an inherent dampening takes place, where the lift coefficient increases or decreases depending on the movement of the yacht. The effect of the waves on the appendages has two effects, firstly the water level at the foil is different and therefore it might lie further under water. Next to this effect, the orbital motions of the wave also affect the inflow speed and angle of attack. The orbital motions of the wave can be calculated using the potential and differentiating it to its corresponding axis, as shown in the following equations.

$$\frac{d\Phi}{dx} = \zeta_a \omega cos(\mu)e^{kz}cos(kxcos(\mu) + kysin(\mu) - \omega t) \tag{4.48}$$

$$\frac{d\Phi}{dy} = \zeta_a \omega sin(\mu)e^{kz}cos(kxcos(\mu) + kysin(\mu) - \omega t) \tag{4.49}$$

$$\frac{d\Phi}{dz} = \zeta_a \omega e^{kz}sin(kxcos(\mu) + kysin(\mu) - \omega t) \tag{4.50}$$

The total inflow for the hydrofoil element then becomes a superposition of the yacht speed, yacht angular velocities, and the wave orbital motions, equation 4.51. This velocity is in the coordinate frame of the yacht, to obtain the velocity on the reference frame of the hydrofoil element a coordinate transformation is performed.

$$V = \vec{V} + \vec{\omega} \times \vec{R} + R_{n,b} \begin{bmatrix} u \\ v \\ w \end{bmatrix}_w \tag{4.51}$$

4.9. Novelty statement

While the DVPP is very similar to those of Kerdraon and Horel, there are some noticeable differences. Firstly, this approach handles the hull geometry similarly to both Kerdraon and Horel. The difference in this method is that the surface mesh is not cut at the waterline; rather, only panels whose center lies under the waterline are selected for the calculation.

Secondly, the resistance is handled differently. While Horel uses only the DSYHS method, this method is deemed inaccurate for Froude numbers higher than 0.75. The DVPP uses a combination of DSYHS and Savitsky to allow for a more accurate resistance calculation at high speeds.

The use of hydrodynamic and wave forces is similar to that of both Kerdraon and Horel. However, Kerdraon uses an additional non-linear correction; however this method is not further explained, so it is unclear what it entails. This leads to the linear approach in this DVPP, which is similar to the method of Horel. Furthermore, a method has been developed to correct for the current displacement in the diffraction and radiation forces; this significantly improves the results, and it is the first time that such a method has been applied and explained. Next to this, it was unclear how the hydrodynamic pressure is implemented in both Kerdraon and Horel, especially if wheeler stretching or a different method is applied. Therefore, this implementation of wheeler stretching is considered new with regard to the state-of-the-art DVPPs for ocean racing yachts.

There is a significant improvement in the aerodynamic forces; as stated, there is a correction for the flapping of sails. This type of correction has never been implemented before and significantly improves the ability to use the ORC method in unsteady environments. Lastly, the appendage forces are modeled similarly to Horel, but an extra correction is performed to account for the 3D effects. Additionally, the waterline is calculated at the location of the appendage. This waterline adds an extra point in the discretization of the foil. This ensures that the force trace remains smooth while the yacht experiences large waves, especially in rough seas where the change in wetted foil is significant.

$$5$$

Validation

In this chapter, three validation cases are presented. One involves a sphere falling in the water, which is meant to check the damping of the model. The second case involves a wigley hull sailing in waves at forward speed, to assess if the hydrodynamic force implementation in combination with the Cummins equation is implemented correctly. Lastly, a grid refinement study will be conducted, where the timestep of the simulation is changed. It's important to note that hydrofoils and resistance forces are not validated, as these are considered 'new' methods. All the simulations are solved with the ODE4 fixed timestep method implemented in Simulink.

5.1. Sphere heave decay

The first validation case consists of the heave decay motion of a sphere of 5 meters. This case is extensively researched with regards to Wave Energy Converters by the International Energy Agency for the sake of verification and validation of numerical modeling (International Energy Agency et al., 2017). In this study, the aim of this validation case is to validate the hydrostatic force model and the handling of the radiation damping that is computed using boundary element methods.

Two heave decay tests are presented, one where the sphere starts at 1.0 meters high and one where the sphere starts at 5.0 meters. Especially the case of 5.0 meters is essential for this study, as in this case, the sphere begins just out of the water and experiences very large changes in displacement and, thus wetted surface. This behavior is also expected in the simulation of a IMOCA 60. The results of the DVPP presented method are compared to those of EC Nantes, ECN. The characteristics of the sphere are shown in table 5.1b.
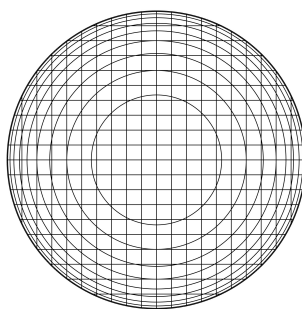
Radius	5.0 m
Weight	$2.618 \cdot 10^5$ kg
CoG z	0.00 m

(a) Linesplan sphere   (b) Characteristics sphere

Figure 5.1: Key data sphere with 5 meters radius

The results of the validation case can be seen in figures 5.2a and 5.2b, where, respectively, the 1.0-meter fall case and the 5.0-meter fall case are shown. Firstly, the results of 1.0 meters, the presented method, has a slight shift in decay; that is, the heave decay has more dampening. At the same time, the size of the excitations is similar. The higher dampening could be explained by the fact that the

integral in the Cummins formulation is approximated by using the BEM results, which only calculate for a finite set of frequencies.

For the 5.0-meter case, the results are in great agreement. The same difference in decay can be seen by the difference in the peak and trough placement, but this effect is way smaller than in the 1m fall. There also is a difference in the decay's peak and trough values. This can be explained by the fact that the hydrostatics are calculated using a finite set of panels. Thus, the water level might be just above the middle of the panel and thus included in the calculation, which could give stiffer results.

(a) Heave decay from 1m fall

(b) heave decay from 5m fall
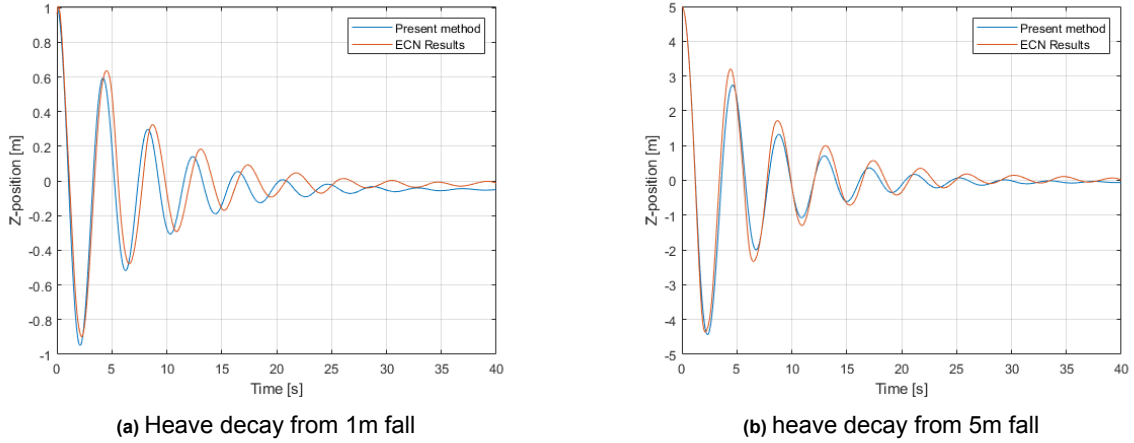
Figure 5.2: Decay sphere radius 5 meters, results are in agreement with the reference data

Overall, the DVPP results agree with those of EC Nantes; therefore, it is concluded that the hydrostatic and radiation forces are validated. The results of the 5.0 meter fall showed excellent agreement with the ECN results.

5.2. Wigley hull RAO in head waves

The second validation case is of a Wigley hull in head waves, previously done by Journee (1992) and Kerdraon (2021). The work focuses on a Wigley III shape, and the linesplan is given in figure 5.3a, and the characteristics are given in table 5.3b.
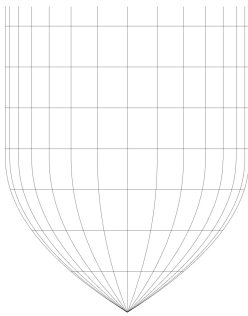
(a) Linesplan Wigley III hull

Length, L_{wl}	3.0	m
Breadth, B	0.3	m
Draft, T	0.1875	m
Displacement, ∇	0.078	m^3
Pitch moment of inertia	43.875	m^4
Center of gravity, KG	0.170	m

(b) Parameters Wigley III hull

Figure 5.3: Key data Wigley III hull

In this test case, the Response Amplifier Operator, RAO, for both heave and pitch is calculated at pre-defined wave periods. The simulations model Airy waves of infinite depth with an amplitude of 0.02 meters and varying wavelengths corresponding to different wave periods. To assess the implementation of the slip-boundary condition in the radiation term, validation is performed at no forward speed and at a case with a forward speed corresponding to a Froude number of 0.20 and 0.40. For each of

these cases, 22 simulations representing 22 different wave periods are carried out, and the RAOs for those wave periods are calculated according to equations 5.1 and 5.2.

$$RAO_{heave}(\omega) = \frac{Z(\omega)}{\zeta(\omega)} \tag{5.1}$$

$$RAO_{pitch}(\omega) = \frac{\theta(\omega) \cdot LWL}{2\pi\zeta} \tag{5.2}$$

The main goal of this validation study is to validate the Froude-Krylov, diffraction, and radiation force modeling. The radiation force modeling is especially important due to its correction for the development of the slip-boundary condition. While the validation case is only at Froude numbers 0.20 and 0.40 and the yacht is sailing at Froude numbers higher than 0.8, this validation with reference data provides insight into whether the results agree in the region between Froude numbers 0.0 and 0.40.

5.2.1. No forward speed
The RAOs of the DVPP without forward speed are shown in figures 5.4a and 5.4b. The DVPP RAOs at the 22 different wave periods are shown in blue, while the orange line is the numerical results of Journee, and the yellow dots are the experimental results of Journee (Journee, 1992) and (Kerdraon, 2021).

(a) RAO heave at Fn=0

(b) RAO pitch at Fn=0
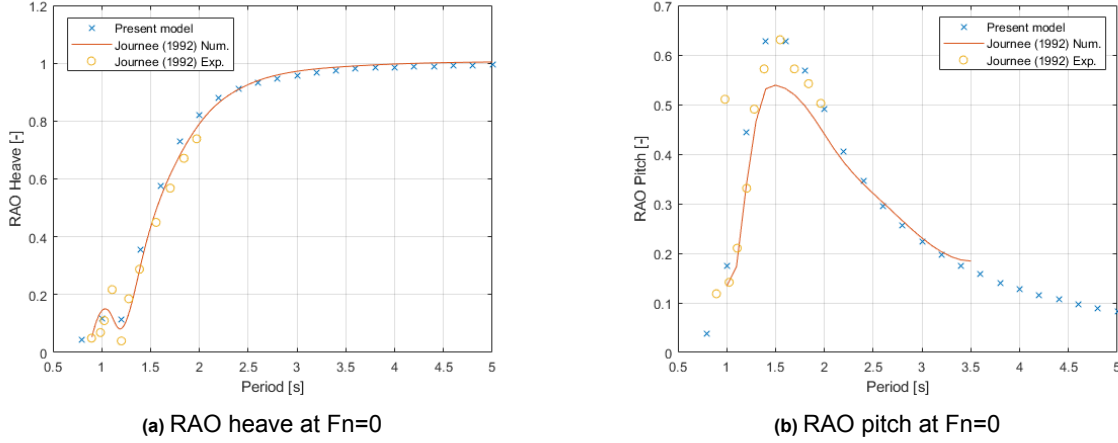
Figure 5.4: RAO of Wigley hull at zero forward speed. Results are in agreement with both reference data.

The results indicate a general agreement between the method presented and Journee's numerical and experimental results. The heave RAOs show excellent agreement with the reference data. However, for the pitch RAOs, figure 5.5b, there is a difference around the peak values, where the DVPP over-estimates the response compared to the numerical values. Nevertheless, the results align with the experimental data, which may be due to the BEM calculations having a different frequency interval and cutoff frequency, which could result in slightly different results. Additionally, Journee uses strip theory instead of the 3D-panel theory used by NEMOH, which could also contribute to this discrepancy.

Around the low-frequency limit, the DVPP's results are in excellent agreement with Journee's results for both the heave and pitch RAOs. These results give confidence in the implementation of the Froude-Krylov, diffraction, and radiation force implementation.

5.2.2. Froude number 0.20
The DVPP results with a forward speed corresponding to a Froude number of 0.20 is shown in figures 5.5a and 5.5b. Where the DVPP results are in blue, Journee's numerical results are in orange, Journee's experimental results are in yellow, and Kerdraon's numerical results are in purple.

(a) RAO heave at Fn=0.2

(b) RAO pitch at Fn=0.2
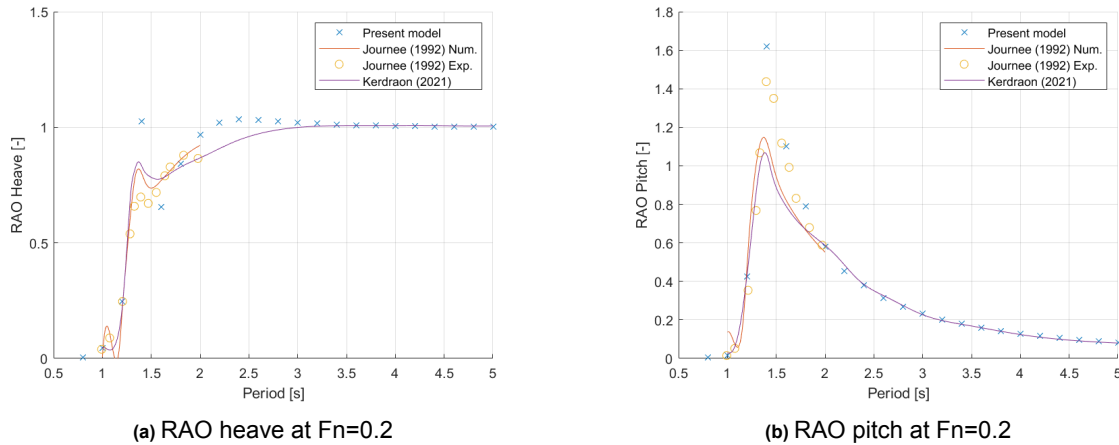
Figure 5.5: RAO of Wigley hull at Froude number 0.20. Results agree with both reference data at larger periods, near the resonance peak overestimation of RAO due to the integration method.

The results generally align with those of Journee and Kerdraon. The RAO curve maintains a consistent shape over the period, particularly for longer waves. The results are especially in good agreement for higher periods. However, when looking at the RAO for heave motion, figure 5.5a, there are discrepancies around the resonance peak. The RAO at the frequency peak is slightly higher than expected, and the RAO for periods just after the peak doesn't match the reference data. In the reference data, the dip is more pronounced, and the return to the low-frequency limit is quicker than the Journee data. Nonetheless, the RAOs predicted by the DVPP are in excellent agreement at higher periods.

In the case of the pitch RAO, 5.5b, there is an overestimation around the resonance peak. However, the DVPP results are similar to Journee's experimental data. Further away from the resonance peak, the pitch RAOs are in excellent agreement with the results of both Journee and Kerdraon.

For both cases, the peak is not accurately represented; it is significantly higher than the results of Journee and Kerdraon. However, the placement of the peak is consistent in the presented method. For the cases that are important for the IMOCA simulation, the low-frequency, high-period waves are dominant. Therefore, it is expected that this overestimation of the peak response will not be an issue.

Near this peak, the dampening forces dominate the ship's response (Journée, 2000). In the DVPP these dampening forces, the radiation forces, are simulated using the cummings representation. Where two integrals are approximated numerically, firstly, the convolution integral and secondly, the impulse response function. The second one approximates the dampening terms between zero and infinite frequency by stopping at a certain frequency. At the same time, the convolution integral is approximated by the trapezium rule and is not calculated for the whole simulation length but is cut off at a certain time. Both these effects limit the dampening and, consequently, lead to an increase in resonance peak in the RAOs (Uchowski and Jackowski, n.d.).

The results generally show great agreement to the numerical and experimental reference data. This gives confidence in the applied method for both the hydrostatic and wave forces for cases with forward speed. The overestimation of peak RAO values should not present an issue in the modeling of an IMOCA 60 in extreme waves, as it is expected that the waves will be near the low-frequency limit. At this region, the presented method of the DVPP accurately estimates a ship's behavior. If such resonance does occur these waves should not be included in the wave spectrum, hereby the output of the DVPP will be more accurate.

5.2.3. Froude number 0.40

The same simulation is performed with a forward speed corresponding to Froude number 0.40. These results are shown in figure 5.6a and 5.6b. The results of the DVPP show excellent agreement to both Journee experimental data and the results of Kerdraon. Like the results with Froude number 0.20, the peak in heave and pitch RAO seems slightly over-estimated, and the corresponding response to the

low-frequency limit looks slightly different. But this effect is way smaller than at Froude number 0.20. At the lower frequency, both heave and pitch RAO results are in excellent agreement with both reference data.

(a) RAO heave at Fn=0.40

(b) RAO pitch at Fn=0.40
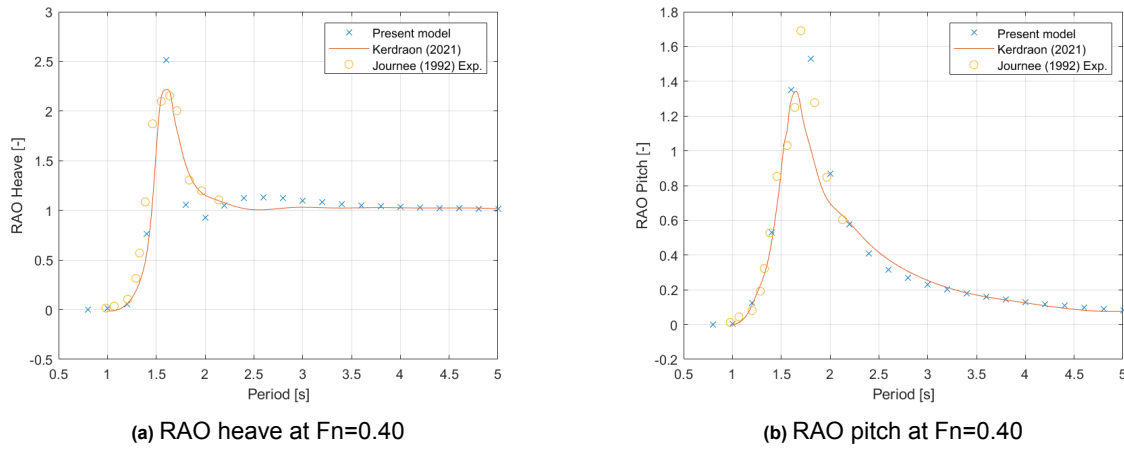
Figure 5.6: RAO of Wigley hull at Froude number 0.40. Results agree with both reference data at larger periods, near the resonance peak overestimation of RAO due to the integration method.

These results at a higher speed give more confidence in the DVPP results at the higher speeds an IMOCA 60 sails at. There still is a slight overestimation at peak values; this effect should be considered when examining the results of subsequent simulations.

5.3. Grid refinement study

A test case has been conducted to assess the effect of the grid, in this case, the time step of the simulation. This is the heave decay of the sphere at 5 meters high, the same as in the first validation case. This study aims to investigate the simulation's dependency on the time step, especially the damping and non-linear hydrostatic force calculation.

This validation case is executed at time intervals of 0.1, 0.01, and 0.001 seconds, and then the results are compared. A smaller time step, in this case 10 times smaller, has two main effects. First, it increases the simulation duration by around 10 times. Second, it requires storing 10 times more data due to the numerical calculation of the convolution integral, which includes previous simulation states stored at each time step. This increase in data storage also leads to higher memory requirements, ultimately impacting simulation time. Therefore, it's important to use the smallest time step possible while still obtaining accurate results.
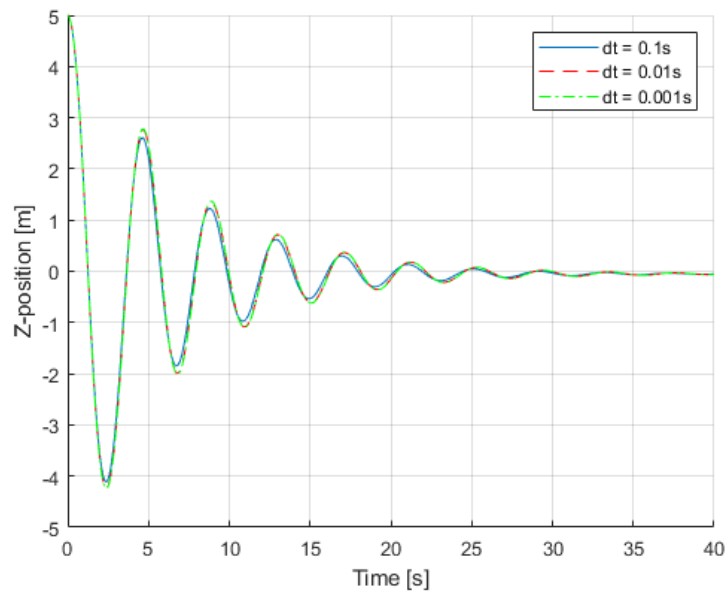
Figure 5.7: Timestep refinement study heave decay sphere. All the timesteps are in agreement with each other, indicating that the results are converged.

The results of the timestep refinement study are presented in figure 5.7. Overall, there is little difference between the different timesteps. The red line representing 0.01 seconds and the green line representing 0.001 seconds show exactly the same results, while the larger timestep of 0.1 seconds does not completely align with these results. Although this difference is extremely minor and only in the initial decay, the overall outcomes are consistent with the smaller time steps. Based on this study, a timestep of 0.01 seconds is recommended for accuracy. If a faster simulation is needed, a timestep of 0.1 seconds can be used, but it will not significantly impact the simulation results.

<div align="right">

6

</div>

Simulation of IMOCA 60 sailing in waves

This chapter shows simulations of an IMOCA 60 sailing in waves, which will be used to qualitatively validate the results with the results of Kerdraon. The goal is to investigate whether the DVPP can be used to simulate an IMOCA 60 in big seas. First, the setup of the DVPP is explained in paragraph 6.1. Based on this setup, the results are shown in section 6.2 and compared with the results of Kerdraon (2021). The simulations are solved with the ODE4 fixed timestep method implemented in Simulink, with a timestep of 0.1 seconds.

6.1. Setup

The DVPP needs several input parameters to obtain a valid solution. These include the yacht's mass and inertia, CoG, hull geometry, hydrodynamic coefficients, sail dimensions, and, lastly, appendage geometry.

To start with the mass properties of the yacht. Since the IMOCA class is highly competitive, very few exact numbers of these properties are known. Luckily, one newer designed yacht has a Rating Certificate, appendix B, a measurement performed by an official party that results in a time rating for ocean races. In this certificate, the mass and center of gravity are given, and the inertia moment is later estimated using BEM Rosetta, (Zabala et al., 2021), an interface for frequency domain analysis. The dimensions of the sails are also given in this certificate; next to the dimensions, the Reef and Flat parameters are also needed. These are found using trial and error and obtaining a steady solution, that is a solution where the boat sails at a steady speed and attitude.

The hydrostatic and Froude-Krylov forces can be calculated using the surface mesh approach, which requires the hull geometry. The hull form was generated in Rhinoceros based on the lines plan in appendix D and then exported as an STL file for the DVPP. It's important to note that the lines plan used for the hull form differs from the one used for the rating certificate, which provided the mass properties. Ideally, the same hull would be used, but since the hull geometry of the yacht with the rating certificate is unknown, a yacht built during a similar time was chosen as a substitute. The foil geometry and assumed values for the foil rake and chord length, 0.60 meters and 3.0 degrees, respectively, are all derived from the same lines plan as the hull.

Finally, the hydrodynamic coefficients are required, as detailed in section 4. A boundary element solution is necessary to compute the A and B matrices, and the diffraction force, which is obtained using NEMOH, as described in Kurnia and Ducrozet (2023). NEMOH requires the hull form and mass properties. The hull form, created in Rhinoceros, is utilized to produce a new STL file of the hull with the appropriate panel spacing, ensuring a minimum of 8 panels per wave; this code can be found in appendix E. The NEMOH results are directly used as inputs for the DVPP.

In addition to the yacht's specifications, it's important to provide the environmental conditions. This includes selecting the wind speed and angle. Since this research focuses on examining the impact of waves on the yacht's downwind sailing performance, the following input for these factors are chosen:

True Wind Speed, TWS = 25 knots, and True Wind Angle, TWA = 145 degrees. These are the same factors Kerdraon uses.

Lastly, it's important to consider the wave conditions for comparison with the results of a previously built Offshore Racing Trimaran DVPP as described in Kerdraon (2021). Similar wave conditions have been chosen: 3 waves, representing low, medium, and high frequencies typical of a wave field in the Southern Ocean (Kerdraon, 2021).

6.2. First Results

The simulation result of an IMOCA 60 in waves is given in figure 6.1. In this figure, the most important outputs of the DVPP are shown; these include the speed, resistance of the hull, z-position of the CoG, the wave elevation at CoG, heel, and trim, and lastly, the AWA. This simulation failed to reach its end time, t=450 seconds, due to an excessive heel angle. This crash in the simulation happened due to the effect the incoming waves have on the apparent wind angle. The incoming wave increases the boat speed, which also has an impact on the apparent wind angle and speed. The AWA is reduced, going from 80 to 40 degrees, and the AWS is increased. Both parameters are taken in to account with the aerodynamic force calculation, where the AWA is used to calculate the lift and drag coefficients. The AWS is used in the total force calculation. Due to the decrease in AWA the Lift coefficient moves to a higher value, this in combination with the increase in AWS results in a higher heeling moment from the sails. This effect is not problematic when it happens gradually; however, if this happens, suddenly, the DVPP does not represent real life. Where optimally trimming the sails cannot occur very suddenly, the sail will start flapping in real life, and there will be less heeling moment and lift force. This effect is apparent when the AWA changes rapidly, as shown in the results.
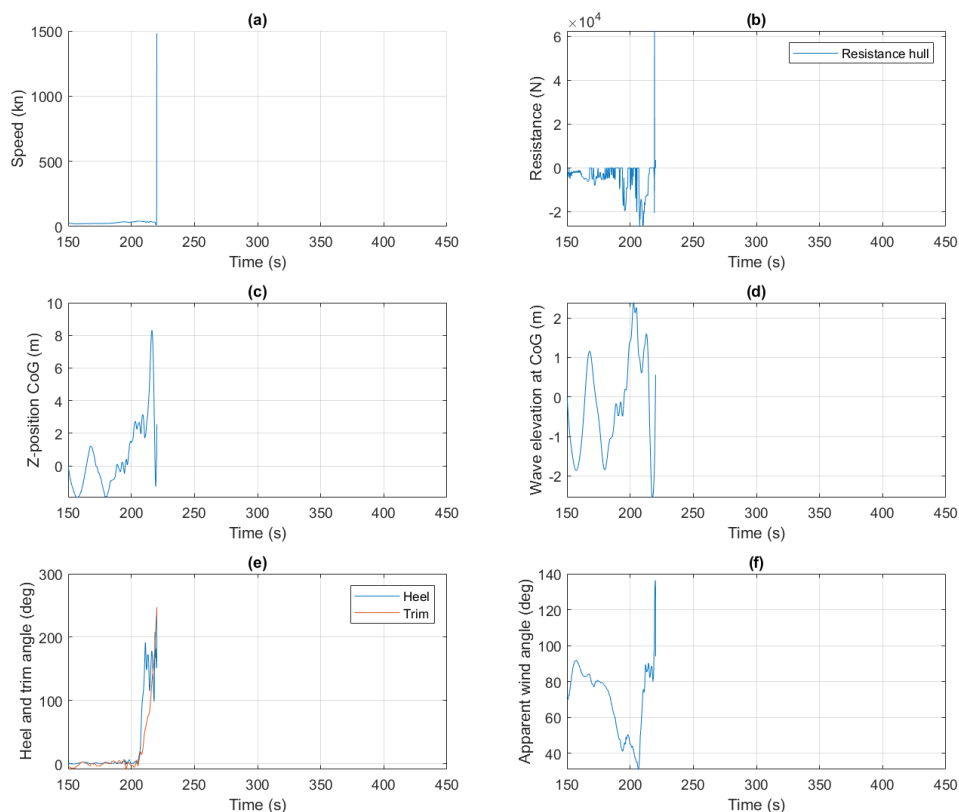
Figure 6.1: Results DVPP southern ocean, wave spectrum as Kerdraon (2021), 25kn TWS, 145 TWA. a) Speed of the yacht, b) Resistance of the hull, c) Z-position of CoG, d) Wave elevation at CoG, e) Heel and Trim angle, and f) Apparent wind angle

6.3. Improvements to the presented DVPP

Two improvements are proposed to account for the deficit in the current presented DVPP that became apparent when simulating big seas: first, on the hydrodynamic forces and second, on the aerodynamic forces, which caused the crash in the previous simulation. These two improvements are presented below.

The decomposition of the hydrodynamical forces into Froude-Krylov, radiation, and diffraction forces poses a linearity issue. Since each is handled with different submerged surfaces, the Froude-Krylov calculation uses the instantaneous wetted surface. In contrast, the radiation and diffraction forces use the BEM results calculated at the still water level. For yachts sailing without foils, where the wetted surface is close to the still water wetted surface, this is not a problem. However, this simplification would lead to mathematical inaccuracies in the case of an IMOCA with a changing wetted surface, which is sometimes not in the water. Namely, when the hull is not in the water, there will not be any hydrodynamical forces, while there are still diffraction and radiation forces on the body, according to the DVPP.

To combat this issue, a rather simple correction is proposed, which uses the identification of the submerged panels in the Froude-Krylov calculation. The diffraction and radiation force is scaled with the ratio between the instantaneous and still water displacement, which is used in the BEM calculation. This formula is shown in equation 6.1

$$S_c = 1 + \frac{\Delta_{inst} - \Delta_{BEM}}{\Delta_{BEM}} \tag{6.1}$$

The initial results of the DVPP indicate a need for an additional correction factor in the aerodynamic forces. The lift and drag coefficients are particularly affected by the flapping effect of sails when the apparent wind angle changes rapidly. Therefore, a correction factor is applied to the lift and drag coefficients on the sails. The ORC method assumes that the sails are always perfectly trimmed. However, this is not the case when the AWA changes rapidly. For example, consider figure 6.2. The left figure illustrates the normal scenario where the yacht is sailing at a steady speed. However, if a wave propels the boat forward, assisted by the lifting foils, the yacht's speed will increase in a short amount of time. This change in boat speed also alters the apparent wind, pushing it further forward and resulting in a smaller apparent wind angle. This change is depicted in the right figure. If this phenomenon occurs rapidly, and the crew is not quick enough to adjust the sails for this change in wind direction, the front of the sail will begin to flap, thus reducing its lift-producing capacity.
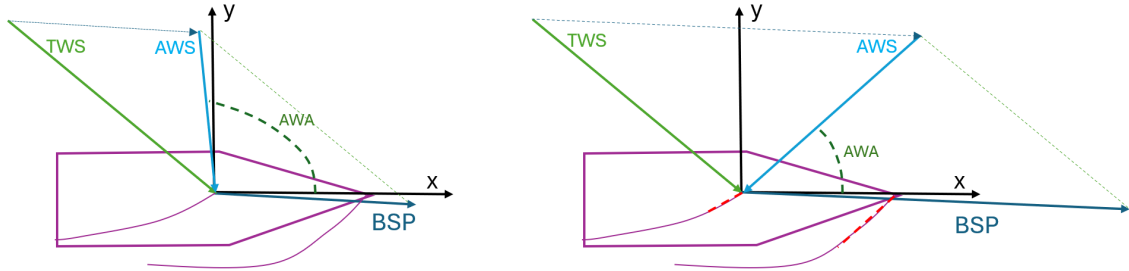
Figure 6.2: Effect extreme waves on the apparent wind angle and speed. The left figure shows normal sailing mode, and the right figure shows the situation when speed increases rapidly. Red stripes indicate area of the sail that is flapping

To account for this a simple solution is proposed, which lowers the lift coefficient by 75% and increases the drag coefficient by 20% when the AWA decreases further than 10 degrees in less than 4 seconds. A second correction takes place if the AWA keeps decreasing to further than 25 degrees. If this happens, the lift coefficient is lowered by 50%, and the drag coefficient is increased by 40%.

6.4. Improved results

The results of the DVPP with this correction to the lift coefficient are shown in figure 6.3. The first important takeaway is that the Z-position follows the wave elevation, which means that the yacht follows the waves. However the resistance plot shows a very jumpy trace, this means that the yacht is not always in contact with the water and thus the hydrofoils are lifting the boat out of the water, while the hull is skimming over the waves.
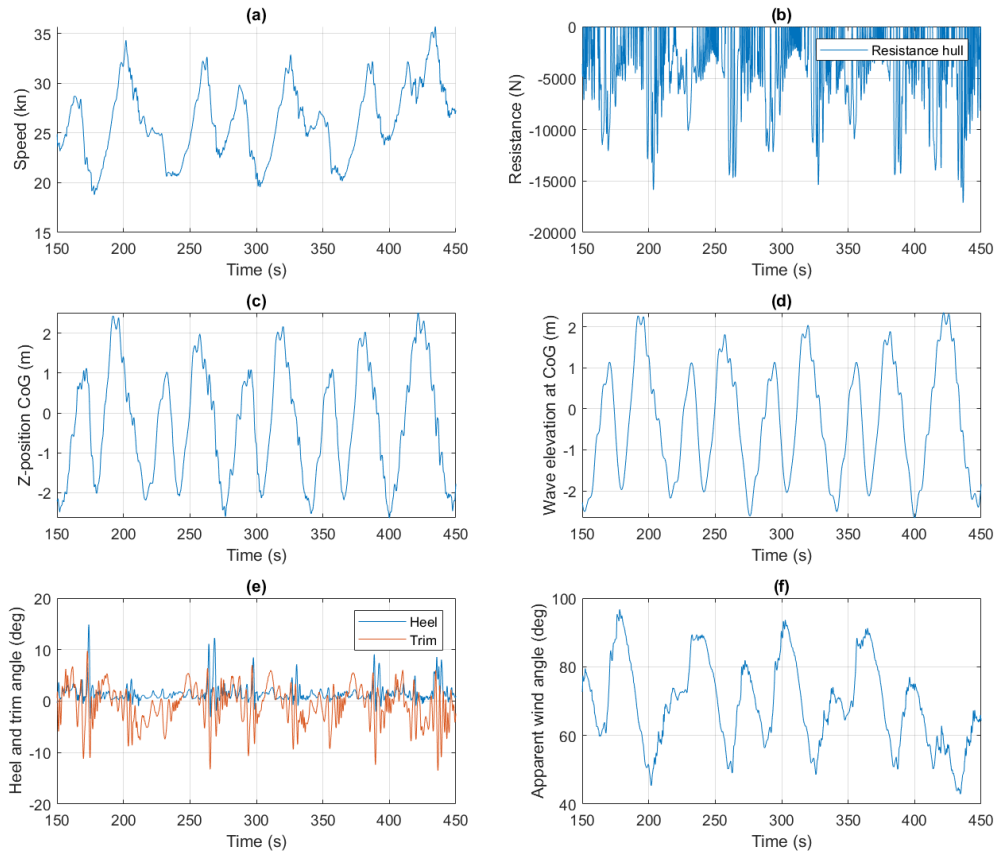
Figure 6.3: Results DVPP southern ocean, 25kn TWS, 145 TWA with sail correction. a) Speed of the yacht, b) Resistance of the hull, c) Z-position of CoG, d) Wave elevation at CoG, e) Heel and Trim angle, and f) Apparent wind angle

In the result of this simulation, the three waves can be distinguished. The high-frequency small wave can easily be seen in the Heel graph; in this plot, a small high-frequency change indicates that the high-frequency wave is rolling the yacht a little bit. The medium frequency component can be seen in the speed graph. In this graph, several dips in speed can be seen around the order of 4 knots. These are probably due to the medium wave slowing the boat down. The low-frequency, high-amplitude wave can be found in the wave elevation; in this plot, a clear sine profile indicates this wave.

Kerdraon (2021) Used this wave profile to simulate a 100ft offshore racing trimaran and explained that the wave's influence on a semi-foiling yacht can be described in a few steps. First, the wave arrives and the yacht accelerates, than the lift increases and the yacht sails at higher speeds, later, the wave overtakes the yacht and the bow pitches up. After that, the yacht loses speed, and lastly, the wave overtakes the yacht, and the yacht is close to the minimal speed. It is not expected that these conclusions can be drawn directly to a monohull-type foiling yacht. But as seen in the plots a similar tendency for the yacht can be seen.

Take the wave at t=400; the wave arrives, and the yacht is displaced upwards and increases in speed.

During this phase, the yacht continues to accelerate; as the wave peak reaches the yacht, the yacht stops accelerating, and the bow starts to pitch up, and the trim angle becomes negative. Than the wave overtakes the yacht and the speed is minimal, this phase cannot be fully seen in the time traces. This is probably due to the bigger effect of small, higher-frequency waves on the results. These waves have more impact on this monohull as their length is shorter than the trimaran Kerdraon used.

Based on this qualitative validation, it is evident that the DVPP can effectively simulate an IMOCA 60 in challenging conditions. These results provide answers to several research questions. Firstly, the methodology of using both nonlinear Froude-Krylov and BEM results effectively captures hydrodynamic forces for both displacement and foiling sailing. Secondly, the aerodynamic forces are especially important, as it is shown that with the current state of the art, the DVPP cannot simulate an IMOCA 60 in big waves. However, with the improvements proposed to take into account the unsteadiness, this is possible. Indicating that the effect of perfect sail trim is significant in these types of DVPPs. Additionally, the results suggest that the DVPP can be used to assess the dynamic stability of an IMOCA 60. This implies that in waves typical of the Southern Ocean, the DVPP can provide a reliable solution.

7

Parametric study DVPP

In this chapter, a parametric study is performed, which looks at the foils' dependency on the yacht's behavior in big waves. With this study, some relationships can be established regarding the effect of waves on the yacht's speed. This parametric study first focuses on the environmental conditions, then on the foil chord length, and mainly on the steady angle of attack of the foil. The setup of these simulations is explained in paragraph 7.1. The results are shown in paragraphs 7.2, 7.3 and 7.4. And a conclusion is shown in paragraph 7.5. All the simulations are solved using the ODE4 fixed timestep method implemented in Simulink, with a timestep of 0.1 s.

7.1. Simulation setup

The first main input for the DVPP is the type of waves that will be used. For this parametric study, it is assumed that the waves will be fully developed, and therefore, each wind speed has its corresponding wave height according to the Bretschneider wave spectrum. This model places a wave height and period relation with the wind speed and fetch. Bretschneider (1964). These formulas can be seen in equations 7.1 and 7.2. Where U is the wind speed and fetch the distance the waves can build.

$$H_s = \frac{U^2}{g} 0.283 \cdot \tanh(0.0125 \cdot \frac{g \cdot fetch^{0.42}}{U^2}) \tag{7.1}$$

$$T_s = \frac{U}{g} 7.54 \cdot \tanh(0.077 \cdot \frac{g \cdot fetch^{0.25}}{U^2}) \tag{7.2}$$

The testing starts with varying the wind and wave conditions, these two are closely related, since wind over long enough fetch creates fully developed waves. To achieve these fully developed waves, the fetch is set to a very high number, fetch $> 10^7$ m. Based on the significant wave height and period, a wave spectrum can be made for these conditions using the following equation (Bretschneider, 1964).

$$S(f) = \frac{5}{16} H_s^2 \frac{f_m^4}{f^5} e^{-\frac{5}{4} \frac{f_m^4}{f^4}} \tag{7.3}$$

In this equation, f_m is the modal frequency, related to Ts with $T_s = 0.95 f_m^{-1}$ (Holthuijsen, 1980). And f is the frequencies for which the spectrum is calculated, thus a range between $[0, \omega]$ rad/s. The selection of the cut-off frequency and the maximum frequency of the spectrum is important for the simulations. Since the radiation and diffraction forces are calculated for a predefined set of frequencies, the spectrum range should be inside this region to limit extrapolations that need to happen.

This spectrum is later discretized into ten waves with their own wave height and frequency based on the defined spectrum. The frequency of these ten waves is linearly spaced in the domain of f. The equation to obtain the wave height, ζ, can be seen in equation 7.4 (Journée, 2000). In this equation, S(f) represents the wave spectrum and df the delta of the ten frequencies. The wave field used in the DVPP is a summation of each wave component obtained using the spectrum.

$$\zeta = \sqrt{2 \cdot S(f) \cdot df} \tag{7.4}$$

Besides the environmental conditions, the foils' effect on the yacht's behavior in waves is important. Therefore, firstly, the foil chord length is changed; this changes the total amount of force the foils can produce, and hence, the effect of the foils is expected to change. The rake (static angle of attack) of the foil is also subject to testing to investigate the effects of the wave's orbital movements on the foil. It is expected that when the input rake is lower, the orbital movement of the waves have a bigger effect on the lift of the foil. A systematic overview of the parametric study can be seen in figure 7.1
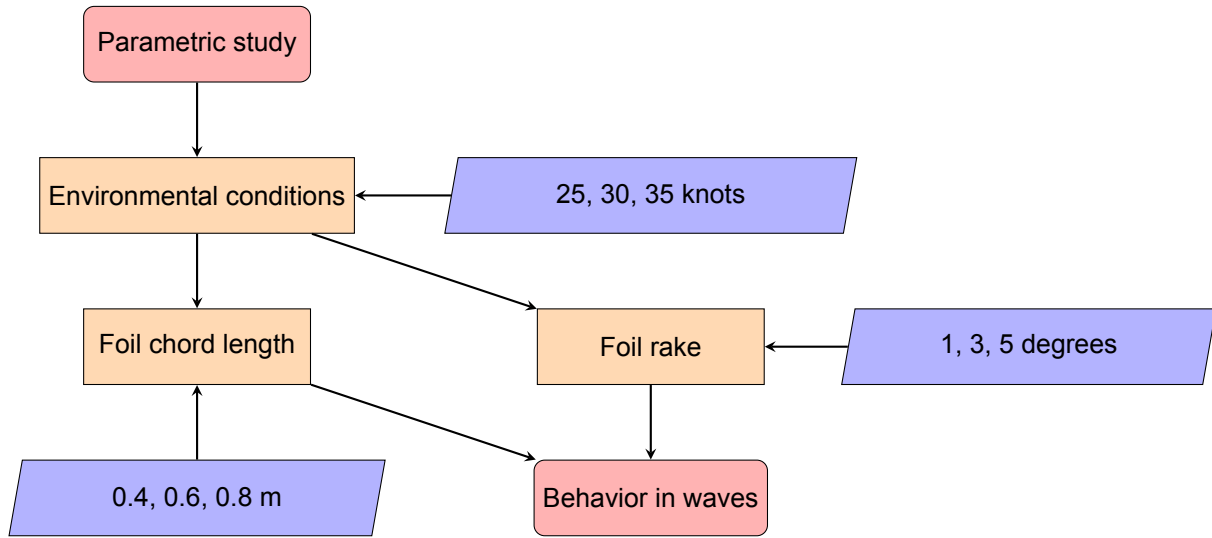
Figure 7.1: Flowchart of the parametric study

For each parameter in the study, corresponding variables are chosen in such a way that it is expected that the behavior in waves is affected. As for the environmental conditions, the range of 25-35 knots is chosen based on drone footage and reports (The Ocean Race, 2024) and (Gorman, 2023). From these videos and reports, it is concluded that the crashes occur in downwind sailing conditions with high waves and wind speeds. The wind angle at which the yacht sails is of particular importance. As the wind angle is too low, TWA under 140 degrees will not result in a crash due to the waves coming too far from the side. But a too-big wind angle TWA over 160 degrees will not be a realistic way of sailing because of how the sails are made (North Sails, 2022). Furthermore, for the later cases, only the 35-knot environmental condition will be used to save computational time, as it is deemed that the outcomes will be similar.

The foil chord length dimensions, 0.4 to 0.8 meters, are chosen because 0.6 meters is a general chord length for a hydrofoil on an IMOCA 60 (Aygor, 2017). The resulting step of 0.2 meters bigger and smaller is chosen as it is deemed to have a good trade-off between big enough steps such that the difference is noticeable in the results and realistic values. The same principle holds for the foil rake, the 3.0 degrees is a base setting for an IMOCA 60 (Aygor, 2017), and the step of 2.0 degrees is chosen to investigate the foil rake's effect.

A base input for the DVPP is needed before starting the study. This consists of Flat and Reef parameters, Keel angle, Foil chord, and rake. The latter two, foil chord and rake, are also subject to change in the test at later stages. However, the middle option is chosen for the first test sequence, respectively 0.6m and 3.0 degrees. For the Flat, Reef, and keel angle parameters, such inputs are selected so that the yacht sails at the highest speed possible while still sailing steadily, that is, with no extreme heel or pitch motion. This is assessed by running the DVPP without waves and looking for a steady-speed solution.

Because a wave spectrum is used to make the wave field, it is evident that the waves the yacht sails in will be different for the environmental cases. However, this also means that for the later cases, where the environmental conditions stay the same, the wave field will differ in each case. This is mainly because the yacht will not be in the same position as it was in the previous test case. If the yacht's speed is very similar to the previous case, the yacht will sail in the same wave conditions, but these cases are limited. Thus, there can be no clear comparison between the two study cases. However, based on the time trace of each case in combination with key data a clear conclusion can be drawn on the effect of each parameter.

The results of each case will be explained in the following sections. In these simulations, the first 150 seconds are taken as setup time; in this time, the equilibrium of the yacht is found, and the waves are gradually turned on. This ensures stable results for the rest of the simulation. Firstly, the cases with changing environmental conditions, meaning TWS, will be presented in section 7.2. For the 35 knot case, the results of changing chord length are shown in section 7.3. Lastly, the results of changing the rake angle are shown in section 7.4.

7.2. Environmental conditions

The first test case is the environmental conditions, with wind increasing from 25 to 35 knots in increments of 5 knots. In this sequence, it is expected that the slowdowns occurring will get bigger due to the higher speeds the yacht will be able to sail and the bigger waves due to a higher wind speed. The results of these tests are shown in figure 7.2, where the red results are 25 knots, black of 30 knots, and blue of 35 knots of wind.
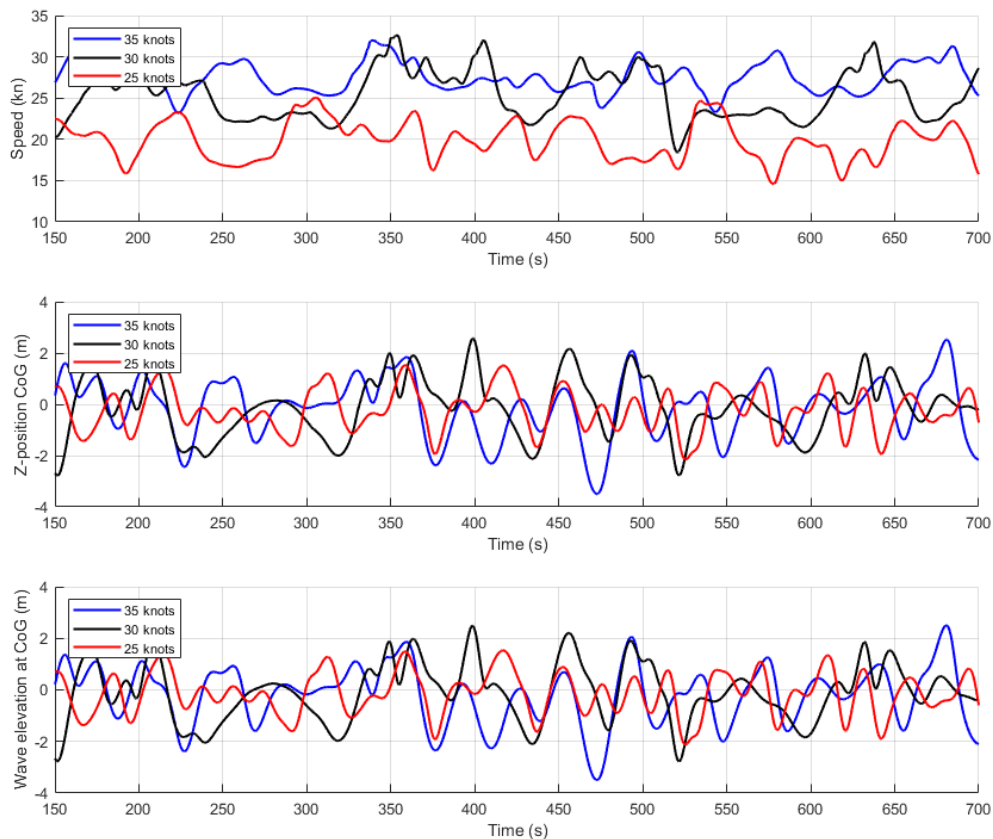
Figure 7.2: Comparison of results of environmental conditions. Red is 25 knots, black is 30 knots, and blue is 35 knots wind. The top figure shows boatspeed, the middle the Z-position of CoG, and the bottom figure is the wave elevation at CoG

It should be noted that for the 35 knot case, the TWA is changed from 150 degrees to 155 degrees. This is done for two reasons; firstly, it represents a case where the yacht is sailing at optimum VMG, making the most speed from the wind. Secondly, a higher TWA is chosen in these higher wind conditions to ensure that the yacht will not capsize.

The speed results in the top figure show that a higher wind speed also corresponds with higher boat speeds. This relationship is rather evident, however, in the 35 knots wind case. the yacht's speed is not considerably higher due to the increased TWA. This increased TWA also leads to an increase in AWA and, therefore, a different lift and drag coefficient of the sails. This lowers the total driving force of the yacht. In the 30-knot case, a slowdown is present, whereas this is not present in the other cases. In the 30 knot results, the yacht's speed, in combination with the speed of the waves, causes this slowdown result. In the 25-knot case, the yacht is not sailing fast enough to be able to crash into the wave in front, and in the 35-knot case, the waves are going too fast in relation to the yacht's speed to produce a significant slowdown. Decreasing the TWA to 150 will lead to higher boat speeds and, therefore, might also lead to a slowdown in this wind range. Additionally, changing the sail parameters to bigger sails could have a similar effect.

Next to the boat speed, it is also clear that the higher environmental conditions produce higher waves, as can be seen by both the wave elevation and the z-position of the yacht's CoG. This is evident as the wave profile is built upon the Bretschneider spectrum, which uses the wind speed to compute a significant wave height, and based on that wave height, an appropriate spectrum is built.

7.3. Foil chord length

For the subsequent studies, the case of 35 knots has been chosen as a base case; in these results, there is no slowdown, but this gives the opportunity to see if changing key parameters actually leads to a slowdown. This approach clarifies the effects of each individual parameter. Two cases that are different from the base case are presented to assess the effect of the chord length on the yacht: a case with a shorter chord length, 0.40 meters instead of 0.60 meters, and a case with a bigger chord length, 0.80 meters

The result of these simulations can be seen in figure 7.3. This figure shows the boat speed, z-position of CoG, and wave elevation. From this figure, it can be concluded that there is little difference between the results of the smaller and normal chord length, the z-position and speed plot are very similar. There are discrepancies where the smaller chord length achieves higher top speeds and lower bottom speeds. Based on the z-position plot, it can be concluded that the yacht is following the wave more, that is due to having less lift; the waves have a bigger influence in pushing the boat when a wave is incoming from behind, and the opposite when the wave has overtaken the yacht.
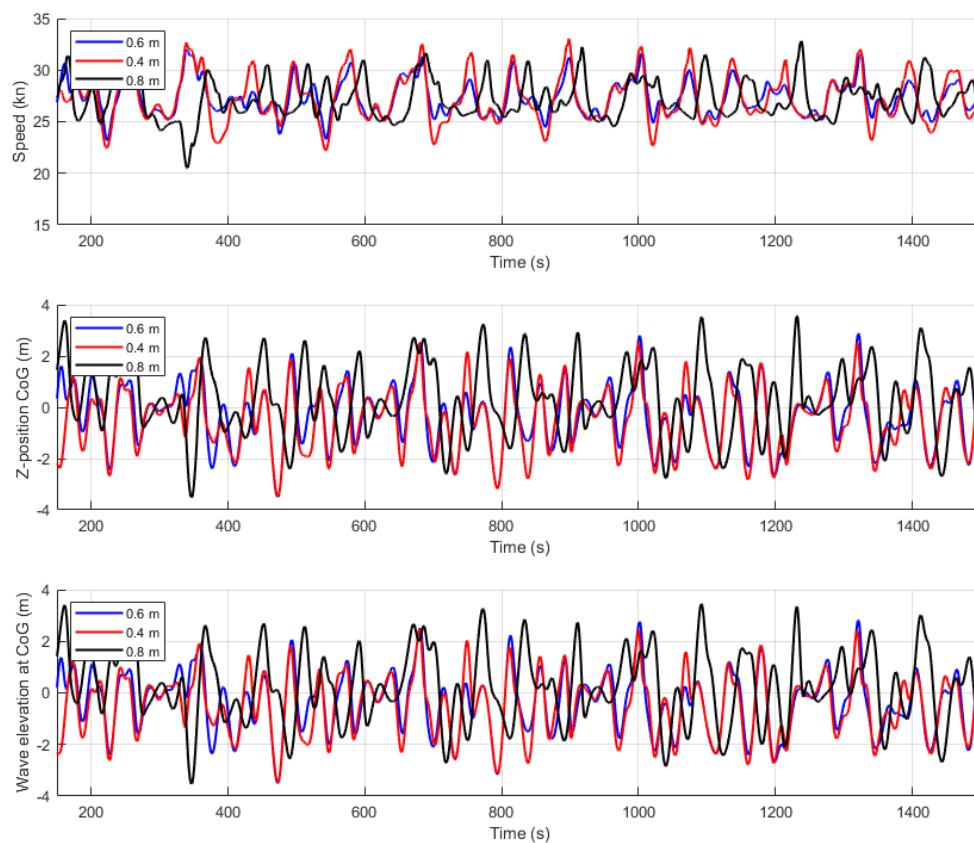
Figure 7.3: Comparison of main output for different chord lengths. Red is 0.40 meters, blue is 0.60 meters, and black is 0.80 meters. The top figure shows boat speed, middle is the Z-position of CoG, and the bottom figure shows the wave elevation at CoG

The longer chord length case, 0.8 meters, provides a different result. The wave elevation shows a different plot, indicating that the yacht is sailing at a different place in the wave field, which makes it difficult to draw conclusions from this data. However, it does not look like the bigger foil gives higher average speeds, which would be expected because the foils can give more lift. This means that the lift drag ratio is not favorable enough to benefit from a larger foil.

These results are also visible in the average speed and standard deviation, table 7.1, where the smaller foil has a bigger standard deviation. And the larger foil has a slightly lower average speed.

	0.60 m	0.40 m	0.80 m
Mean speed (kn)	27.31	27.27	27.18
Std. speed (kn)	1.66	2.26	1.89
Mean heel (deg)	0.68	1.17	0.58

Table 7.1: Mean speed, standard deviation of speed, and mean heel angle for different foil chord length

From this analysis, it can be concluded that the chord length does not significantly change the yacht's behavior in waves. It would suggest that a smaller chord length does increase the effect the waves have on the yacht due to more of the hull being in the water, and therefore, there is a bigger effect of the hydrodynamic forces of the waves.

7.4. Foil rake angle

Lastly, the effect of the foil rake is assessed; the goal of this assessment is to investigate whether the wave orbital movements significantly impact the yacht's behavior when the foil rake is lower. Due to a lower rake, the effect of the orbital movements should be more pronounced as the angle of attack can become more negative, and therefore, it is expected that in the low rake result, the waves have a bigger effect. The results of the three simulations with varying rake angles can be seen in figure 7.4; in this figure, the blue plot is the base case with a 3.0-degree rake. The red plot has a lower rake angle of 1.0 degrees, and the black plot shows a higher rake of 5.0 degrees.
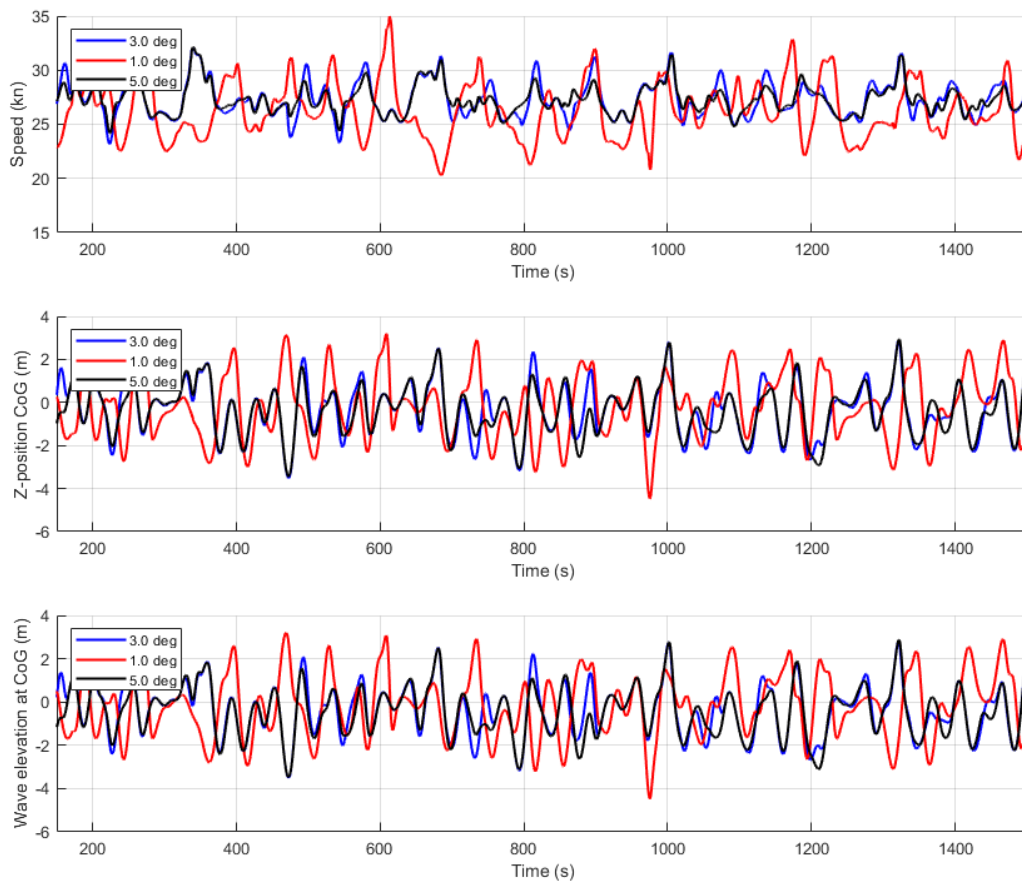
Figure 7.4: Comparison of results of foil rake angle. Red is 1.0 degrees, blue is 3.0 degrees, and black is 5.0 degrees rake angle. The top figure shows boat speed, the middle the Z-position of CoG, and the bottom figure is the wave elevation at CoG

What stands out in this figure is that the results of the higher rake, 5.0 degrees, are similar to those of 3.0 degrees. This can be seen in all the plots: the speed, Z-position, and wave elevation are very similar over time. This is expected from a higher rake angle, which means that the orbital movements will have less effect on the foils. This is because the orbital movement will not be able to cause the foil's angle of attack to become too negative and, therefore, give a loss of lift.

As for the case with a lower rake, these are very different than the other results. The yacht is sailing in a different place in the wave field. From these results, it can be seen that the lower rake case has higher peak and trough speeds. This can be explained by the fact that the lower rake case is affected more by orbital movements. As the yacht comes up a wave, the orbital movements cause an increase in the angle of attack on the hydrofoil, which gives the yacht more lift and, therefore, more speed. This is reversed when the yacht sails in a wave trough.

Further, the key numbers are shown in table 7.2. It can be concluded that the overall speed during the whole simulation is rather similar for all the simulations, except for the lower rake angle case, where the average speed is 1.0 knot slower. This, in combination with the standard deviation also being 1.0 higher, shows that the rake angle does have a significant influence on the behavior of the IMOCA 60 in waves. A higher rake angle will lead to higher average speeds and lower standard deviation.

	3.0 deg	1.0 deg	5.0 deg
Mean speed (kn)	27.31	26.29	27.29
Std. speed (kn)	1.65	2.62	1.32
Mean heel (deg)	0.68	1.55	0.54

Table 7.2: Mean speed, standard deviation of the speed, and mean heel angle for different foil chord length

The analysis shows that a lower rake angle on the yacht leads to greater slowdowns in waves. This is because a smaller rake angle reduces lift, causing the hull to be in the water more often, making it more prone to the hydrodynamic forces of the waves. On the other hand, a higher rake angle allows the yacht to sail at higher speeds by reducing resistance. A yacht with a higher rake angle will recover quicker from a crash, resulting in smaller speed reductions.

7.5. Conclusion

Based on the results of the parametric study, a conclusion can be drawn about the effects of the environmental conditions and the foils' characteristics on the behavior of an IMOCA 60 in high waves. First, the environmental conditions: a clear relationship between higher wind and wave and larger boat speed variation was present. The larger hydrodynamic forces and the larger effect of the orbital movements on the hydrofoils easily explain this. However, there is a limit; if the waves are going too fast, the yacht cannot accelerate to a speed that leads to negative encounter frequencies and, therefore, cannot crash into the wave in front.

As for the chord length, there seems to be a correlation between a larger chord length and less effect of the waves on the yacht. However, there is no effect on the average speed of the yacht. There only seems to be a little difference in the peak and trough speeds.

Lastly, the rake angle. It is concluded that a lower rake angle has a relatively big effect on the behavior of the yacht in waves. This is mainly due to the orbital movements of the waves, which have a bigger effect. This is due to being in a different part of the lift vs. angle of attack curve. When the orbital movement lowers the angle of attack, the angle can become negative, leading to negative lift.

8

Identification and simulation of a crashing event

This chapter shows how the DVPP will be used to investigate the crashing tendency of an IMOCA 60 sailing in waves. First, the identification of a crashing event will be explained in paragraph 8.1, what a crash means, and how it is defined in this report. Secondly, the simulation method is explained in paragraph 8.2. Lastly, the results are presented in paragraph 8.3. As for the previous situations the equations are numerically solved using the ODE4 fixed timestep method.

8.1. Identification

To determine whether a crashing event occurs, a clear definition is needed to distinguish between a slowdown and an actual crash effectively. For this study, a crash is defined as:

A deceleration higher than 0.45 G

This criterion is based on the study of Uchowski and Jackowski (n.d.) that cites that this threshold is where seatbelts lock in cars. Therefore, it is assumed that this deceleration results in a person being disconnected from their place, and injury can occur.

However, this criterion alone may lead to false positives, where the yacht's speed decreases significantly due to factors unrelated to wave encounters. To address this, an additional condition is introduced: the crash must be directly caused by the interaction with a wave. In addition to this definition, the results are visually inspected.

8.2. Simulation method

The aim of the build DVPP is to use it to investigate if it can predict the occurrence of crashes in IMOCA 60, which sails around the world. This phenomenon came to light during the Ocean Race, where IMOCA 60 sailboats, crewed by 4 persons, sail around the world. The route of this race is shown in figure 8.1. Particularly during the leg which goes from Cape Town to Itajai, this crashing has come to light. During this leg onboard the IMOCA 60 Malizia, a crew member was thrown off their bed during a slowdown in a wave, which resulted in serious head injury (The Ocean Race, 2024).

Figure 8.1: Ocean race route 2022-2023, important leg for this study is from Cape Town to Itajai as the most wind and waves are present there (Abratis, 2021)

The largest waves and wind conditions are found in the Pacific Ocean, close to Cape Horn. The main reason for this is that the prevailing winds are strong westerlies, combining this with the fact that there is little land in this region, this means that the waves generated by the wind can build over long distances. (NOAA, 2024).

A closer look at the route of this leg and the general wind at this leg is shown in figure 8.2, Where the historical wind data of this period, obtained from the ECMWF ERA5 dataset (ECMWF, 2024), is combined with the steady state speeds of the yacht. This ERA5 data set is a reanalysis dataset, which means that the state-of-the-art forecast model is combined with observation data to generate a new data set that represents the earth's atmosphere over time (Jeppesen, 2023). By selecting the period of the leg from Cape Town to Itajai, the weather conditions are taken as they were when it was last sailed.

By using this analysis data in combination with the steady state speed, an optimal route can be calculated, that is, the route that takes the yacht the least amount of time to complete. This is calculated by discretizing the area between the start and end locations in a grid. From the starting point it is calculated how long it takes to get to the surrounding grid points. This calculation is repeated for each surrounding grid point to its surrounding grid points, and the route that takes the shortest time from start to finish is deemed the most optimal (Wheeler and Henson, 2023).

This calculation is done by using the commercial software Expedition Marine, which is the industry standard for calculating optimal routes in sailboat racing (White, n.d.). The resulting optimum route is shown in figure 8.2a, where the black line is the optimal route and the colors indicate the wind speed, with blue being 4 knots and red being 40 knots. Besides this figure, table 8.2b, a table which represents the wind speed and the percentage of time sailed at that wind speed in shown.

TWS	% of time
40	4%
36	9%
32	16%
28	15%
24	17%
20	15%
16	15%
12	8%
8	1%
4	0%

(b)

(a)
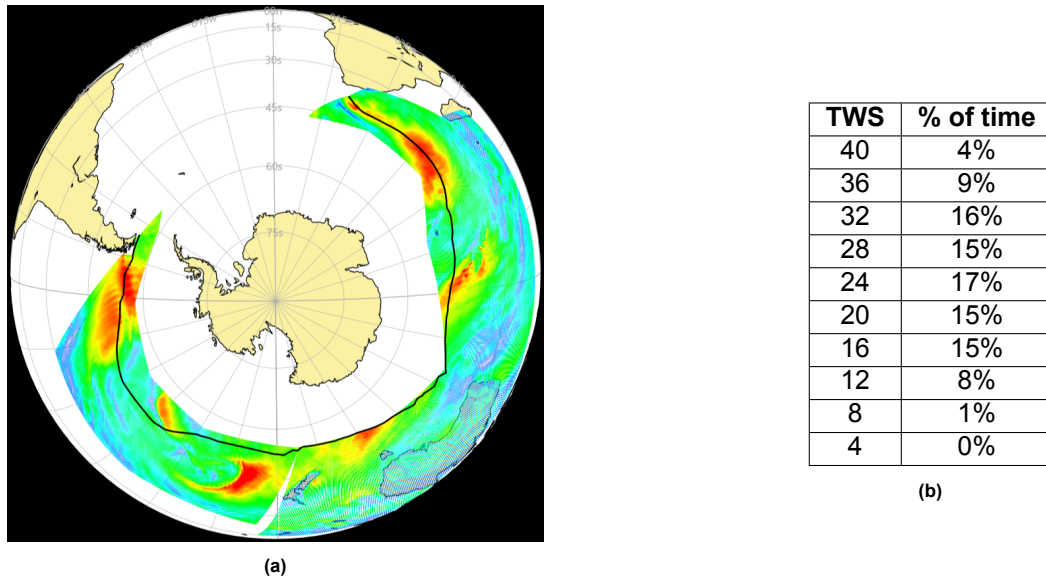
Figure 8.2: Optimal route IMOCA 60 Southern Ocean, colored with wind speed and probability of wind speed

The resulting black line, showing the optimal route, goes closely along the south pole, but not closer than around 55 degrees longitudes. This is due to imposed boundaries by the race committee, which keeps the boat out of ice fields (Rusch, 2023). Furthermore, from this line and the colors, which show the wind on that location at the time the yacht is there, it can be concluded that the yacht will sail multiple times in winds around 40 knots. This accounts for only 4% of the time spent in this leg, as shown in table 8.2b, indicating that this is the upper limit the boat will sail. Based on this analysis, a wind condition of 40 knots was chosen, in combination with a True Wind Angle of 155 degrees.

With the wind speed of 40 knots, a corresponding Bretschneider spectrum is discretized into 10 wave components, and a superposition of these is used as the wave field the yacht is sailing in as explained in section 7.1. Besides these environmental conditions, the foil parameters need to be chosen. Based on the parametric study, the base case of a chord length of 0.60 meters and 3.0 degrees is selected, which is deemed the 'normal' condition.

Lastly, the sail parameters are chosen. Based on the parametric study it is concluded that the yacht should be sailing at the limit, that is maximum power in the sails. This means that the sail parameters are set to produce extremely high boat speeds, but it also leads to potential instability. The instability could result in the yacht crashing into a wave, which is the goal, or capsizing due to the increased heeling force of the sails.

It is assumed that if the simulation is long enough, there will be an extreme event in the wave case. This means that the different wave components will align, and a 'monster' wave will occur, potentially causing the IMOCA to crash into the wave. To determine if such an event will happen, the chosen simulation time is 4000 seconds, which corresponds to 1 hour and 10 minutes.

The main hypothesis of this study is that a high wave approaching from behind will accelerate the boat to extreme speeds due to the hydrofoils lifting the yacht out of the water. This increase in speed will cause the yacht to sail towards the wave in front of it. If this oncoming wave is high enough and the yacht is on its foils, the yacht will move into the wave instead of following the next wave. This is because the hydrostatic and Froude-Krylov effects are not present when there is no hull in the water, resulting in little response to the incoming wave.

8.3. Simulation results

The simulation results in 40 knots of wind and with a TWA of 155 degrees is shown in figure 8.3. The top plot shows the boat speed, while the bottom plot shows the g-force experienced at the yacht's center of gravity. This G-force is the vector norm of all three components of the acceleration of the yacht.

Based on the results, it can be seen that multiple times the G-force goes higher than the specified threshold of 0.45 G. The reductions in speed corresponding to these high G-forces can clearly be seen in the speed plot, where the yacht is decelerated from over 40 knots to around 25 knots.
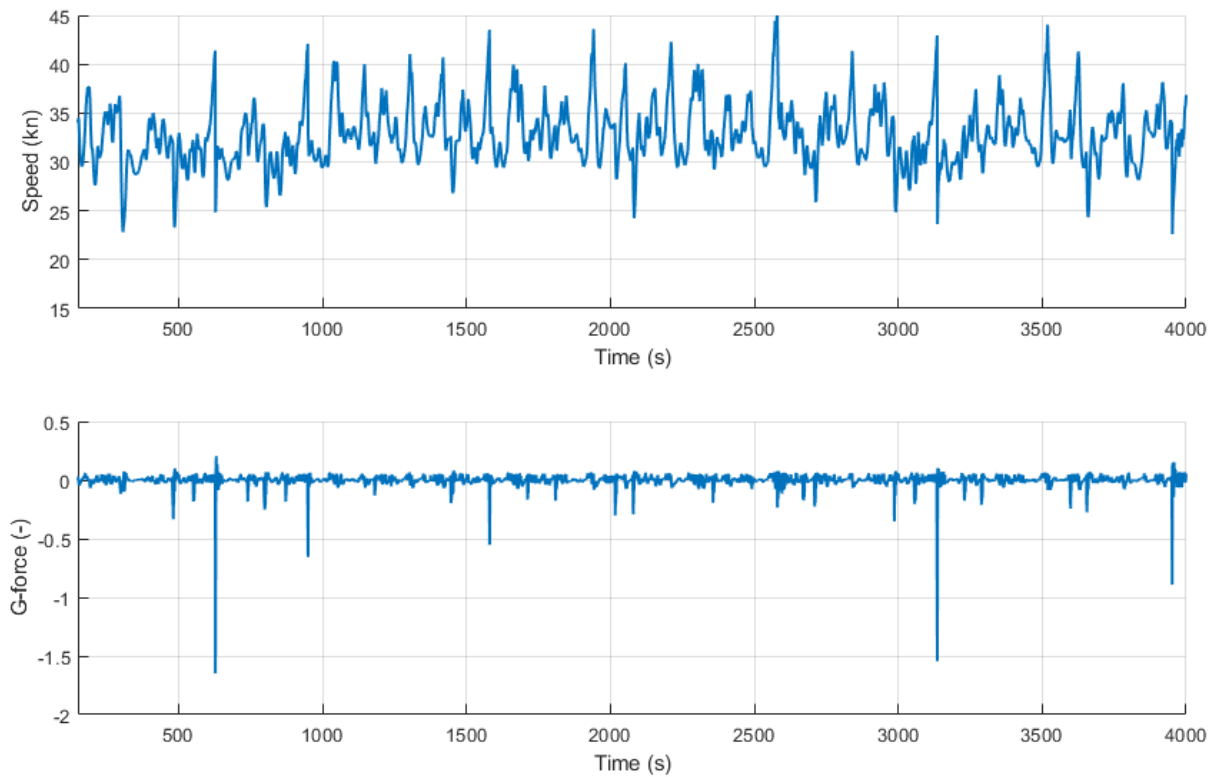
Figure 8.3: DVPP results with 40kn wind, 155 TWA, 1.0 reef 1.0 flat. The top plot shows the yacht's speed, and the plot below the G-force.

The crash at t = 3135 seconds is looked at with more detail, in figure 8.4, which shows the speed, resistance, z-position at CoG, Heel and trim angle, angle of attack of the foils, G-force and the drag coefficient are shown for a period before and after the crash.

This figure shows the deceleration at 3135 seconds in the speed plot, where the speed goes from 42 knots to 25 knots in around a second. Before the crash the yacht is sailing in foiling mode, which can be seen by the hull's resistance being zero. During this time, the yacht's speed increases from around 35 to 42 knots. This acceleration halts near the bottom of the wave, wherein the resistance of both hull and foil increases to over 10000 N. This leads to a big deceleration where the G-force increases to over 1.5 G.

The foil's increased resistance is due to the larger angle of attack, which increases the drag coefficient. This increase in resistance is enlarged by the fact that the foil is becoming more in the water, and therefore, there is more wetted surface of the foil. This gives the first deceleration, and then an extra deceleration happens when the hull comes in contact with the water, and the hull's resistance increases significantly.

The increase in the wetted surface of the foil can be explained by the yacht's speed in the z-direction, coming from moving off the wave, and the yacht not being submerged but in a fully foiling condition. The yacht's response, when it enters the through of the wave, is slightly delayed, as there are no hydrostatic and hydrodynamic forces. This means that only the foils provide force in the z-direction and are responsible for the yacht following the waves. Since this response is not big enough, the foils will get submerged further till the yacht is in the water and the hydrostatic and dynamic forces take over.
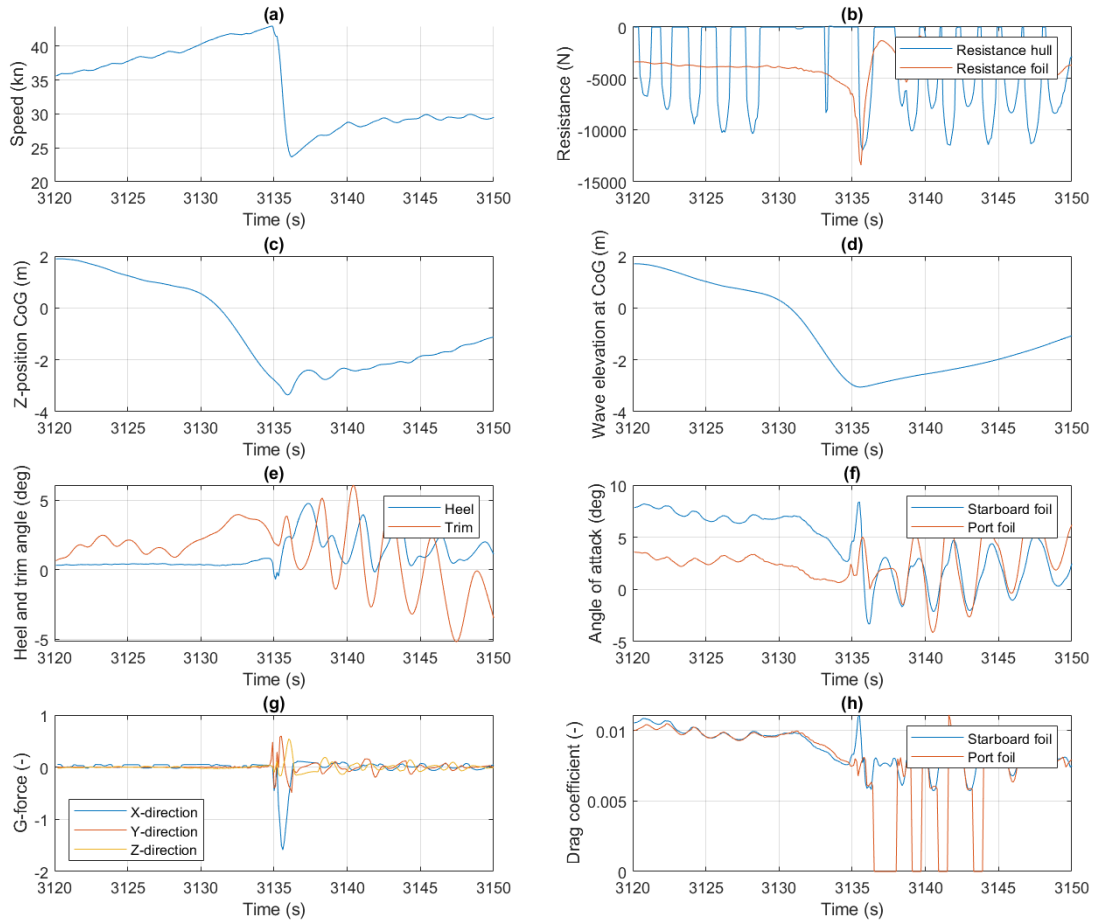
Figure 8.4: Simulation results zoomed in at t=3135 seconds. a) Speed of the yacht, b) Resistance of the hull, c) Z-position of CoG, d) Wave elevation at CoG, e) Heel and Trim angle, f) Apparent wind angle, g) G-force, and h) drag coefficient

It should be noted that the results after the crash should be taken with a grain of salt, since the non-linear corrections, for both the foil forces as the hydrodynamical forces, do not represent completely accurately the behavior of the yacht. For the foil forces, the ventilation is not taken into account, which is expected when the foil submergence changes quickly. The same hold true for the hydrodynamical forces, when the submerged volume changes the nonlinear correction changes. However, this correction factor is not physics-based and does not accurately represent the force. Over time, these limitations dampen out, and the DVPP does provide accurate results.

8.4. Conclusion

Based on this longer simulation, the DVPP with the newly introduced parts can be used to access the crashing behavior of IMOCA 60s. These newly proposed parts, resistance with Savitksy, handling of the foil geometry and downwash effects, non-linear corrections on the diffraction and radiation forces, and the correction on the aerodynamic forces, allow the DVPP to be able to simulate the extreme environmental case. Based on the simulation results, several peaks with G-forces higher than 0.45 G were found, and based on analysis of one deceleration case, two crucial factors were identified. First, deceleration is due to changes in the angle of attack and submergence of the foil, and second, deceleration is due to the hull getting in contact with the water.

Based on the parameter analysis, it is concluded that to limit the effect of waves on the yacht, it is

advised that the chord length should be long and the rake angle big. A second simulation is done with a chord length of 0.80 meters and a rake angle of 5.0 degrees. The results are presented in figure 8.5. It is clear from these results that the G-force in slowdowns is considerably lower, a maximum of 0.6 instead of 1.7 G. This can also be seen in the standard deviation of the speed, which is 2.74 knots for the optimized results and 3.04 knots in the previous results. This indicates that the waves have less effect on the behavior of the yacht.
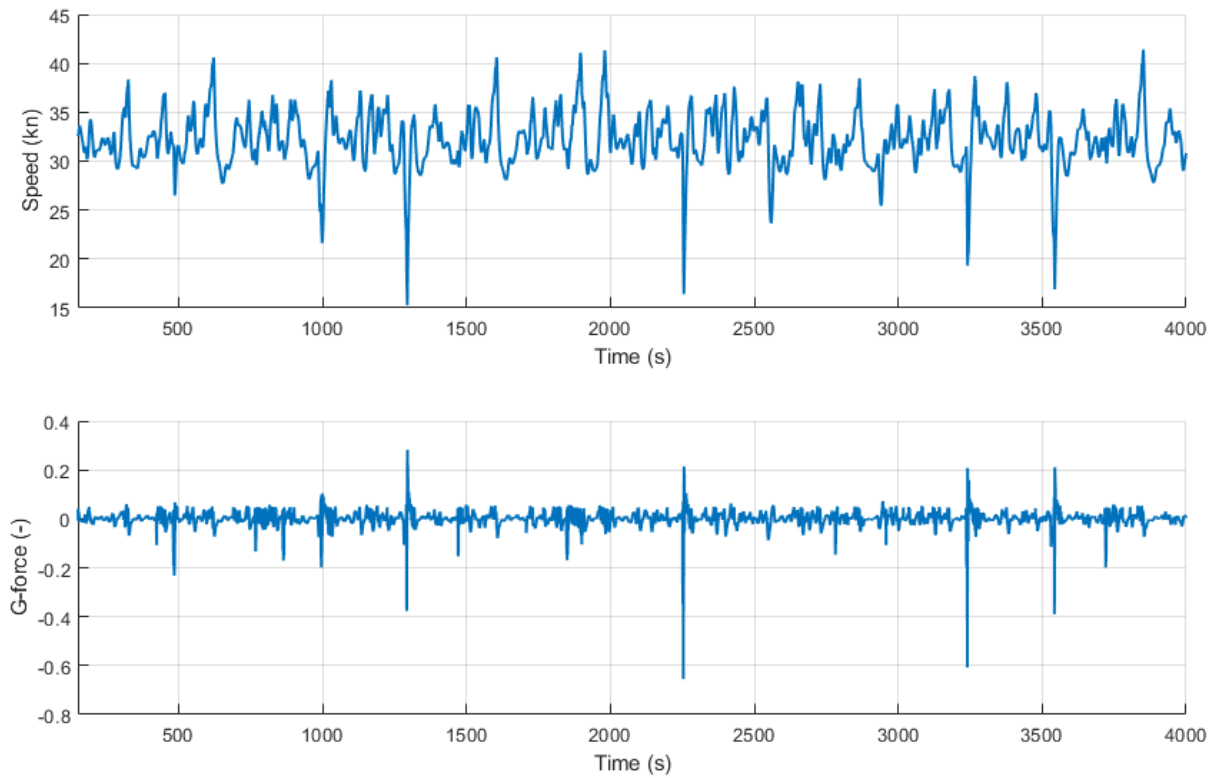
Figure 8.5: Simulation results with larger chord length and higher rake angle. Results show a decrease in G force by around 60%

9
Discussion

This study provided a numerical way to simulate an IMOCA 60 sailing in big waves. Secondly, it was concluded that the applied method is applicable for simulating the occurrence of crashes of these yachts. Based on this study further improvements and a discussion on the applied methodology and results are formulated. These are shown below:

- **The methodology** Several improvements can be applied to the methodology, mainly focusing in the validation. There is no validation case of a yacht that is fully foiling. Therefore, it is hard to assess whether or not the simulation is accurate for a foiling sailing yacht. This could either be done by full CFD simulation of an IMOCA 60 or with tank tests. These additional validation cases where not done due to time constraints, further research could build upon the knowledge gained from this thesis and try to simulate a similar crash to validate these case.

- **System-based approach** The system-based approach implemented in the DVPP does not consider the interactions between individual components. For example, the effect of the foils on the flow around the hull is not considered. As these effects are deemed to be rather small in comparison to the total force, it is expected that the inclusion of these effects does not significantly alter the results of the DVPP. Secondly, in this approach, the boat is modeled as a rigid body, while the yacht has certain movable systems, such as the keel and water ballast. To include, these effects during the simulation a multi-body system would be advised.

- **Appendage forces** The approach using lift and drag coefficients obtained from 2-dimensional simulations does provide a time-efficient method. However, even with the correction for free-surface effects and 3-dimensional effects, complex phenomena such as cavitation or ventilation are not fully captured. These effects could alter the results of the extreme cases of the DVPP due to the frequent change in submergence of the hydrofoil.

- **Resistance** As for the resistance of the hull a solution was proposed which combined the DSYHS with the method of Savitsky. Which is assumed to be a more accurate method for calculating the resistance of a hull sailing at high Froude numbers. However, since both methods are limited in the ability to model the resistance of a high-performance sailing vessel, it is recommended that the DSYHS is expanded with newer high-performance sailing vessels sailing at high Froude numbers.

- **Hydrodynamic forces** The hydrodynamic forces were part of the leading research topic of this report. Due to the high waves combined with the relatively 'small' boat, a nonlinear method was applied. However, this method stretches the applicability of the potential theory used. It was shown that the nonlinear hydrodynamic force, in combination with a correction factor on the diffraction and radiation forces, produces a numerically fast and time-efficient way to simulate an IMOCA 60 in big waves. However, further research is recommended to obtain a fully nonlinear wave model that does not need engineering solutions to get stable results. Another solution might be to conduct a full CFD simulation of a yacht in waves. However, as the literature explains, this does take significant time, and the computational power required is rather large.

- **Aerodynamic forces** Based on the literature, the ORC method was recommended, and it was noted that unsteady aerodynamics could significantly affect the usefulness of a DVPP. This re-

search showed that this unsteadiness, most noticeably, the effect of flapping of sails if the apparent wind angle changes too fast. Has a significant impact on the simulation. Due to the perfect sail trim, assumed in the ORC method, the yacht will capsize if this effect is not considered. The engineering solution of reducing the lift coefficient based on the change in apparent wind angle provides a numerically fast way to correct this behavior. However, this method has little scientific backing. Therefore, it is recommended that further research should be conducted on imperfect sail trim and the effect of this on the force the sail can produce.

- **Results** Firstly, the results of the parametric study. These results indicated that a larger foil in combination with a higher rake angle leads to fewer slowdowns in waves. This effect is plausible, since more lift of the hydrofoils means that the hull will be less in the water and thus less effect of the hydrodynamic forces. However, in real life, these higher lift forces need to be handled by the hull and rigging. This could be an issue since these extremely high forces could lead to structural failure. Secondly, based on the limitations of the DVPP given in the earlier points, the results of the DVPP, especially during phases where the wetted surface changes quickly, are not entirely accurate. This mostly comes from the corrections in hydrodynamic forces. This effect can be seen when the yacht crashes in a wave, where the yacht is rolling and pitching frequently. A CFD calculation is advised for further investigation into the forces occurring in this phase.

10

Conclusion

This report aims to comprehensively understand if the dynamics of ocean-going IMOCA 60 yachts, particularly when encountering large waves while sailing downwind, can be numerically simulated. In these conditions, the yachts can accelerate to high speeds, leading to a situation where the yacht crashes into the wave in front of it, causing decelerations that have led to injury onboard. The guiding research question is: Can the occurrence of wave-induced crashing events be investigated by numerically simulating an IMOCA 60 in high waves?

The literature study concluded that a Dynamic Velocity Prediction Program (DVPP) could be used to numerically simulate an IMOCA 60. However, there has been no research on using a DVPP for an IMOCA 60 in combination with big waves. This research aims to close this gap by investigating if a DVPP can be used to simulate the wave-induced crashes that occur in IMOCA 60s. The current literature forms the foundation for building DVPP by using a system-based approach to model the forces on the yacht.

Several changes to the current state-of-the-art methods are implemented to better model a foiling yacht in waves; these focus on the hydrodynamical, aerodynamic, and resistance forces. Firstly, for the hydrodynamical forces, the DVPP uses a discretization of the hull geometry to calculate the static and dynamic pressure over the hull using the instantaneous water line. For this pressure, wheeler stretching is applied, and the total force is calculated by integrating over the submerged surface. Besides the hydrodynamic forces, the diffraction and radiation forces are linearly modeled in the frequency domain and converted to the time domain using the Cummins formulation. However, since the yacht is sailing at very varying displacements, sometimes with the bare hull out of the water, a nonlinear method is preferred. Therefore, a correction to consider the current displacement has been developed.

Secondly, most current DVPPs use a steady aerodynamics model, which means that the sails are assumed to be sailing at optimal lift and drag at all times. However, in the case of big waves, this assumption does not hold, as when the yacht is accelerating, the wind angle changes quickly, and the sail starts flapping. To take this effect into account, a factor has been applied that looks at the change in wind angle over 4 seconds.

Lastly, the resistance of semi-foiling yachts is considered, as current literature uses either CFD results or the DSYHS. For this research CFD results where not in the timeframe, therefore, DSYHS is used. However, this series is valid up to Froude number 0.75, whereas these boats are sailing at higher Froude numbers. Therefore, the method for planing hulls of Savitsky has been implemented above Froude number 0.75, and a transition region between Froude number 0.6-0.75 to gradually transition between these to methods.

The DVPP is validated in both quantitative and qualitative ways. For quantitative validation, sphere heave decay tests and RAOs of a Wigley hull are conducted. For qualitative validation, a simulation of waves and wind typical for the southern Ocean is compared to a similar DVPP. The results of the quantitative validation showed great agreement to reference data for both heave decay and RAOs. Only near the resonance peak, there was a slight overestimation of the response of the yacht. Based on these results, it is concluded that the DVPP accurately models the hydrostatic, hydrodynamic, radiation, and diffraction forces for both no forward speed and with forward speed.

The qualitative validation was performed on the DVPP without the improvements and with the improvements to the current state-of-the-art DVPP. The current state-of-the-art DVPP results show significant limitations, mostly due to the steady aerodynamic forces. The DVPP crashes due to the excessive heeling of the yacht. With the proposed improvement, the DVPP does not crash, and the yacht shows the same behavior as described in Kerdraon (2021).

Further investigation has been conducted on the key factors of the yacht when sailing in big waves: environmental conditions and foil parameters. The results showed that higher environmental conditions lead to more considerable slowdowns. However, the relationship between the wave's speed and the yacht's speed is also important. Regarding the foil parameters, a smaller chord length and rake angle also lead to larger slowdowns, mainly due to the increase in hydrodynamic force acting on the hull in combination with the larger effect of orbital movements on the foil's angle of attack.

The last research question still open is the ability of the DVPP to be used in the occurrence of crashing events due to waves. To investigate this, a longer simulation was performed with a wind speed of 40 knots, accompanied by a wave spectrum corresponding to this wind speed. The results show several slowdowns with a g-force higher than the threshold of 0.45 G. Indicating that the DVPP can be used to assess the dynamic stability in big waves.

Upon further analysis of one crash, it was concluded that the yacht first accelerates and goes into a fully foiling mode. This foiling mode reduces the yacht's ability to follow the waves. The yacht then sails off the front of the incoming wave. During this phase, the trim angle of the yacht changes. The crash happens when the yacht enters the wave through. At this point, the yacht touches the water, and a combination with a change in trim increases the resistance of both hull and foil greatly, leading to a slowdown that is large enough to be classified as a crash.

Based on the research, it is concluded that the occurrence of crashing events can be investigated by numerically simulating an IMOCA 60 in a Dynamic Velocity Prediction Program. Several improvements to the current state of the art were necessary to obtain valid results; these are wheeler stretching of the hydrodynamic pressure, correction of the dynamic forces based on the submerged volume, correction of the aerodynamic forces, and extra corrections on the appendage forces to take into account the 3d effects.

References

11th-Hour-Racing-Team (Mar. 29, 2023). *EPIC drone footage of IMOCA Southern Ocean sailing!* URL: https://www.youtube.com/watch?v=k_CfRK2XYow (visited on 10/04/2024).

Abratis, Ralf (Dec. 20, 2021). *Kieler Comeback beim The Ocean Race 2023*. URL: https://offshoreteamgermany.com/kieler-comeback-beim-the-ocean-race-2023-2/.

Airy (1845). "Tides and Waves". In: *Encyclopedia Metropolotana, London* Vol. 5, pp. 341–396.

Angelou, Manolis and Kostas J. Spyrou (Sept. 29, 2017). "Towards a New Mathematical Model for Investigating Course Stability and Maneuvering Motions of Sailing Yachts". In: *Journal of Sailing Technology* 2017-06. DOI: 10.5957/csys-2016-010. URL: https://doi.org/10.5957/csys-2016-010.

Angelou, Manolis and Kostas J. Spyrou (Feb. 1, 2019). "Modeling of transient hydrodynamic lifting forces of sailing yachts and study of their effect on maneuvering in waves". In: *Ocean Engineering* 173, pp. 531–547. DOI: 10.1016/j.oceaneng.2019.01.021. URL: https://doi.org/10.1016/j.oceaneng.2019.01.021.

Angelou, Manolis and Kostas J. Spyrou (June 1, 2021). "Dynamic stability assessment of yacht downwind sailing in regular waves". In: *Applied Ocean Research* 111, p. 102651. DOI: 10.1016/j.apor.2021.102651. URL: https://doi.org/10.1016/j.apor.2021.102651.

Armesto, José A. et al. (June 13, 2015). "Comparative analysis of the methods to compute the radiation term in Cummins' equation". In: *Journal of Ocean Engineering and Marine Energy* 1(4), pp. 377–393. DOI: 10.1007/s40722-015-0027-1. URL: https://doi.org/10.1007/s40722-015-0027-1.

Aygor, Teksen (Feb. 2017). *Analyses of Foil Configurations of IMOCA Open 60s with Towing Tank Test Results*. URL: https://matheo.uliege.be/bitstream/2268.2/4411/1/AYGOR%20Teksen%2C%20MAster%20Thesis%20%28SOLENT%2C%20ZUT%29%20New.pdf.

Batt, K. L., R. P. Morison, and M. S. Speer (July 5, 2000). "Direct verification of forecasts from a very high resolution numerical weather prediction (NWP) model". In: *Meteorology and Atmospheric Physics* 74(1-4), pp. 117–127. DOI: 10.1007/s007030070029. URL: https://www.researchgate.net/publication/253409451_Direct_verification_of_forecasts_from_a_very_high_resolution_numerical_weather_prediction_NWP_model.

Boef, W.J.C. (Mar. 1, 1992). "Launch and Impact of Free-fall Lifeboats. Part I. Impact Theory". In: *Ocean Engineering* 19(2), pp. 119–138. DOI: 10.1016/0029-8018(92)90011-r. URL: https://doi.org/10.1016/0029-8018(92)90011-r.

Bretschneider, Charles L (Sept. 1, 1964). "Generation of Waves by Wind: state of the art". In: *International Summer Course Lunteren*. URL: https://apps.dtic.mil/dtic/tr/fulltext/u2/612006.pdf.

Buchner, Bas (May 1, 1995). "The impact of green water on FPSO design". In: *All Days*. DOI: 10.4043/7698-ms. URL: https://doi.org/10.4043/7698-ms.

Chuang, Wei□Liang, Ting-Chieh Lin, and Y. Wang (Nov. 1, 2023). "Greenwater due to plunging breaking wave impingement on a deck structure. Part 1: Experimental Investigation on Fluid Kinematics". In: *Ocean Engineering* 287, p. 115859. DOI: 10.1016/j.oceaneng.2023.115859. URL: https://doi.org/10.1016/j.oceaneng.2023.115859.

Cox, Daniel T. and J. Alberto Ortega (Nov. 1, 2002). "Laboratory observations of green water overtopping a fixed deck". In: *Ocean Engineering* 29(14), pp. 1827–1840. DOI: 10.1016/s0029-8018(02)00011-2. URL: https://doi.org/10.1016/s0029-8018(02)00011-2.

Cummins, W.E. (Oct. 1, 1962). "THE IMPULSE RESPONSE FUNCTION AND SHIP MOTIONS". In: *Schiffstechnik* 9, pp. 101–109. URL: https://apps.dtic.mil/sti/citations/AD0288277.

Day, Sandy et al. (Dec. 4, 2002). "Vpp Vs Ppp: Challenges In The Time-Domain Prediction of Sailing Yacht Performance". In: *High Performance Yacht Design Conference*. DOI: 10.3940/rina.ya.2002.07. URL: https://doi.org/10.3940/rina.ya.2002.07.

Defi-Azimut (2024). *Des runs de très haute volée*. URL: https://www.defi-azimut.net/fr/actualites/des-runs-de-tres-haute-volee (visited on 10/04/2024).

Delhommeau and Kobus (1987). *Méthode approchée de calcul du comportement sur houle avec vitesse d'avance*. Vol. 467. Bulletin de l'Ass ociation Technique Maritime et Aéronautique.

ECMWF (Oct. 2, 2024). *ERA5-Land hourly data from 1950 to present*. URL: https://cds.climate.copernicus.eu/datasets/reanalysis-era5-land?tab=overview (visited on 10/02/2024).

Faltinsen, O M (2005). *Hydrodynamics of high-speed marine vehicles*. URL: https://tudelft.on.worldcat.org/search/detail/58468113?queryString=Hydrodynamics%20of%20High-Speed%20Marine%20Vehicles.

Fenton, John D. (Mar. 1, 1985). "A Fifth￭Order Stokes theory for steady waves". In: *Journal of waterway, port, coastal, and ocean engineering* 111(2), pp. 216–234. DOI: 10.1061/(asce)0733-950x(1985)111:2(216). URL: https://doi.org/10.1061/(asce)0733-950x(1985)111:2(216).

Fjellstad, Ola Erik et al. (Aug. 1994). *Quaternion Feedback Regulation of Underwater Vehicles*. URL: https://www.fossen.biz/publications/1994%20Fjellstad%20and%20Fossen%20CCA.pdf.

Fossen, Thor I. (Apr. 8, 2011). *Handbook of Marine Craft Hydrodynamics and Motion Control*. DOI: 10.1002/9781119994138. URL: https://doi.org/10.1002/9781119994138.

Gatin, Inno et al. (Oct. 1, 2017). "Enhanced coupling of solid body motion and fluid flow in finite volume framework". In: *Ocean Engineering* 143, pp. 295–304. DOI: 10.1016/j.oceaneng.2017.08.009. URL: https://doi.org/10.1016/j.oceaneng.2017.08.009.

Gerhardt, Frederik C. et al. (Mar. 20, 2009). "Tacking in the Wind Tunnel". In: *Chasepeake sailing yacht symposium*. DOI: 10.5957/csys-2009-012. URL: https://doi.org/10.5957/csys-2009-012.

Gorman (Apr. 12, 2023). *Richomme learns the solo ropes in IMOCA by leading the charge east*. URL: https://www.imoca.org/en/news/news/richomme-learns-the-solo-ropes-in-imoca-by-leading-the-charge-east (visited on 08/13/2024).

Holthuijsen, I. H. (1980). *Methode voor golfvoorspelling*. Vol. Deel 1. Technische adviescommissie voor de waterkeringen.

Horel, B. et al. (June 9, 2013). "A Method of Immersed Surface Capture for Broaching Application". In: *ASME 2013 32nd International Conference on Ocean, Offshore and Arctic Engineering*. DOI: 10.1115/omae2013-11527. URL: https://doi.org/10.1115/omae2013-11527.

Horel, Boris (Jan. 1, 2019). "System-based modelling of a foiling catamaran". In: *Ocean Engineering* 171, pp. 108–119. DOI: 10.1016/j.oceaneng.2018.10.046. URL: https://doi.org/10.1016/j.oceaneng.2018.10.046.

Horel, Boris and Mathieu Durand (June 1, 2019). "Application of System-based Modelling and Simplified-FSI to a foiling open 60 monohull". In: *Journal of sailing technology* 4(01), pp. 114–141. DOI: 10.5957/jst.2019.4.1.114. URL: https://doi.org/10.5957/jst.2019.4.1.114.

Huang, Luofeng et al. (July 1, 2021). "CFD analyses on the water entry process of a freefall lifeboat". In: *Ocean Engineering* 232, p. 109115. DOI: 10.1016/j.oceaneng.2021.109115. URL: https://doi.org/10.1016/j.oceaneng.2021.109115.

Huetz, Lionel and B. Alessandrini (Jan. 1, 2011). "Systematic Study of the Hydrodynamic Forces on a Sailing Yacht Hull Using Parametric Design and CFD". In: *30th International Conference on Offshore Mechanics and Arctic Engineering*. DOI: 10.1115/omae2011-50263. URL: https://doi.org/10.1115/omae2011-50263.

IMOCA Class (n.d.). *About the IMOCA Class*. URL: https://www.imoca.org/en/imoca/about.

International Energy Agency et al. (Oct. 2017). "Wave Energy Converter Modeling Verification and Validation". In: URL: https://www.nrel.gov/docs/fy18osti/68465.pdf.

, Jacques (Mar. 13, 2023). *Evolution of the Whitbread yachts' hull design, from 1974 to the Ocean Race 2023 - PART THREE*. URL: https://chevaliertaglang.blogspot.com/2023/03/evolution-of-whitbread-yachts-hull.html.

Jeppesen, Joanne (Aug. 23, 2023). "Fact sheet: Reanalysis". In: URL: https://www.ecmwf.int/en/about/media-centre/focus/2023/fact-sheet-reanalysis.

Journée (2000). *Offshore Hydromechanics*. 3rd ed. TU Delft.

Journee, Johan M.J. (Jan. 1, 1992). *Experiments and Calculations on Four Wigley Hullforms*. 909. URL: https://repository.tudelft.nl/islandora/object/uuid%3A52a76d0b-5db1-4902-a254-a81491b9cf99.

Karimirad, Madjid (Jan. 1, 2014). *Wave and Wind Theories*, pp. 165–186. DOI: 10.1007/978-3-319-12175-8_8. URL: https://link.springer.com/chapter/10.1007/978-3-319-12175-8_8.

Kerdraon, Paul (Jan. 22, 2021). *Modeling of unsteady hydrodynamic phenomena on an offshore racing trimaran.* URL: https://theses.hal.science/tel-03274068.

Kerdraon, Paul et al. (Sept. 1, 2020). "Development of a 6-DOF dynamic velocity prediction program for offshore racing yachts". In: *Ocean Engineering* 212, p. 107668. DOI: 10.1016/j.oceaneng.2020.107668. URL: https://doi.org/10.1016/j.oceaneng.2020.107668.

Keuning, J A and M Katgert (Jan. 1, 2008). "A bare hull resistance prediction method derived from the results of the Delft Systematic Yacht hull series extended to higher speeds". In: *Proceeding of the International conference innovation in high performance sailing yachts*, pp. 13–21.

Keuning, J. A., K. J. Vermeulen, and E. J. De Ridder (Mar. 4, 2005). "A Generic Mathematical Model for the Maneuvering and Tacking of a Sailing Yacht". In: *SNAME 17th Chesapeake Sailing Yacht Symposium*. DOI: 10.5957/csys-2005-012. URL: https://doi.org/10.5957/csys-2005-012.

Kim, Sungeun Peter (Mar. 1, 2011). "CFD as a seakeeping tool for ship design". In: *International Journal of Naval Architecture and Ocean Engineering* 3(1), pp. 65–71. DOI: 10.2478/ijnaoe-2013-0046. URL: https://doi.org/10.2478/ijnaoe-2013-0046.

Kleefsman, K.M. Theresa and Arthur Veldman (Jan. 1, 2004). "An Improved Volume-of-Fluid Method for Wave Impact". In: *European Congress on Computational Methods in Applied Sciences and Engineering*. URL: https://pure.rug.nl/ws/files/2945542/2004ProcECCOMASKleefsman.pdf.

Knudsen, Stig Staghoi et al. (June 10, 2022). "Towards the Dynamic Velocity Prediction of a NACRA 17". In: *SNAME 24th Chasepeake Sailing Yacht Symposium*. DOI: 10.5957/csys-2022-002. URL: https://doi.org/10.5957/csys-2022-002.

Kurnia, Ruddy and Guillaume Ducrozet (Nov. 1, 2023). "NEMOH: Open-source boundary element solver for computation of first- and second-order hydrodynamic loads in the frequency domain". In: *Computer Physics Communications* 292, p. 108885. DOI: 10.1016/j.cpc.2023.108885. URL: https://www.sciencedirect.com/science/article/pii/S0010465523002308.

Levin, Rickard Lindstrand and Lars Larsson (Nov. 1, 2017). "Sailing yacht performance prediction based on coupled CFD and rigid body dynamics in 6 degrees of freedom". In: *Ocean Engineering* 144, pp. 362–373. DOI: 10.1016/j.oceaneng.2017.09.052. URL: https://doi.org/10.1016/j.oceaneng.2017.09.052.

Liao, Kangping et al. (Jan. 8, 2021). "Numerical simulation of green water on deck with a hybrid Eulerian-Lagrangian method". In: *Journal of Ship Research* 66(01), pp. 73–90. DOI: 10.5957/josr.03190015. URL: https://doi.org/10.5957/josr.03190015.

Matusiak, Jerzy (Jan. 1, 2010). "On the non-linearities of ship's restoring and the Froude-Krylov wave load part". In: *ResearchGate*. URL: https://www.researchgate.net/publication/313627506_On_the_non-linearities_of_ship's_restoring_and_the_Froude-Krylov_wave_load_part.

Matworks (n.d.). *Simulink - Simulation and Model-Based Design*. URL: https://www.mathworks.com/products/simulink.html.

NOAA (2024). *Waves*. URL: https://www.noaa.gov/jetstream/ocean/waves (visited on 10/07/2024).

North Sails (Aug. 7, 2022). *Building Sails for the IMOCA*. URL: https://www.northsails.com/en-nl/blogs/north-sails-blog/building-3di-sails-for-the-imoca-north-sails-france (visited on 08/13/2024).

Offshore Racing Congress (Jan. 2022). *ORC VPP Documentation 2022*. URL: https://orc.staging.daytwo.no/uploads/files/Rules-Regulations/ORC-VPP-Documentation-2022.pdf.

Ogilvie, T. Francis (Jan. 1, 1964). "Recent progress toward the understanding and prediction of ship motions". In: *Proc. Symp. 5th on Naval Hydrodyn, Washington D.C.* URL: https://ci.nii.ac.jp/naid/20000327176/.

Orcaflex (n.d.). *Vessel theory: Impulse response and convolution*. URL: https://www.orcina.com/webhelp/OrcaFlex/Content/html/Vesseltheory,Impulseresponseandconvolution.htm.

Orihara, Hideo and Hideaki Miyata (Oct. 1, 2003). "Evaluation of added resistance in regular incident waves by computational fluid dynamics motion simulation using an overlapping grid system". In: *Journal of Marine Science and Technology* 8(2), pp. 47–60. DOI: 10.1007/s00773-003-0163-5. URL: https://doi.org/10.1007/s00773-003-0163-5.

Park, Dong-Min et al. (Dec. 20, 2014). "Systematic Experimental and Numerical Analyses on Added Resistance in Waves". In: *Journal of the Society of Naval Architects of Korea* 51(6), pp. 459–479. DOI: 10.3744/snak.2014.51.6.459. URL: https://oak.go.kr/central/journallist/journaldetail.do?article_seq=16924.

Payne, Peter R. (Jan. 1, 1981). "The vertical impact of a wedge on a fluid". In: *Ocean Engineering* 8(4), pp. 421–436. DOI: 10.1016/0029-8018(81)90035-4. URL: https://doi.org/10.1016/0029-8018(81)90035-4.

Rahman, M. (Jan. 1, 1970). "Fundamentals concerning Stokes waves". In: *WIT transactions on engineering sciences* 9. DOI: 10.2495/afm960271. URL: https://www.witpress.com/Secure/elibrary/papers/AFM96/AFM96027FU.pdf.

Rieker, Jochen (Jan. 19, 2024). *The Ocean Race: Why the sails could decide the race*. URL: https://www.yacht.de/en/the-ocean-race/the-ocean-race-why-the-sails-could-decide-the-race/.

Robin, Pierre et al. (May 29, 2023). "Tackling Modern Sailing Challenges with a CFD-based Dynamic VPP". In: *Innov'Sail 2023*. URL: https://hal.science/hal-04102794.

Roux, J.P. Le (Apr. 1, 2008a). "An extension of the airy theory for linear waves into shallow water". In: *Coastal Engineering* 55(4), pp. 295–301. DOI: 10.1016/j.coastaleng.2007.11.003. URL: https://doi.org/10.1016/j.coastaleng.2007.11.003.

Roux, J.P. Le (Aug. 1, 2008b). "Profiles of fully developed (Airy) waves in different water depths". In: *Coastal Engineering* 55(9), pp. 701–703. DOI: 10.1016/j.coastaleng.2008.02.003. URL: https://doi.org/10.1016/j.coastaleng.2008.02.003.

Roux, Yann et al. (Jan. 1, 2008). "Strongly coupled VPP and CFD RANSE Code for Sailing Yacht Performance Prediction". In: *HAL (Le Centre pour la Communication Scientifique Directe)*. URL: https://hal.science/hal-01156261.

Rusch, P. (Mar. 15, 2023). *Managing the ice limit*. URL: https://www.theoceanrace.com/en/news/13635_Managing-the-ice-limit (visited on 10/09/2024).

Ryu, Yonguk, Kuang An Chang, and Richard Mercier (July 1, 2007). "Application of dam-break flow to green water prediction". In: *Applied Ocean Research* 29(3), pp. 128–136. DOI: 10.1016/j.apor.2007.10.002. URL: https://doi.org/10.1016/j.apor.2007.10.002.

Savitsky, Daniel (Oct. 1, 1964). "Hydrodynamic Design of Planing Hulls". In: *Marine Technology and SNAME News* 1(04), pp. 71–95. DOI: 10.5957/mt1.1964.1.4.71. URL: https://doi.org/10.5957/mt1.1964.1.4.71.

Sheng, Wanan et al. (May 13, 2022). "Time-Domain Implementation and Analyses of Multi-Motion Modes of Floating Structures". In: *Journal of Marine Science and Engineering* 10(5), p. 662. DOI: 10.3390/jmse10050662. URL: https://www.mdpi.com/2077-1312/10/5/662.

Stengel, Robert F. (Nov. 1, 2022). *Flight dynamics. Second Edition*. Princeton University Press.

Stokes, George Gabriel (Jan. 1, 1847). "On the theory of oscillatory waves". In: *Math. Phys. Papers* 8, pp. 441–473. URL: http://ci.nii.ac.jp/naid/10016936381.

The Ocean Race (Mar. 26, 2023). *Team Malizia's Rosalin Kuiper suffers a head injury near Cape Horn*. URL: https://www.theoceanrace.com/en/news/13749_Team-Malizia-s-Rosalin-Kuiper-suffers-a-head-injury-near-Cape-Horn-she-is-conscious-stable-and-recovering (visited on 10/02/2024).

The Ocean Race (Mar. 11, 2024). *Most Increadible Drone Shots from The Ocean Race*. URL: https://www.youtube.com/watch?v=4Q6SAAbf6mY&t=165s (visited on 08/13/2024).

Uchowski, Andrzej and Jerzy Jackowski (n.d.). "ANALYSIS OF PROPERTIES OF OPERATION OF THE SUPPORTING EQUIPMENT FOR THE SEAT BELTS". In: *ResearchGate* (). URL: https://www.researchgate.net/publication/267989061_ANALYSIS_OF_PROPERTIES_OF_OPERATION_OF_THE_SUPPORTING_EQUIPMENT_FOR_THE_SEAT_BELTS#pf4.

Veldman, Arthur, Henk Seubers, Peter Van Der Plas, et al. (May 1, 2017). "Accelerated free-surface flow simulations with interactively moving bodies". In: *36th International Conference on Ocean, Offshore and Arctic Engineering*, pp. 604–615. URL: https://pure.rug.nl/ws/files/65689390/Marine2017_paper568.pdf.

Veldman, Arthur, Henk Seubers, S. M. Hosseini Zahraei, et al. (May 13, 2019). "The ComMotion project: Computational methods for moving and deforming objects in extreme waves". In: *VIII International Conference on Computational Methods in Marine Engineering*, pp. 820–831. URL: https://pure.rug.nl/ws/files/101835023/MARINE2019_Veldman.pdf.

Von Kármán, Th. (Oct. 1, 1929). "The impact on seaplane floats during landing". In: *NACA TN No. 321*. URL: https://digital.library.unt.edu/ark:/67531/metadc54062/m2/1/high_res_d/19930081174.pdf.

Wheeler, Mark and Bill Henson (Mar. 2023). *Weather routing – speed or comfort?* URL: https://fremantlesailingclub.com.au/wp-content/uploads/2023/04/Weather-routing.pdf.

White, N. (n.d.). *Expedition Marine*. URL: https://www.expeditionmarine.com/.

Wikipedia contributors (Apr. 17, 2024). *IMOCA 60*. URL: `https://en.wikipedia.org/wiki/IMOCA_60#/media/File:IMOCA_plan.png`.

"BEMRosetta: An open-source hydrodynamic coefficients converter and viewer integrated with Nemoh and FOAMM" (Sept. 5, 2021). In: ed. by Zabala et al. 14th European Wave and Tidal Energy Conference: Plymouth, gb.

<div style="text-align: right; font-size: 3em;">A</div>
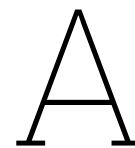
Background literature impact dynamics, CFD calculation of floating bodies and green water

A.1. Impact dynamics

The most basic and researched subject in impact dynamics is a 2-dimensional falling wedge, which was first described by Von Kármán (1929). In this paper, an analytical model based on momentum conservation is made to predict the impact forces on a wedge falling into the water. This 2d falling object can be seen as a ship section that is slamming into waves. This research is validated by Payne (1981) who compared the results of this theory and theories expanding on the work of Von Kármán (1929), he concluded that the original method presented by Von Karman gives good agreement with experiments however, it does not account for the acceleration of water mass in spray regions. Furthermore, the improvements proposed by other authors have little effect or can even be harmful to the results.

This theory is extended by Boef (1992) who provides an impact theory for the impact of free-fall lifeboats. In this work the momentum theorem and added mass concept are used to calculate the impact for cylinders. In his equation of motion the added mass term is changed by using a max-function to obtain correct results for when the cylinder starts rising. During this phase, there is no momentum gained from the loss of added mass, and the motion equation is changed such that this does not happen. The equations are changed for a boat by calculating the forces on an infinitesimal small cross-section and integrating this over the length of the boat. He concludes that the results agree well with observations of small-scale experiments.

Apart from using analytical equations Huang et al. (2021) models the impact of a lifeboat free-falling into the water using CFD. From Veldman, Seubers, Van Der Plas, et al. (2017) he concluded that using a relative speed approach, where the lifeboat is standing still and the water is moving at a relative flow against the body, is inaccurate because it is incapable of accounting for the large added mass due to the accelerations during the water entry. Therefore he uses a finite volume and overset mesh approach to analyse the free-fall of lifeboats. These results are verified based on full-scale measurements. Based on the results he concludes that the presented method can accurately predict the hull slamming forces and that the peak pressure impacts are captured accurately.

A.2. CFD calculation of floating bodies

Wave impact and ridged body motions simulated in CFD are also a source of literature. A way to use the Volume-Of-Fluid, VOF, method with a height function for wave impact on bodies is presented in Kleefsman and Veldman (2004). In his presented method the mass conservation in each cell is conserved by using a height function, this method is incorporated in the ComFLOW software. The results are validated by wedge drops and dam break simulations with known experimental results. This work

is used in Veldman, Seubers, Zahraei, et al. (2019) where computational methods for adding moving and elastic objects in waves are added to the software. In his work the traditional coupling method, where information is exchanged once per time step, is changed to a method where the body dynamics are solved simultaneously with the fluid.

Orihara and Miyata (2003) presented a different coupling scheme to obtain more accurate resistance calculations in waves. In the presented method the solution of the motion of the ship and the solution of the flow computation is combined to simultaneously solve the motion of the ship. To accurately take into account the effect of the ship's motion on the flow a predictor-corrector scheme is employed. The hydrodynamic force and moment are calculated using the flow solution of the present time and based on that the ship motions are calculated, based on this the body force is evaluated and from that solution, a corrector of the hydrodynamical force is calculated. Based on this a corrector for the body motions can be calculated and from that a corrector of the flow field and static pressure is calculated. From this solution a flow field of the new time is obtained.

Kim (2011) uses the same kind of predictor-corrector scheme on a CFD simulation of a container vessel and validates the results with segmented model tests. Based on this study it was concluded that the fully nonlinear seakeeping analysis by CFD can successfully calculate the nonlinear structural loads. Also it was demonstrated that the method used can be seen as a reliable method for fully nonlinear seakeeping analysis. Gatin et al. (2017) presents a different method for coupling body motions and fluid flow in CFD simulations. In this method the motion equations are solved in the PISO loop after each pressure correction, leading to more accurate results. The method also requires fewer PISO correction cycles than conventional coupling algorithms to achieve satisfactory results, which leads to lower CPU time.

Based on this research Chuang, Lin, and Wang (2023) examined the BIV and PIV model further and concluded that there is a transition zone between the over-topping wave to the green water flow. When the flow is in a green water regime the Ritter solutions with the initial water depth obtained from Ryu can capture the velocity distribution. The Ritter solution however fails to describe the free surface elevation of the greenwater flow. Besides the assessment of the Ritter solutions they investigated the self-similar U velocity distribution described in Ryu, Chang, and Mercier (2007). The equation that they derived was modified such that random waves can be used. With this modification, it is shown that the equations hold potential for the utility in engineering applications.

Liao et al. (2021) Provided next to the dam-break solution a numerical method to solve green water on a deck. He employed a hybrid Eulerain-Langrangian method which solves the flow on a Eulerian framework where the rigid body of the ship is represented as a set of surface particles. These particles are described by a lagragian framework by solving the 6-DOF rigid body motion equations. This method can solve problems involving large amplitudes of body motion by having the mesh of the flow solver fixed. Based on experiments on a box and Wigley hull he concluded that the pressure results are in good agreement with experimental data, also the body motions are captured with reasonable accuracy. However the peak pressures are still difficult to predict because of the involvement of spray and air entrapment.

A.3. Green water

Green water impact on an FPSE in head waves is modelled by Buchner (1995). He concluded that the occurrence of such impact can be split into 4 sequences, the relative wave motion comes above the freeboard, the water flows onto the deck, a shallow water wave flows over the deck, and water hits a structure. He concluded that the ship motions can be linearly modeled using RAOs. Based on this research Cox and Ortega (2002) concluded that the wave collapse and its propagation is similar to a dam-break problem and that those shallow water equations can be used. However in the case of green water impact there is a non-zero initial horizontal velocity.

Ryu, Chang, and Mercier (2007) used a new kind of particle image velocimetry called bubble image

velocimetry velocity, BIV, and showed that the current Ritter's dam-break flow solution is suitable for green water flow on offshore structures. However it does not predict the shape of the velocity profile, it gives an accurate prediction of the cross-sectional velocity and of the front velocity of the green water flow. However, the determination of the initial water depth is the most difficult task in obtaining a correct solution. To overcome this problem he proposed two approaches to solve this initial water depth. The first method is to approximate the height by taking the difference between the height of the incoming wave and the freeboard. The second approach is to match the front velocity of the green water flow with that of the dam-break solution and back calculating the initial water depth.

B

Rating certificate Imoca 60
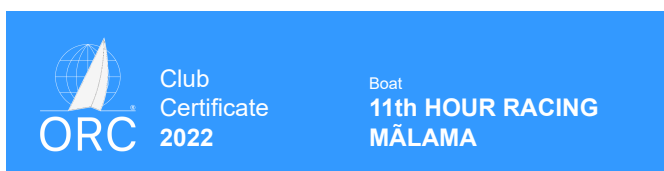
ORC	Club Certificate **2022**	Boat **11th HOUR RACING MÃLAMA**

Centre de Calcul FFVoile
52 rue Sénac de Meilhan
17000 - La Rochelle
France

FFVoile

11TH HOUR RACING MÃLAMA

Mainsail = 160.71 m²
Headsail = 147.75 m²
Headsail flying = 313.09 m²
Asymmetric = 425.75 m²

APH: 346.5   **CDL: 18.462**

GPH: **391.1**   CertNo: **22302b**

BOAT

Class	**IMOCA 60**
Designer	**Guillaume VERDIER**
Builder	**CDK Technologie**
Age date	**08/2021**
Series date	**08/2021**
Offset file	**11thHour.off**
Data file	**11thHOUR_22302b**

HULL

Length Overall	**18.280 m**
Maximum Beam	**5.346 m**
Draft	**4.498 m**
Displacement	**9,100 kg**
DLR	**1.5959**
IMS Division	**Performance**
Dynamic Allowance	**0.001%**
Age Allowance	**0.033%**

PROPELLER

Installation	**Shaft exposed**
Type	**Folding 2 blades**
Diameter	**0.499m**

CREW

Maximum weight	**1,575 kg**	
Minimum weight	**1,181 kg**	* when applied
Non Manual Power	**Rig**	
Crew Arm Extension		

SAIL AREAS (m²)

	Measured	Rated
Mainsail	**160.71**	**167.72**
Headsail Luffed	**147.75**	**147.75**
Headsail Flying	**313.09**	**313.09**
Symmetric		
Asymmetric	**425.75**	**425.75**

(1 asymmetric(s) with SHW/SFL < 85%)

STORM SAIL AREAS (m²)

Trysail	**35.45**
Storm Jib	**35.03**
Heavy Weather Jib	**94.58**

SAIL LIMITS

Headsails	**8**
Spinnakers	**6**

STABILITY

Righting Moment	**930.7 kg·m**
Stability Index	**N/A**

COMMENTS

All measures taken from IMOCA measurement (R.Boulaire) or from 2D/3D files / Offset file: designer's file

The owner and any other person in charge is responsible that boat is complying with her certificate in accordance with RRS 78.1 and ORC Rule 304.
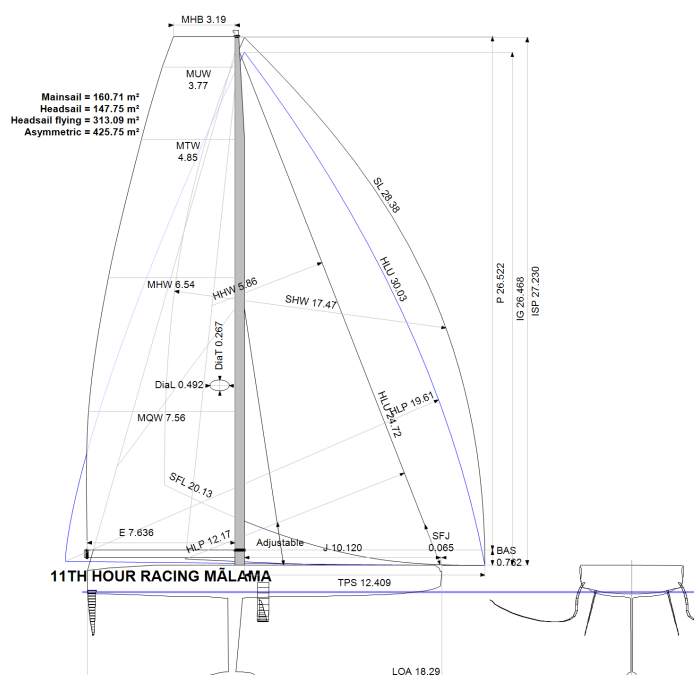
Rated boat velocities in knots							
Wind Velocity	6 kt	8 kt	10 kt	12 kt	14 kt	16 kt	20 kt
Beat Angles	47.1°	43.0°	40.2°	39.1°	38.1°	37.0°	36.1°
Beat VMG	5.27	6.38	6.97	7.35	7.61	7.87	8.09
52°	8.34	9.69	10.25	10.70	11.13	11.61	12.32
60°	9.09	10.17	10.83	11.51	12.04	12.50	13.43
75°	9.86	10.82	11.94	12.82	13.60	14.23	15.28
90°	10.07	11.40	12.71	13.85	14.68	15.49	16.54
110°	9.84	11.26	12.97	14.40	15.54	16.53	18.35
120°	9.37	10.72	12.20	14.09	15.66	16.82	19.08
135°	7.47	9.49	10.87	12.52	14.51	16.04	19.12
150°	6.18	8.00	9.52	10.73	12.33	14.02	18.00
Run VMG	5.35	6.93	8.24	9.30	10.67	12.14	15.59
Gybe Angles	139.7°	141.7°	146.9°	146.9°	143.5°	144.1°	145.9°

ORC Club Certificate 2022

Boat
11th HOUR RACING MĀLAMA

Centre de Calcul FFVoile
52 rue Sénac de Meilhan
17000 - La Rochelle
France

FFVoile

Time Allowances in secs/NM							
Wind Velocity	**6 kt**	**8 kt**	**10 kt**	**12 kt**	**14 kt**	**16 kt**	**20 kt**
Beat VMG	683.5	563.9	516.6	489.9	473.3	457.6	444.8
52°	431.7	371.7	351.3	336.4	323.6	310.1	292.2
60°	395.9	354.1	332.4	312.8	299.0	288.0	268.0
75°	364.9	332.7	301.5	280.7	264.6	252.9	235.6
90°	357.6	315.9	283.2	260.0	245.2	232.4	217.7
110°	366.0	319.8	277.5	250.1	231.7	217.7	196.2
120°	384.1	335.9	295.1	255.6	229.9	214.1	188.7
135°	481.8	379.5	331.3	287.5	248.1	224.5	188.3
150°	582.7	449.7	378.3	335.4	292.1	256.9	200.0
Run VMG	672.9	519.3	436.8	387.3	337.3	296.6	231.0
Selected Courses							
Windward / Leeward	678.2	541.6	476.7	438.6	405.3	377.1	337.9
All purpose	498.8	413.4	367.9	337.6	313.3	293.7	266.2

Single Number Scoring Options		
Course	**Time On Distance**	**Time On Time**
Windward / Leeward	450.6	1.3314
All purpose	346.5	1.7318

Custom scoring options for France

Single Number	Time On Distance	Time On Time
Triple Number Coastal/Long Distance Low	456.1	1.3155
Triple Number Coastal/Long Distance Medium	347.9	1.7245
Triple Number Coastal/Long Distance High	288.3	2.0814
Triple Number Windward/Leeward Low	609.9	0.9838
Triple Number Windward/Leeward Medium	451.6	1.3287
Triple Number Windward/Leeward High	369.5	1.6240

Club Certificate 2022 — ORC

Boat
11th HOUR RACING MĀLAMA

Centre de Calcul FFVoile
52 rue Sénac de Meilhan
17000 - La Rochelle
France

FFVoile

Data in **meters/kilograms (Metric)**

HULL AND APPENDAGES (Lightship Trim)

Class	**IMOCA 60**	LOA	**18.280**	VCGD	**-0.398**	Water ballast weight	**2,385**	
Measurement		Max. Beam	**5.346**	VCGM	**-0.406**	Water ballast LCG	**5.76**	
HIN		Draft	**4.498**	RM Measured (kg·m)	**930.7**	Water ballast VCG	**0.14**	
Plan review		Displacement	**9,100**	RM Default (kg·m)	**837.6**	Water ballast TCG	**0.80**	
Hull construction	**Carbon**	Wetted area	**65.77**	Limit of positive stability(°)	**N/A**	List angle	**7.5**	
Aramid Hull Core	**No**	IMS L	**18.342**	Stability Index	**N/A**	Canting keel angle	**38.0**	
Carbon Rudder	**Yes**	LSM0	**17.864**	BLR index	**0.8749**			
Light stanchions	**Yes**	Acc. length	**17.375**					
Trim tab	**No**	Sink (kg/mm)	**54.81**					

PROPELLER

Propeller Type	**Folding 2 blades**									
Installation	**Shaft exposed**	PRD	**0.499**	PSD	**0.022**	PSA	**12.5°**	ST1	**0.044**	ST4 **0.047**
Twin screw	**No**	PBW	**0.129**	PHD	**0.052**	ESL	**1.452**	ST2	**0.088**	ST5 **0.245**
Hydro generator	**No**	PIPA	**0.0036**	PHL	**0.137**			ST3		

RIG

Forestay tension	**Aft & Forward**	P	**26.522**	E	**7.636**	
Inner stay	**Adjustable**	IG	**26.468**	J	**10.120**	
Carbon mast	**Yes**	ISP	**27.230**	BAS	**0.762**	
Headsail furler	**No**	MDT1	**0.267**	FSD	**No Foil**	
Mainsail furler	**No**	MDL1	**0.492**	SFJ	**0.065**	
Articulated bowsprit	**No**	MDT2	**0.151**	SPL		
Non-circular rigging	**No**	MDL2	**0.195**	WPL		
Fiber rigging	**Yes**	TL	**5.202**	TPS	**12.409**	
Runners/Checkstays	**2**	MW	**0.195**	BD	**0.375**	
Spreaders	**0**	GO	**0.195**	MWT		
				MCG		

Flying Headsail Foretriangles

Id	ISP	TPS
2	26.468	10.597
1	26.468	12.409

FLOTATION AND STABILITY

Calculation method	**VCG entered directly**	SFFP	**0.800**	SAFP	**18.288**
Flotation Date	**23/08/2021**	FFM		FAM	
Measurer		FF	**1.390**	FA	**1.123**
Comment		LCFcl	**10.917**	LCFsh	**11.213**
		SG	**1.0243**	HBI	**1.393**

INVENTORY

BALLAST

Id	Kind	Description	Weight	LCG	VCG	TCG
Aft Tank	Movable	Aft water ballast - Port / XCG = 17.16 (from stern)	952	1.12	0.12	0.00
Mid Tank	Movable	Central water ballast - Port / XCG = 12.07 (from stern)	998	6.21	0.21	1.92
Forward Tank	Movable	Forward water ballast - Central / XCG = 3.39 (from stern)	435	14.89	0.05	0.00
		Fixed Ballast Total	**0**			

ORC

| Club Certificate 2022 | Boat **11th HOUR RACING MĀLAMA** | Centre de Calcul FFVoile 52 rue Sénac de Meilhan 17000 - La Rochelle France | FFVoile |

MAINSAIL

Id	MHB	MUW	MTW	MHW	MQW	Area	Meas.Date	Maker	Material	Comment
MN	3.19	3.77	4.85	6.54	7.56	160.71	13/05/2022	North Sails	Dyneema	Course

HEADSAIL

Id	HHB	HUW	HTW	HHW	HQW	HLP	HLU	Btn	Flying	FT	Area	Meas.Date	Maker	Material	Comment
MH0-2	0.13	2.86	5.59	10.90	15.62	19.61	30.03	No	Yes	1	313.09	13/05/2022	North Sails	Dyneema	Course
A6.5	0.11	2.80	5.49	10.64	15.00	18.21	25.33	No	Yes	1	252.69	13/05/2022	North Sails	Dyneema	Course
A7	0.18	2.45	4.79	9.25	13.32	17.05	24.90	No	Yes	1	222.68	13/05/2022	North Sails	Unknown	Course
J0	0.13	1.86	3.64	7.24	10.93	14.87	29.67	Yes	Yes	0	217.64	13/05/2022	North Sails	Dyneema	Course
FR0	0.15	1.75	3.43	6.89	10.45	14.13	25.54	No	Yes	2	178.31	13/05/2022	North Sails	Unknown	Course
J1.5	0.14	1.53	2.94	5.86	8.91	12.17	24.72	Yes	No		147.75	13/05/2022	North Sails	Dyneema	Light
J2	0.14	1.36	2.63	5.20	7.93	10.87	23.68	Yes	No		126.10	13/05/2022	North Sails	Dyneema	Medium
J3	0.14	1.01	1.89	3.72	5.63	7.65	16.62	Yes	No		62.95	13/05/2022	North Sails	Dyneema	Lourd

ASYMMETRIC SPINNAKER

Id	SLU	SLE	SL	SHW	SFL	Ratio	Area	Meas.Date	Maker	Material	Comment
A2.2	30.16	26.60	28.38	17.47	20.13	87%	425.75	13/05/2022	North Sails	Polyester	Medium
A2	30.90	26.61	28.76	16.52	20.24	82%	413.69	13/05/2022	North Sails	Polyester	Medium

C

Section approach hydrostatic force calculation

To combat the limitation of the surface mesh method, a sectional approach is presented. In this method, for each section, the underwater intersection between the section and the waterline is computed. This point, and the other points of the section lying under the waterline, are used to calculate the hydrostatical forces on each section. The total hydrostatical force is then computed by integrating all the sections.

To obtain the intersection points between the water level and the section two equations are solved, the equation of the wave height and the interpolation between the points lying just above and just below the water level, as a function of Y needs to be solved.

$$\zeta = \zeta_a \cdot cos(-\omega t + kx + kY) \tag{C.1}$$

$$interpolation = z_p + (z_{p-1} - z_p) \cdot \frac{Y - z_p}{z_{p-1} - z_p} \tag{C.2}$$

These intersection points and the underwater points give the exact representation of the section lying under the water surface. From these points, the midpoints can be calculated; these midpoints lie exactly in the middle of the underwater points. On these midpoints, the hydrostatical force is calculated using its underwater position as z and the difference in the z-axis of the underwater points as length.

$$F_{hs} = \rho \cdot g \cdot z_{mid} \cdot dz_{underwater} \tag{C.3}$$

This gives the hydrostatical force for each midpoint. To obtain the total hydrostatical force on a section, the hydrostatical force is integrated over the section. To obtain the hydrostatical force on the entire yacht, the hydrostatical forces of all the sections are integrated over the yacht's length.
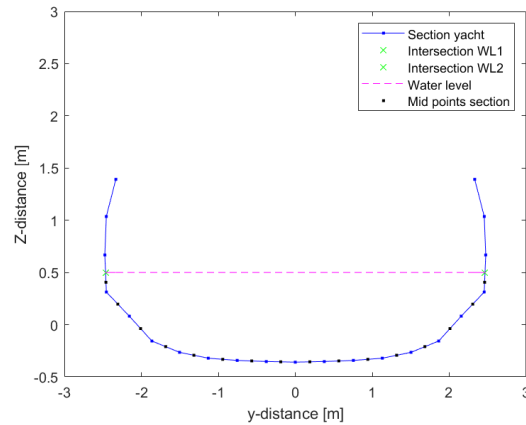
Figure C.1: One section of yacht hydrostatical forces

In figure C.1 one section of the yacht can be seen as the blue line. The pink line represents the water level, the green crosses the intersection points of the waterline with the section of the yacht and the black points the mid points.

This method provides a numerically fast way to calculate the hydrostatic force, but it assumes that there is only a hull between the sections and, thus, not a stern plane or a bow shape. Therefore, in the case that there is only water on the stern, no force in the longitudinal direction is present. This poses an issue for the simulation in big waves, where the yacht accelerates due to a wave hitting its stern.

D

Lines plan IMOCA 60
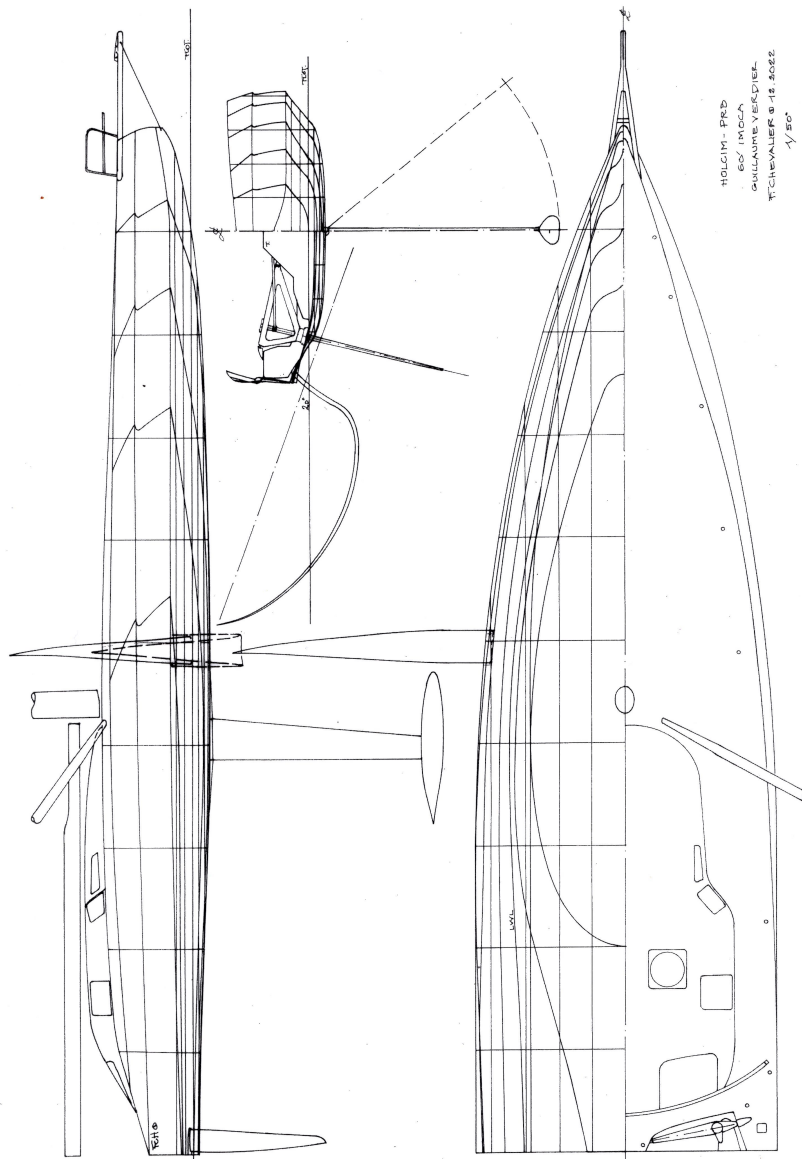
Figure D.1: Lines plan Holcim PRC (J. , 2023)]

E
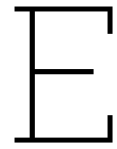
Panel length determination BEM

```matlab
%% calculation of panel size for NEMOH
% Define constants
g = 9.81; % Acceleration due to gravity (m/s^2)
N = 8; % Number of panels per wavelength,

% Define the frequency range
f_min = 0.1/(2*pi); % Minimum frequency (Hz)
f_max = 5.0/(2*pi); % Maximum frequency (Hz)
f = linspace(f_min, f_max, 100); % Frequency range (Hz)

% Calculate wavelength and panel size
lambda = g ./ (2 * pi * f.^2); % Wavelength (m)
panel_size = lambda / N; % Panel size (m)

% Plot the panel size as a function of frequency
figure;
plot(f, panel_size);
xlabel('Frequency (Hz)');
ylabel('Panel Size (m)');
title('Panel Size as a Function of Frequency');
grid on;

disp(panel_size(end))
```

Prony's approximation

In the DVPP, the Prony's approximation is used (Armesto et al., 2015). In this method, the impulse response function is approximated using a sum of exponential functions.

$$K(t) \approx \sum_{k=1}^{N_0} \alpha_k e^{\beta_k t} \tag{F.1}$$

In this approximation, N_0 is the order of the approximation, and coefficients α_k and β_k can be found using the Matlab code from Sheng et al. (2022) and the calculated A and B from the frequency domain analysis. To obtain the memory effect a recursive method is employed as explained by Sheng et al. (2022).

$$I(t) = \sum_{k=1}^{N_0} i_k(t) \tag{F.2}$$

$$i_k(t + \Delta t) = i_k(t) e^{\beta_k \Delta t} + \alpha_k e^{\frac{\beta_k \Delta t}{2}} \Delta x(t) \tag{F.3}$$

The prony approximation gives an issue with regard to the approximation of the α and β coefficients. Since, in an ideal situation, the effect of forward speed would be included in the memory effect. However, this means that for every time step, the coefficients should be recalculated, this poses an increase in computational effort. Therefore, in the DVPP, only the infinite frequency A and B matrices are corrected for the effect of forward speed, and for the memory term, the impulse response function for a case with zero forward speed is used. This impulse response K can be seen in the following formula.

$$K(\tau, U) = \frac{2}{\pi} \int_0^\infty B(\omega) cos(\omega \tau) d\omega \tag{F.4}$$